

NORTHWESTERN UNIVERSITY

Dysregulation of External Globus Pallidus-Subthalamic Nucleus Network Dynamics in
Parkinsonian Mice During Cortical Slow-Wave Activity and Activation.

A DISSERTATION

SUBMITTED TO THE GRADUATE SCHOOL IN PARTIAL FULFILLMENT OF ITS
REQUIREMENTS

for the degree of

DOCTOR OF PHILOSOPHY

Field of Northwestern University Interdepartmental Neuroscience Program (NUIN)

By

Ryan F. Kovaleski

EVANSTON, ILLINOIS

June 2020

Abstract

The basal ganglia are a remarkably complicated and interconnected tangle of subcortical nuclei whose exact function and composition are hotly debated to this day. What is plainly obvious, however, is that loss of dopaminergic modulation in the basal ganglia, as is the case in Parkinson's disease (PD) following the progressive degeneration of dopaminergic substantia nigra neurons, leads to catastrophic movement deficits. Further, excessively irregular, temporally offset, and possibly oscillatory activity in the reciprocally connected external globus pallidus (GPe) and subthalamic nucleus (STN) of the indirect pathway of the basal ganglia are tightly linked with motor dysfunction. Precisely which network interactions underlie the emergence, persistence, or amplification of pathologically associated basal ganglia activity following dopamine depletion remain contested. In efforts to address these questions, many formative studies of dopamine depletion leveraged anesthetized preparations to interrogate the transmission of cortically generated activity patterns throughout the basal ganglia but did so without access to cell-class specific manipulations or recording techniques. This dissertation is aimed at extending prior findings in urethane anesthetized rats acquired during slow wave activity (SWA) and activation (ACT) to mice and more rigorously testing several hypotheses regarding the origin or propagation of abnormal basal ganglia activity following dopamine depletion.

Here we applied multi-structure extracellular recordings in the unilateral 6-hydroxydopamine mouse model of PD to study network dynamics in the indirect pathway following dopamine depletion. Cell class-specific *in vivo* optogenetic inhibition was used to both identify neurons and determine their contribution to activity in connected nuclei. We found that following dopamine depletion: D2 dopamine receptor-expressing striatal projection neurons (D2-SPNs), upstream of

GPe, were hyperactive during cortical SWA and ACT; prototypic parvalbumin-expressing GPe (PV GPe) neuron activity was excessively suppressed when D2-SPNs were active during cortical SWA and ACT despite elevated autonomous activity; optogenetic suppression of D2-SPN activity largely alleviated abnormal patterning of GPe neurons during SWA; STN firing rates were unaltered during SWA or ACT, but were less entrained to cortical SWA; optogenetic inhibition of PV GPe neuron activity almost entirely eliminated vestigial STN responsiveness to cortical SWA; optogenetic inhibition of STN neurons exacerbated abnormal entrainment of GPe neurons to cortical SWA; excessive oscillatory activity in broad neuronal populations was not detected using traditional methods. Together these findings challenge several theories of basal ganglia dysfunction following dopamine depletion and provide both a framework to test similar hypotheses under awake conditions and a valuable link between the rat and mouse literature with some potentially crucial differences.

Acknowledgments

Firstly, I would like to thank my thesis committee, especially Dr. Mark Bevan for his mentorship and steadfast willingness to apply himself tirelessly to the betterment of the people and projects under his stewardship and his commitment to the rigorous pursuit of truth in science. May he be forever funded. Secondly, but by no means less importantly, I thank my parents for their unending and cherished support and encouragement. If we all emulated their behavior the world would shine so much brighter than it does. Thirdly, and at this point I'm really questioning the usefulness of the numbering scheme I feel compelled to apply here, I thank my partner, Mary Thomas, for the adventures we share that keep me sane, without whom I would have likely starved to death in my distraction, and who beckons me into a future worth sharing through both her personal affection and professional activism. Lastly, I would be remiss not to extend a hearty thanks to the members of the Bevan Lab who have always been there to lend a hand (or ear) when two would not suffice – special mentions for Drs. Jeremy Atherton and Joshua Callahan in alphabetical order.

The following work (including methods and results sections, verbatim) is published in The Journal of Physiology (Kovaleski et al., 2020). *In vivo* and *ex vivo* experiments were performed at Northwestern University and University of Bordeaux, respectively. M.D.B, R.F.K, and J.W.C conceived of the study. R.F.K, J.W.C., and M.C. acquired the data and were joined in analysis and interpretation by M.D.B., J.B. and D.L.W. The first draft of the manuscript was generated by R.F.K. and M.D.B. All authors contributed meaningfully to revision and intellectual content.

List of Abbreviations

6-OHDA – 6-hydroxydopamine

AAV – adeno-associated virus

ACSF – artificial cerebrospinal fluid

ACT – tail pinch-evoked cortical activation

AMPA - α -amino-3-hydroxy-5-methyl-4-isoxazolepropionic acid

AP – anterior-posterior

Arch-GFP – archaerhodopsin fused GFP

CV – coefficient of variance of the interspike interval

EEG – intracranial electrocorticogram

D1-SPN – type 1 dopamine receptor-expressing striatal projection neuron

D2-SPN – type 2 dopamine receptor-expressing striatal projection neuron

DV – dorsal-ventral

GABA – gamma-aminobutyric acid

GFP – green fluorescent protein

GPe – globus pallidus external segment

GPi – globus pallidus internal segment

HBS – HEPES-buffered saline

IC – internal capsule

IQR – interquartile range (25th-75th percentile)

ISI - interspike interval

LFP – local field potential

M1 – primary motor cortex

MFB – medial forebrain bundle

ML – medial-lateral

MWU – Mann-Whitney U test

MPTP – 1-methyl-4phenyl-1,2,3,6-tetrahydropyridine

NMDA – N-methyl-D-aspartate

NMDAR – N-methyl-D-aspartate receptor

P# - correction factor for multiple comparisons tests, # stands for the correction factor applied

PB – phosphate-buffer

PBS – phosphate-buffered saline

PBS-T - mixture of PBS, 0.5 % Triton X-100

PD – Parkinson's disease

PV – parvalbumin

RT – room temperature

SD – standard deviation

SN – substantia nigra

SNr – substantia nigra pars reticulata

SPN – striatal projection neuron

STN – subthalamic nucleus

SWA – cortical slow wave activity

TH – tyrosine hydroxylase

ZI – zona incerta

Table of Contents

ABSTRACT.....	2
ACKNOWLEDGMENTS	4
LIST OF ABBREVIATIONS.....	5
LIST OF FIGURES AND TABLES.....	9
CHAPTER 1: INTRODUCTION.....	11
1.1: PARKINSON’S DISEASE	11
1.2: BASIC ANATOMY.....	13
1.3: THE BASAL GANGLIA AND DOPAMINE: FUNCTION AND DYSFUNCTION.....	15
1.4: ANESTHETIZED AND AWAKE BASAL GANGLIA RECORDINGS.....	19
1.5: PRIOR STUDIES - SIGNIFICANCE.....	21
CHAPTER 2: METHODOLOGY	24
2.1: EXPERIMENTAL APPROACH.....	24
2.2: ANIMALS.....	28
2.3: 6-OHDA/VEHICLE AND ADENO-ASSOCIATED VIRUS (AAV) VECTOR INJECTION.....	28
2.4: <i>IN VIVO</i> ELECTROPHYSIOLOGICAL RECORDING.....	29
2.5: HISTOLOGICAL PROCESSING OF <i>IN VIVO</i> TISSUE	31
2.6: <i>IN VIVO</i> ELECTROPHYSIOLOGICAL ANALYSIS	33
2.7: <i>EX VIVO</i> ELECTROPHYSIOLOGICAL RECORDING.....	36
2.8: HISTOLOGICAL PROCESSING FOR <i>EX VIVO</i> EXPERIMENTS	37
2.8: STATISTICAL ANALYSIS.....	39
CHAPTER 3: RESULTS.....	41

	8
3.1: DURING CORTICAL SWA THE FREQUENCY OF D2-SPN ACTIVITY IS GREATER IN 6-OHDA- INJECTED MICE.....	41
3.2: IN DOPAMINE-DEPLETED MICE PV GPE NEURON ACTIVITY IS RELATIVELY ANTIPHASIC TO CORTICAL SWA.....	46
3.3: DURING CORTICAL SWA, D2-SPNS CONTRIBUTE TO THE ANTIPHASIC FIRING OF GPE NEURONS IN 6-OHDA-INJECTED MICE.....	51
3.4: FOLLOWING LOSS OF DOPAMINE THE AUTONOMOUS FIRING OF PV GPE NEURONS IS SIGNIFICANTLY ELEVATED.....	55
3.5: THE STN OPPOSES RATHER THAN FACILITATES ANTIPHASIC GPE NEURON ACTIVITY.....	59
3.6: DOPAMINE DEPLETION REDUCES PHASE LOCKING OF STN NEURON FIRING TO CORTICAL SWA.....	66
3.7: PV GPE NEURON ACTIVITY ENHANCES STN NEURON ENTRAINMENT TO CORTICAL SWA IN CONTROL- AND DOPAMINE-DEPLETED MICE.....	69
3.8: LOSS OF DOPAMINE PROFOUNDLY ALTERS THE RESPONSES OF D2-SPNS AND PROTOTYPIC PV GPE NEURONS TO CORTICAL ACT, WHEREAS STN ACTIVITY IS RELATIVELY UNAFFECTED.	74
CHAPTER 4: DISCUSSION.....	79
4.1: EXPERIMENTAL FINDINGS IN BRIEF.....	79
4.2: IMPLICATIONS OF D2-SPN HYPERACTIVITY.....	80
4.3: EXCESSIVE PATTERNING OF PROTOTYPIC GPE NEURONS.....	82
4.4: PATTERNING OF STN NEURON ACTIVITY.....	85
4.5: STN'S ROLE IN GPE PATTERNING.....	87
4.6: CONCLUDING REMARKS.....	88
REFERENCES.....	90

List of Figures and Tables

FIGURE 2.1.1 SCHEMATIC REPRESENTATION OF ELECTRODE RECORDING SITES.	25
TABLE 2.1.1 TH IMMUNOREACTIVITY IN THE STRIATUM OF VEHICLE- AND 6-OHDA-INJECTED MICE	26
TABLE 2.1.2 SPECTRAL PROPERTIES OF THE EEG DURING CORTICAL SWA AND ACT IN VEHICLE- AND 6-OHDA-INJECTED MICE	26
TABLE 2.1.3 SPECTRAL ANALYSIS OF LFPS IN THE GPE AND STN DURING CORTICAL SWA AND ACT IN VEHICLE- AND 6-OHDA-INJECTED MICE.....	27
FIGURE 3.1.1 DURING CORTICAL SWA THE FREQUENCY OF D2-SPN ACTIVITY IS GREATER IN 6-OHDA-INJECTED MICE	44
FIGURE 3.2.1 IN 6-OHDA-INJECTED MICE PV GPE NEURON ACTIVITY IS RELATIVELY ANTIPHASIC TO CORTICAL SWA.....	50
FIGURE 3.3.1 OPTOGENETIC INHIBITION OF D2-SPNS REDUCES ANTIPHASIC GPE ACTIVITY IN 6-OHDA-INJECTED MICE.....	53
FIGURE 3.4.1 IN 6-OHDA-INJECTED MICE THE FREQUENCY OF AUTONOMOUS PV GPE NEURON ACTIVITY <i>EX VIVO</i> IS ELEVATED	57
FIGURE 3.5.1 EFFECT OF OPTOGENETIC INHIBITION OF THE STN ON GPE ACTIVITY	62
FIGURE 3.5.2 OPTOGENETIC INHIBITION OF STN NEURONS DECREASES THE FIRING RATE OF UNIDENTIFIED AND PUTATIVE PV GPE NEURONS AND INCREASES THEIR ANTIPHASIC ACTIVITY IN 6-OHDA-INJECTED MICE	64

FIGURE 3.6.1 IN 6-OHDA-INJECTED MICE PHASE LOCKING OF STN FIRING TO CORTICAL SWA IS REDUCED	10 68
FIGURE 3.7.1 OPTOGENETIC INHIBITION OF PV GPE NEURONS DISINHIBITS STN NEURONS AND REDUCES THEIR PHASE LOCKING TO CORTICAL SWA IN BOTH VEHICLE- AND 6-OHDA-INJECTED MICE.....	72
FIGURE 3.8.1 EFFECTS OF TAIL PINCH-EVOKED CORTICAL ACT ON D2-SPNS, PV GPE NEURONS, AND STN NEURONS IN VEHICLE- AND 6-OHDA INJECTED MICE ...	77

Chapter 1: Introduction

1.1: Parkinson's disease

Parkinson's disease (PD) is the second most common neurodegenerative disorder (Kalia and Lang, 2015) and is especially common in aging populations affecting ~1% of people over 63 years old (Hirtz et al., 2007). The long-established consensus view is that PD results from the progressive degeneration of dopaminergic substantia nigra (SN) neurons. Dopaminergic SN neurons project massively to the striatum and less so to other basal ganglia structures providing neuromodulatory input associated with habit formation, learning, and movement initiation (Yin and Knowlton, 2006; Redgrave et al., 2010; Keeler et al., 2014; Klaus et al., 2019; Mallet et al., 2019). The disease progression is staged, with neural degeneration taking place long before symptom onset (Postuma et al., 2012). A fractional number of PD patients develop the disease due to known genetic factors; the rest are idiopathic but accumulated evidence suggests a combination of genetic and environmental risk factors are to blame (Kalia and Lang, 2015). PD is a movement disorder characterized by akinesia, rigidity, bradykinesia, shuffling gait, and tremor (Postuma et al., 2015) among a host of lesser studied motor and cognitive dysfunctions (Faivre et al., 2019) and sleep disorders (St Louis et al., 2017) that can manifest several at once or arise over time.

One of the major challenges of PD treatment is the lack of early detection methods. The long-range synaptic connections of dopaminergic SN neurons are established during development and cannot be replaced by any current methodology once lost. Because early intervention is impossible at present, most current therapies are targeted to patients after symptom onset

(Kordower et al., 2013). Because approximately \sim 50-60% of dopaminergic SN neurons degenerate before symptom onset, it is likely that homeostatic mechanisms within the basal ganglia spare motor behavior from the consequences of such a loss until a critical threshold of dopamine depletion is exceeded (Blesa et al., 2017; Villalba and Smith, 2018). It is also possible that once striatal dopamine loss reaches a critical level the circuit modifications that were permissive of relatively normal motor activity up to that point become detrimental in the profoundly dopamine depleted state (Blesa et al., 2017; Villalba and Smith, 2018; Mallet et al., 2019; McGregor and Nelson, 2019). Indeed, modifications to both the rate and pattern of basal ganglia nuclei have been shown to develop as circuits adapt to dopamine depletion (Leblois et al., 2006; Hammond et al., 2007; Quiroga-Varela et al., 2013). For instance, synchronization of basal ganglia nuclei to stereotyped oscillations in various frequency bands that emerges in the weeks following acute dopamine depletion in monkey and rodent animal models (Bergman et al., 1994; Leblois et al., 2006; Mallet et al., 2008a; Sanders et al., 2013; Sharott et al., 2017) has been demonstrated as a hallmark of and possible cause of parkinsonian network activity. While it remains the case that treatments are focused on symptomatic patients whose dopamine depletion is already pervasive and who have already undergone adaptation to dopamine depletion it is critical to develop a deeper understanding of how abnormal activity patterns in this state are transmitted throughout the basal ganglia. In order to intelligently propose further research targeted at mitigating the transmission of maladaptive activity and restoring motor function, we must systematically interrogate the dopamine depleted circuit to determine which nodes within the basal ganglia interact to generate or mitigate abnormal patterning.

1.2: Basic anatomy

Here I will outline the basic anatomy of the basal ganglia pertinent to motor aspects of PD. Most current therapies for PD focus on the gross motor aspects of parkinsonism (bradykinesia, akinesia, etc.) because they are the most frequently debilitating aspects of the disease. However, this is not to minimize non-motor components which can be devastating in some patients and are not well treated by existing therapies (Pfeiffer, 2016). This will restrict our discussion of anatomy leaving off the parallel limbic and associative cortico-basal ganglia thalamocortical loops, neuromodulatory inputs other than dopamine, and sensorimotor feedback.

Most cortical areas project to the striatum, the primary input structure of the basal ganglia, and have overlapping glutamatergic input (Mailly et al., 2013; Averbeck et al., 2014). Temporally and spatially convergent corticostriatal (mostly axospinous) input is required to induce firing in GABAergic striatal projection neurons (SPNs) which make up more than 90 % of neurons in the striatum (Gerfen and Bolam, 2016). The classic model of basal ganglia circuitry posits two anatomically defined and opposed ‘direct’ and ‘indirect’ pathways that are differentially affected by dopamine modulation (Albin et al., 1989; DeLong, 1990). The direct pathway, traditionally thought of as movement promoting, consists of GABAergic D1 dopamine receptor-expressing SPNs (D1-SPNs) that project to the GABAergic output nuclei of the basal ganglia, the substantia nigra *pars reticulata* (SNr) and globus pallidus internal segment (GPi, or its rodent analog the entopeduncular nucleus) (Gerfen et al., 1990; Deng et al., 2006). According to the classic model, D1-SPNs excited by cortical input suppress SNr/GPi activity thereby disinhibiting brainstem and thalamocortical neurons (Parent and Parent, 2004) and releasing them from tonic inhibition generated by SNr/GPi to promote movement via cortical and brainstem excitation (Albin et al.,

1989; Alexander and Crutcher, 1990; DeLong, 1990; Goldberg et al., 2013). The indirect pathway, traditionally thought of as movement suppressing, begins with D2 dopamine receptor-expressing SPNs (D2-SPNs) that project to the GABAergic globus pallidus external segment (GPe) (Gerfen et al., 1990; Deng et al., 2006) which in turn projects to SNr/GPi and the glutamatergic subthalamic nucleus (STN). STN also projects to SNr/GPi and back to GPe (Smith et al., 1998). Overall, cortical stimulation of D2-SPNs was thought to suppress GPe activity, release SNr/GPi and STN from inhibition whereby STN adds excitatory glutamatergic input to the now disinhibited output nuclei, elevating inhibitory output of the basal ganglia and suppressing movement by reducing activity of thalamocortical neurons and brainstem nuclei (Albin et al., 1989; Alexander and Crutcher, 1990; DeLong, 1990; Frank et al., 2007; Tachibana et al., 2008).

Because D1-SPNs are excited by dopamine stimulation and D2-SPN activity is suppressed, dopamine stimulation favors the direct, movement promoting pathway (DeLong, 1990; Gerfen et al., 1990; Gerfen and Surmeier, 2011). In the dopamine depleted state, however, the balance was thought to shift in favor of the movement-suppressing indirect pathway. The classic model's anatomical description outlined above, while accurate, is not complete. Cortical input directly to STN (the hyperdirect pathway) (Nambu et al., 2002), reciprocal connections between STN and GPe (Bevan et al., 2002), and bridging collaterals from D1-SPNs to GPe (Wu et al., 2000) have been recognized for many years yet are not often incorporated in functional models of basal ganglia activity. Recently identified novel cell classes, such as arkypallidal GPe neurons that project exclusively to striatum (Mallet et al., 2012; Abdi et al., 2015; Dodson et al., 2015; Mallet et al., 2016), have also been identified and whose role in motor activity are just beginning to be

understood. Inaccessible (i.e. deep, miniscule, and/or cellularly diverse) circuit components such as di- and mesencephalic locomotor regions and tectum as well as intralaminar thalamic nuclei, each project to numerous basal ganglia structures and provide sensorimotor feedback that presumably updates circuit activity about motor outcomes and alters information processing yet remain poorly understood and understudied because techniques to permit interrogation of such neuronal populations are only now emerging (Grillner and Robertson, 2015). How feedback from these circuit elements influences basal ganglia activity in the presence of movement disorders where movement kinematics are by definition impaired, for instance, is virtually unaddressed despite a shift in the field towards awake-behaving experimental preparations where this issue is more prevalent. Going forward, studies designed to address these caveats will be necessary to untangle basal ganglia circuit function and dysfunction.

1.3: The basal ganglia and dopamine: function and dysfunction

While it is true that dopamine has the expected effects on excitability of direct and indirect pathway SPNs (Gerfen et al., 1990; Planert et al., 2013) and optogenetic excitation of D1- and D2-SPNs also recapitulates the classic role of direct and indirect pathway activity on gross motor output (Kravitz et al., 2010), the usefulness of the classic model has come into question in recent years. Firstly, inactivation of GPi (Inase et al., 1996) or lesion of GPe (Soares et al., 2004) in normal monkeys does not adversely affect motor function, therefore rate is not an irreplaceable feature of the motor circuit. Further, recent studies point to coactivation of D1- and D2-SPNs during movement initiation (Cui et al., 2013; Markowitz et al., 2018; Parker et al., 2018) which is required for the execution of motor sequences (Tecuapetla et al., 2016). Indeed, ensemble activity of D1- and D2-SPNs occurs during the execution of specific motor sequences with

decorrelations on the sub-second timescale (less than ~ 300 ms) and co-activity during transition from one behavioral sequence to another (Markowitz et al., 2018). With these (and other; McGregor and Nelson, 2019) complications in the classic rate model, attention has shifted towards how the pattern of activity passing through cortico-basal ganglia-thalamocortical loops are abnormally altered following dopamine depletion.

A wildly complex admixture of neural activity likely governs normal basal ganglia activity representing, at a minimum, convergent corticostriatal synaptic innervation of individual SPNs originating in many cortical areas (Mailly et al., 2013; Averbeck et al., 2014; Gerfen and Bolam, 2016), collateral inhibition among SPNs (Burke et al., 2017), engagement of the local striatal microcircuitry composed of more than a dozen interneuron subtypes (Burke et al., 2017; Tepper et al., 2018), complex GPe/STN interactions (Bevan et al., 2002) coupled with hyperdirect cortical input to STN (Nambu et al., 2002), arky pallidal GPe neuron innervation of striatum (Mallet et al., 2012; Abdi et al., 2015), nigrostriatal GABAergic feedback (Haber et al., 2000; Lerner et al., 2015), dopaminergic and other neuromodulatory input to striatum/GPe/STN (Mena-Segovia et al., 2004; Parent et al., 2011; Bolam and Ellender, 2016; Mena-Segovia, 2016; Mallet et al., 2019; Tanimura et al., 2019), and spatiotemporal convergence of these signals in the output nuclei in combination with long loop effects of cortico-basal ganglia-thalamocortical activity and nudged by sensorimotor feedback from brainstem motor regions and thalamus (Mena-Segovia et al., 2004; Galvan and Smith, 2011; Grillner and Robertson, 2015; Mena-Segovia, 2016) as movements progress and achieve favorable or unfavorable results. Among all these candidate structures for the locus of abnormal basal ganglia activity, no one key signature of the parkinsonian circuit activity has been identified that perfectly correlates with severity of

motor symptoms across studies and animal models. However, reliable differences in activity pattern across structures have been observed. Among the most reliably observed, increase burst/pause propensity (irregularity) and synchrony of neural populations in STN, GPe, and GPi/SNr (Magill et al., 2001; Bevan et al., 2002; Hammond et al., 2007; Walters et al., 2007; Quiroga-Varela et al., 2013; Sanders et al., 2013; Willard et al., 2019). In keeping with these observations, somatotopic representations are less distinct in the basal ganglia following dopamine depletion and increased recruitment and synchronization of specific neural populations during movement have been observed (Bergman et al., 1994; Cho et al., 2002; Pessiglione et al., 2005; Leblois et al., 2006; Mallet et al., 2008b; Nambu, 2011; Ketzef et al., 2017; Sharott et al., 2017; Maltese et al., 2019).

Exaggerated and abnormally persistent rhythmic oscillatory activity, especially in the extended beta band (8-35 Hz), remains discussed as a potential disease mechanism whereby the dopamine depleted basal ganglia become susceptible to oscillatory activity in the extended beta band that occludes or actively disrupts activity underlying normal movement. The presence of these abnormal oscillations in PD patients and experimental models of PD in rats and monkeys has been well documented (Mallet et al., 2008b; Kuhn et al., 2009; Sanders et al., 2013; Devergnas et al., 2014; Delaville et al., 2015; Sharott et al., 2017). The evidence of their participation in motor pathology is, unfortunately largely correlational and occasionally inconsistent: on an individual basis severity of motor symptoms in MPTP-treated monkeys can fail to correlate with periods of excessive abnormal oscillations (Muralidharan et al., 2016); motor symptoms in MPTP-treated monkeys can precede emergence of abnormal oscillations (Leblois et al., 2007); and abnormal oscillations are not observed in all PD patients (Rosa et al., 2011). To date, no reports of

abnormal oscillatory activity have been reported in profoundly dopamine depleted mice (McGregor and Nelson, 2019). Because dopamine depleted mice develop parkinsonian phenotypes, this raises an important question about the applicability of the mouse model to PD or the etiological nature of extended beta band oscillations. The fact that the most common treatments for PD symptoms in humans are also therapeutic in dopamine depleted mice, rats, and monkeys (dopamine replacement and DBS; Brown et al., 2001; Heimer et al., 2002; Sharott et al., 2005; Kuhn et al., 2009; Eusebio et al., 2012; Li et al., 2012; Whitmer et al., 2012; Brazhnik et al., 2014; Sanders and Jaeger, 2016) suggests etiological mechanisms underlying motor dysfunction following dopamine depletion are relatively preserved across mammals.

What mechanisms underly emergence of abnormally phasic and possibly oscillatory activity in the basal ganglia following dopamine depletion? There are a variety of possible explanations. The most parsimonious explanation would be that D2-SPNs are hyperactive and respond to cortical and/or thalamic stimulation with a higher degree of synchrony or neuron recruitment following dopamine depletion and this entrains downstream circuitry as a function of the loss of inhibitory dopaminergic modulation in these cells (Albin et al., 1989; DeLong, 1990; Gerfen et al., 1990). There is some evidence that D2-SPNs become hyperexcitable in mice and rats (Mallet et al., 2006; Ballion et al., 2009; Escande et al., 2016; Sharott et al., 2017; Parker et al., 2018; Ryan et al., 2018) although metrics of coactivity at rest appear unaltered and even decreased during movement (Parker et al., 2018). On the other hand, studies like Parker et al. are generally restricted to relatively narrow cross-sectional examination of three-dimensional structures, do not differentiate between striosome and matrix compartments, and take place in mice with large cortical lesions in the vicinity of motor cortex (which overlies dorsolateral striatum) to make

room for the lenses used to acquire calcium imaging data from striatum (Markowitz et al., 2018; Parker et al., 2018). Therefore, it is possible that coactivity is underestimated by these methods. Another recent study showed that the proportion of D2-SPNs active over a period of rest or locomotion is elevated following dopamine depletion (Maltese et al., 2019). This suggests that even if individual neurons are not broadly hyperactive or more phase locked to cortical inputs, downstream structures could still receive abnormally powerful GABAergic input on the basis of additional neuron recruitment. One suggested alternative is that downstream structures, like GPe and STN, lose their autonomous firing properties and this makes them more vulnerable to patterning by synchronous inputs (Zhu et al., 2002; Ballion et al., 2009; Chan et al., 2011; Pavlides et al., 2015; Shouno et al., 2017; McIver et al., 2019) or that GPe-STN reciprocal interactions might play a role in generating or amplifying oscillatory activity (Moran et al., 2011; Tachibana et al., 2011; Fan et al., 2012). Phase offset of GPe and STN activity has also been proposed to converge at the level of the output nuclei to create coincident disinhibition and excitation leading to abnormal bursting activity in SNr/GPi (Shink et al., 1996; Walters et al., 2007; Moran et al., 2011; Tachibana et al., 2011; Shouno et al., 2017; Willard et al., 2019).

1.4: Anesthetized and awake basal ganglia recordings

There are costs and benefits associated with the interrogation of circuit activity in both anesthetized and awake recording preparations. Older studies relied on anesthesia due to technical limitations of neural recording but enjoyed several benefits lacking in awake preparations. It was in this environment of predominantly anesthetized recordings that many of the theories of basal ganglia function were first developed and tested. The primary benefit of anesthesia is that it produces a stereotyped cortical activity state analogous to slow wave sleep

(Steriade, 2000) often referred to as cortical slow wave activity (SWA). Under these conditions, cortical activity alternates between active and inactive phases with a period of ~ 1 Hz, animals are immobile, and sensorimotor feedback to the basal ganglia is largely suppressed (West, 1998). These predictable alternating phases of activity create an opportunity to trace the impact of synchronous activity as it propagates through the basal ganglia in the absence of sensorimotor feedback which is inherently distorted due to the degradation of movement kinematics in animal models of PD. This is convenient for PD research because several prevailing theories of how abnormal basal ganglia activity leads to movement pathology involve the propagation of abnormally synchronous activity patterns. Alterations of synaptic strength and convergent interactions of various pathways can be tested in this preparation because the input to basal ganglia is cyclical in nature.

In awake conditions, this is far from the truth; on a moment to moment basis, state transitions are clearly visible at the level of intracranial electroencephalogram (EEG) and local field potential (LFP) that may be governed by attention, intention, action initiation/abortion, or sensorimotor feedback. On the other hand, awake recordings are invaluable for determining what neural activity is *for* and whether or not specific interventions are therapeutic. However, in order to make that determination, experimenters are often forced to train or overtrain animals on tasks that restrict the variability in neural activity to a parameter space with some semantic relevance. The interpretation of such results can be challenging or misleading such as when parameterization of “therapeutic” interventions is overly narrow, e.g. in studies where mice run more or faster in an open field during optogenetic stimulation but movement kinematics are not analyzed and do not appear remotely normal in example videos (e.g. Mastro et al., 2017).

Therefore, preparations that are designed to reduce the complexity of network activity to isolate circuit components *in vivo* remain valuable in our search to understand basal ganglia dysfunction.

1.5: Prior studies - Significance

In order to understand the significance of the study we carried out it is necessary to examine the scientific context in which it was initiated. A fairly comprehensive study of indirect pathway abnormal activity under anesthesia in rats (Walters et al., 2007), drawing upon earlier work (Magill et al., 2001), found that following dopamine depletion unidentified striatal neurons fire more during SWA and maintain in-phase firing with the active phase of SWA; unidentified GPe neurons developed pauses that were largely coincident with striatal bursting; STN was active primarily during periods where GPe was silent (coincident with hyperdirect input as well) and a higher proportion of bursting STN neurons were detected. This study suggested that it is D2-SPN hyperactivity that entrains the indirect pathway to cortical oscillations. Following up on this conclusion, another study in anesthetized rats sought to demonstrate that by suppressing activity of striatopallidal SPNs using an NMDAR antagonist (D-APV), the pauses in GPe activity could be largely alleviated (Zold et al., 2012). Around the same time, another group solidified the identification of arkypallidal GPe neurons (Mallet et al., 2012; Abdi et al., 2015) highlighting the need for additional experiments separating GPe neuron subtypes with further studies showing the emergence of cortical beta band (13-30 Hz) oscillations represented in GPe and STN neurons in rats, especially during desynchronized cortical states (Mallet et al., 2008a; Mallet et al., 2008b; Delaville et al., 2015). Since this time, calcium imaging and extracellular electrode recordings have extended these findings, regarding D2-SPN activity, to awake mice (Parker et al., 2018;

Ryan et al., 2018). Of particular interest, are results pointing to increases of D2-SPN activity in awake immobile but not locomoting mice (Parker et al., 2018; Ryan et al., 2018) suggesting that perhaps excessive D2-SPN activity must be overcome in order for locomotion to occur.

In this context, our study was designed to revisit and extend these findings in mice. Due to the broad range of genetic tools available for circuit dissection in mice, this animal model is relied upon more and more to interrogate basal ganglia activity and the consequences of dopamine depletion. Therefore, it is critical to confirm findings that are often taken for granted as true in mice that have only ever been tested in rats using non-cell-type-specific techniques. Until now, for example, no pathway-specific suppression of SPN activity has demonstrated that D2-SPNs, specifically, are responsible for abnormal cortical SWA-associated activity of GPe neurons following dopamine depletion in mice or rats and no recordings of prototypic GPe neurons in anesthetized mice have been performed that could be compared to findings in rats discussed above. STN recordings in dopamine depleted mice are also rare, especially in conjunction with recordings from other structures. Therefore, we set out to perform an optogenetic interrogation of the indirect pathway following unilateral 6-hydroxydopamine (6-OHDA) dopamine depletion, with special attention to the GPe-STN network, using transgenic cre-driver mouse lines and cre-dependent viral constructs to enable optogenetic inhibition of D2-SPNs, parvalbumin-expressing GPe (PV GPe) neurons that account for the majority of prototypic neurons and have privileged GPe-STN input (Abdi et al., 2015; Hernandez et al., 2015), and STN neurons in separate experiments while recording downstream activity and EEG. Optogenetic inhibition was used both to enable identification of these specific cell types during *in vivo* urethane anesthetized

recordings and to determine their contribution to abnormal activity in connected nuclei in dopamine-depleted relative to -intact mice.

Chapter 2: Methodology

2.1: Experimental Approach

To determine the activity patterns of D2-SPNs, PV GPe neurons, and STN neurons, and their impact on GPe-STN network activity *in vivo*, neurons were identified and their activities manipulated through activation of the inhibitory opsin Arch-GFP (Chow et al., 2010). Arch-GFP was expressed virally in a cre-dependent manner in D2-SPNs, PV GPe neurons, and STN neurons in A2A-cre, PV-cre, and GABRR3-cre mice, respectively. In addition, mice received ipsilateral injections of 6-OHDA or vehicle in the MFB to lesion midbrain dopamine neurons and to control for surgical injection, respectively. Two-three weeks after surgery, mice were anesthetized with a combination of urethane and ketamine/xylazine and ipsilateral neuronal activity was recorded and manipulated optogenetically using silicon tetrodes/optrodes. Concurrent cortical activity was assessed from the EEG. After recording, mice were perfuse-fixed and the locations of recording tetrodes/optrodes were determined histologically (Fig. 2.1.1). Dopaminergic innervation of the striatum was quantified through immunohistochemistry for TH (Table 2.1.1). During cortical SWA and ACT, the relative powers of oscillatory activity in the EEG and LFPs in the GPe and STN in the 0.5-1.5 Hz, 10-39.9 Hz, and 40-250 Hz bands were similar in vehicle- and 6-OHDA-injected mice (Tables 2 and 3, respectively).

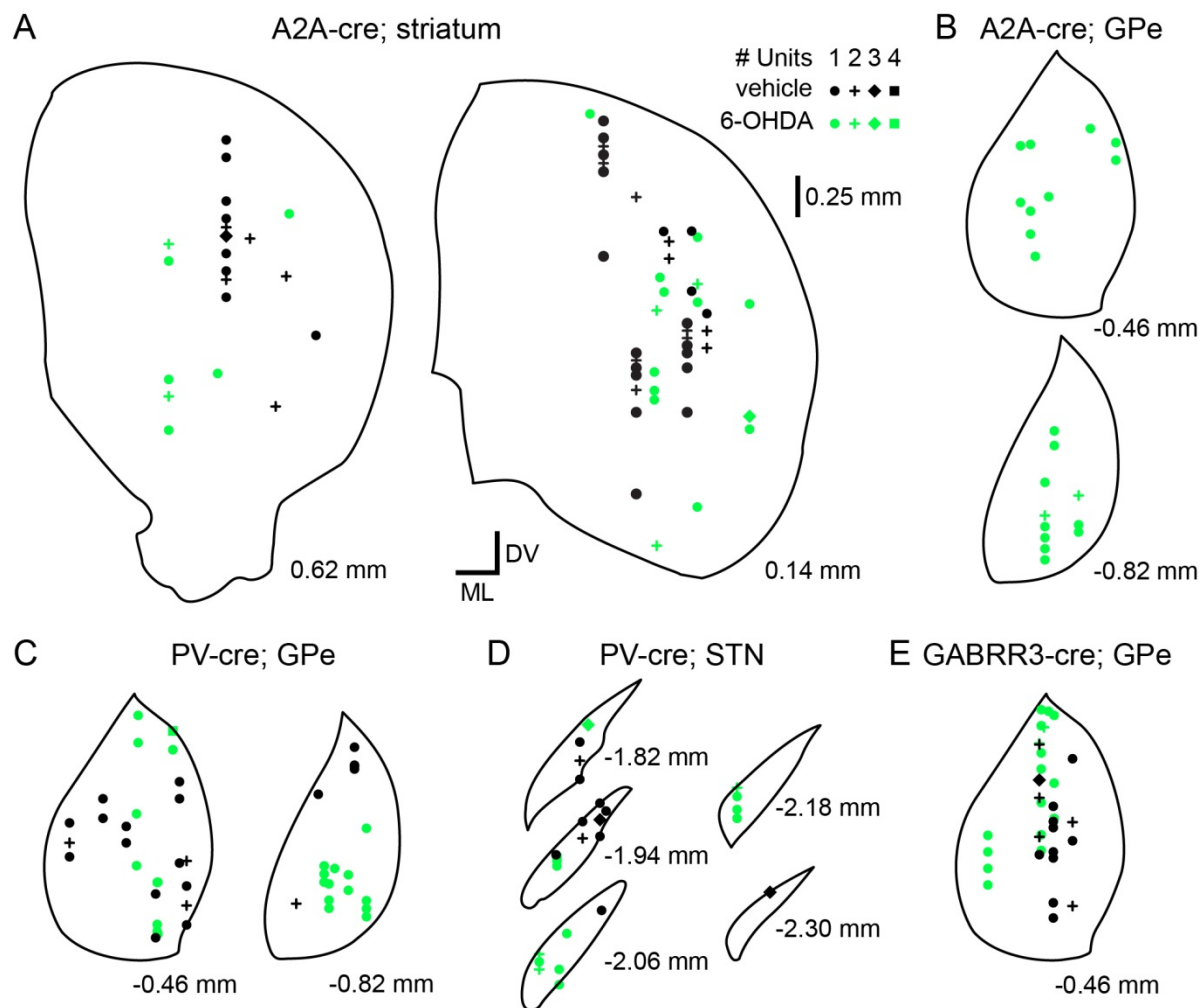


Figure 2.1.1 Schematic representation of electrode recording sites

A-E, maps of electrode recording sites used in this study. Recording sites in vehicle- and 6-OHDA-injected mice are plotted as black and green, respectively. The rostrocaudal location of each map is denoted relative to Bregma. The dorsoventral (DV) and mediolateral (ML) axes, scale bar, and recording key denoted in *A* refer to each panel. The number of units per recording site is denoted by a marker symbol. *A*, electrode sites in the striatum of A2A-cre mice. *B*, GPe electrode sites in A2A-Cre mice. *C*, GPe electrode sites in PV-Cre mice. *D*, STN recording sites in PV-Cre mice. *E*, GPe electrode sites in GABRR3-Cre mice.

Table 2.1.1 TH immunoreactivity in the striatum of vehicle- and 6-OHDA-injected mice

Mouse Line/Cell Type	vehicle: TH immunoreactivity (%)	6-OHDA: TH immunoreactivity (%)	p - value
A2A-cre/D2-SPNs	101, 98-105; n = 6	4, 11-4; n = 9	p = 0.0004*
A2A-cre/GPe	-----	4, 11-5 ; n = 8	-----
PV-cre/PV GPe	103, 96-105; n = 7	1, 11-3; n = 6	p = 0.0012*
PV-cre/STN	103, 96-106; n = 6	0, 16-1; n = 5	p = 0.0043*
PV-cre X Ai9/PV GPe	99, 99-131; n = 3	15, 29-6; n = 7	p = 0.0167*
GABRR3-cre/GPe	102, 96-104; n = 3	3, 34-2; n = 4	p = 0.0571

TH immunoreactivity in the ipsilateral dorsal striatum expressed as a percentage of immunoreactivity in the non-injected contralateral hemisphere, stratified by mouse line and recorded cell type. *, p < 0.05 (MWU).

Table 2.1.2 Spectral properties of the EEG during cortical SWA and ACT in vehicle- and 6-OHDA-injected mice

Frequency Band (Hz)	vehicle: Relative Power	6-OHDA: Relative Power	p - value	vehicle: Peak Frequency (Hz)	6-OHDA: Peak Frequency (Hz)	p - value	n (vehicle/6-OHDA)
0.5-1.5 (SWA)	0.247, 0.169-0.375	0.233, 0.124-0.335,	0.2769	1.22, 0.855-1.34	1.1, 0.855-1.40	0.7042	60/69
10-39.9 (SWA)	(0.792, 0.53-1.23) x 10 ⁻²	(0.827, 0.617-1.21) x 10 ⁻²	0.6455	10.4, 10.1-11.4	10.9, 10.3-12.3	0.0121*	60/69
40-250 (SWA)	(0.332, 0.235-0.565) x 10 ⁻²	(0.341, 0.193-0.523) x 10 ⁻²	0.4576	48.3, 44.1-54.1	45.0, 41.9-49.7	0.0090*	60/69
0.5-1.5 (ACT)	(6.97, 3.43-13.4) x 10 ⁻²	(7.21, 4.39-12.3) x 10 ⁻²	0.9121	0.610, 0.610-1.22	0.610, 0.610-1.47	0.7522	39/35
10-39.9 (ACT)	(2.55, 0.798-4.15) x 10 ⁻²	(2.51, 1.88-4.18) x 10 ⁻²	0.2175	11, 10.1-12.7	11.5, 10.5-14.7	0.2907	39/35
40-250 (ACT)	(1.39, 0.608-2.44) x 10 ⁻²	(1.47, 0.674-2.11) x 10 ⁻²	0.9549	45.7, 41.8-51.5	42.7, 41.0-44.7	0.0103*	39/35

Relative power and peak frequency in the EEG of vehicle- and 6-OHDA-injected mice during cortical SWA or ACT in the 0.5-1.5 Hz, 10-39.9 Hz, and 40-250 Hz frequency bands. Power in each band was normalized to the power in the 0-250 Hz range. *, p < 0.05 (MWU).

Table 2.1.3 Spectral analysis of LFPs in the GPe and STN during cortical SWA and ACT in vehicle- and 6-OHDA-injected mice

Frequency Band (Hz)	vehicle: Relative Power	6-OHDA: Relative Power	p - value	vehicle: Peak Frequency (Hz)	6-OHDA: Peak Frequency (Hz)	p - value	n (vehicle/6-OHDA)
GPe 0.5-1.5 (SWA)	0.408, 0.248 - 0.446	0.272, 0.135 - 0.347	0.0014	1.22, 0.977 - 1.34	0.977, 0.732 - 1.31	0.0749	25/48
GPe 10-39.9 (SWA)	(0.912, 0.504 - 1.67) x 10 ⁻²	(0.548, 0.281 - 0.124) x 10 ⁻²	0.0705	10.6, 10.0 - 11.8	10.4, 10.2 - 11.4	0.9464	25/48
GPe 40-250 (SWA)	(4.06, 2.19 - 6.90) x 10 ⁻³	(3.33, 2.18 - 9.48) x 10 ⁻³	0.7509	180, 59.8 - 180	180, 60.1 - 180	0.4841	25/48
GPe 0.5-1.5 (ACT)	(3.61, 1.97 - 8.47) x 10 ⁻²	(4.09, 2.40 - 8.58) x 10 ⁻²	0.5502	0.610, 0.610 - 1.22	0.610, 0.610 - 0.732	0.9704	21/24
GPe 10-39.9 (ACT)	(2.66, 1.74 - 4.98) x 10 ⁻²	(3.82, 1.29 - 4.64) x 10 ⁻²	0.8659	11.2, 10.3 - 12.8	10.7, 10.1 - 11.8	0.2312	21/24
GPe 40-250 (ACT)	(1.48, 0.611 - 2.82) x 10 ⁻²	(1.61, 0.573 - 3.29) x 10 ⁻²	0.5963	180, 43.3 - 180	60.2, 45.5 - 180	0.5834	21/24
STN 0.5-1.5 (SWA)	0.194, 0.103 - 0.336	0.0878, 0.0506 - 0.161	0.0754	0.977, 0.763 - 1.31	1.34, 1.22 - 1.47	0.0303	8/11
STN 10-39.9 (SWA)	(1.76, 0.622 - 2.90) x 10 ⁻²	(0.913, 0.78 - 1.42) x 10 ⁻²	0.4421	11.5, 10.7 - 12.4	10.9, 10.3 - 12	0.5282	8/11
STN 40-250 (SWA)	(2.19, 0.601 - 3.48) x 10 ⁻²	(1.2, 0.71 - 1.47) x 10 ⁻²	0.3100	120, 60.0 - 180	180, 59.8 - 180	0.9525	8/11
STN 0.5-1.5 (ACT)	(5.43, 1.66 - 9.75) x 10 ⁻²	(5.32, 3.92 - 6.61) x 10 ⁻²	0.9015	0.610, 0.610 - 0.610	0.610, 0.610 - 0.732	0.7308	7/7
STN 10-39.9 (ACT)	(1.98, 0.853 - 3.39) x 10 ⁻²	(1.3, 0.754 - 2.65) x 10 ⁻²	0.4557	11.2, 10.7 - 13.4	23.2, 14.8 - 30.5	0.0390	7/7
STN 40-250 (ACT)	(2.40, 0.435 - 4.10) x 10 ⁻²	(1.24, 1.22 - 2.14) x 10 ⁻²	0.8048	180, 59.8 - 180	180, 45.3 - 180	0.6503	7/7

Relative power and peak frequency in the LFPs of vehicle- and 6-OHDA-injected mice during cortical SWA or ACT in the 0.5-1.5 Hz, 10-39.9 Hz, and 40-250 Hz frequency bands. Power in each band was normalized to the power in the 0-250 Hz range. *, p < 0.05 (MWU).

2.2: Animals

Descriptive data are presented as median and interquartile range (IQR). Adult male mice including A2A-cre (Tg(Adora2a-cre)KG139Gsat, RRID:MMRRC_031168-UCD; 163, 104-196 days old; n = 18), PV-cre (B6.Cg-Pvalb^{tm1.1(cre)}Aibs/J, RRID:IMSR_JAX:012358; 151, 126-167 days old; n = 14), PV-cre X Ai9 mice (B6.129P2-Pvalb^{tm1(cre)}Arbr/J X B6.Cg-Gt(ROSA)26Sor^{tm9(CAG-tdTomato)Hze}/J, RRID:IMSR_JAX:017320 X RRID:IMSR_JAX:007909; 69.5, 67-71 days old; n = 14), and GABRR3-cre (Tg(Gabrr3-cre)KC112Gsat, RRID:MMRRC_030709-UCD; 169, 68-293 days old; n = 7) mice were used. Mice were bred in-house and housed under a 14h/10h (*in vivo* experiments) or 12h/12h (*ex vivo* experiments) light/dark cycle, with food and water *ad libitum*. Mice received regular veterinary inspection and underwent only those procedures detailed here and tail-clipping for the purpose of genotyping. Experiments were performed during the light cycle.

2.3: 6-OHDA/vehicle and adeno-associated virus (AAV) vector injection

6-OHDA/vehicle and AAVs were injected using a stereotaxic instrument (Neurostar, Tübingen, Germany; David Kopf Instruments, Tujunga, CA, USA). Anesthesia was induced with vaporized 3-4 % isoflurane (Smiths Medical ASD, Inc., Dublin, OH, USA; Tem-Sega, Inc., Pessac, France) before injection of ketamine/xylazine (75/10 or 87/13 mg/kg, respectively, IP). Within 2-5 minutes, desipramine (25 mg/kg, IP) and pargyline (50 mg/kg, IP) were injected to enhance the selectivity and toxicity of intracerebral 6-OHDA injections, respectively. After placing the mouse in the stereotaxic instrument, anesthesia was maintained with 1-2 % isoflurane. 1-2 µl of 6-OHDA (3-5 mg/ml) in HEPES buffered saline (HBS; in mM: 140 NaCl, 23 glucose, 15

HEPES, 3 KCl, 1.5 MgCl₂, 1.6 CaCl₂; pH 7.2 with NaOH; 300–310 mOsm/L) plus 0.02 % ascorbate or vehicle (HBS plus 0.02 % ascorbate) was then injected into the MFB (from Bregma: AP, -0.7 mm; ML, 1.2 mm; DV, 4.7 mm) over a 10 minute period. The injectate was then allowed to diffuse for a further 10 minutes prior to retraction of the syringe. For D2-SPN, GPe, or STN neuron identification/silencing experiments in which A2A-cre, PV-cre, or GABRR3-cre transgenic mice were used, AAV expressing AAV9.CBA.Flex.Arch-GFP.WPRE.SV40 (Addgene viral prep #22222-AAV9, RRID: Addgene_22222; Chow et al., 2010) was injected into each target structure (striatum: 4 x 300 nl; AP, 0.4 mm and 0.9 mm; ML, 2.2 mm; DV, 3.7 mm and 2.7 mm; GPe: 2 x 300 nl; AP, -0.27 mm; ML, 2 mm; DV, 3.95 mm and 3.45 mm; STN: 500 nl; AP, -2.0 mm; ML, 1.6 mm; DV, 4.65 mm). Each AAV injection took place over 5 minutes, followed by a further 5-minute period prior to syringe retraction.

2.4: *In vivo* electrophysiological recording

Two-Three weeks (18.5, 15-21 days) following surgery, mice were briefly anesthetized with 3-4 % isoflurane in order to inject urethane (1.25 g/kg, IP). Mice were then allowed to rest in their homecage for 1 hour and then injected with ketamine/xylazine (16/0.8 mg/kg, respectively, IP) every 10-20 minutes until the toe-pinch withdrawal reflex was abolished. Mice were then placed into a stereotaxic instrument (David Kopf Instruments) for the duration of the recording session and ketamine/xylazine supplements were administered as needed to maintain anesthesia. Craniotomies were drilled over the ipsilateral motor cortex (AP, 1.4 mm; ML, 1.5 mm) and two recording sites among the striatum (AP, 0.5 mm; ML, 2.5 mm), GPe (AP, -0.3 mm; ML, 2.0 mm), and STN (AP, -1.7 mm; ML, 1.6 mm) depending on the experiment. A peridural screw “electrode” (MS-51960-1; McMaster-Carr, Chicago, IL, USA) was implanted over primary

motor cortex from which the EEG was recorded. Extracellular single unit recordings and LFPs were acquired using silicon tetrode arrays (A1x4-tet-10mm-100-121-A16; NeuroNexus Technologies, Ann Arbor, MI, USA) connected to a 64-channel Digital Lynx (Neuralynx, Bozeman, MT, USA) data acquisition system with a unity gain headstage, at a sampling frequency of 40 kHz, a gain of 14 X, with reference wire implanted opposed to the ipsilateral temporal musculature. Online digital finite impulse response filters were applied. Single unit activity was band pass filtered between 200-9000 Hz and LFP and EEG signals were band pass filtered between 0.1-400 Hz. Optogenetic stimulation was delivered using a custom 577 nm laser system (Genesis MX STM 577-500 OPSL CW; Coherent Inc., Santa Clara, CA, USA) that was fiber coupled to an optrode with an identical array of tetrodes (A1x4-tet-10mm-100-121-OA16; NeuroNexus Technologies). Silicon probes were dipped in a lipophilic fluorescent dye (DiI; 20 mg/ml in 50 % acetone/methanol; D282; ThermoFisher Scientific, Waltham, MA, USA) prior to initial penetration to identify sites of recording in histological sections.

Unit activity, LFP, and EEG were simultaneously recorded for several minutes during cortical SWA. This was followed by at least two periods of optogenetic stimulation of Arch-GFP (< 6 mW) for 5 seconds, with each stimulation period being separated by at least three minutes. Laser power was measured at the optrode tip prior to probe implantation and verified at the conclusion of each experiment. Cortical ACT was evoked by tail pinch using a custom pneumatic device. After cortical SWA had stabilized following ACT, another tail pinch was applied. This sequence was repeated until at least three trials had been recorded or units were lost.

2.5: Histological processing of *in vivo* tissue

Following recording, mice were given a lethal dose of anesthetic and transcardially perfused with saline for 2 minutes followed by 4 % w/v paraformaldehyde in 0.1 M PB, pH 7.4 for approximately 20 minutes. The brain was then removed, held in the same fixative overnight, and then washed in 0.01 M phosphate-buffered saline, pH 7.4 (PBS; P3813; Millipore Sigma, Darmstadt, Germany) before being sectioned in the coronal plane at 70 μm using a vibratome (VT1000S; Leica Microsystems Inc., Richmond, Illinois, USA). Sections were then washed 3 times in PBS before incubation for 48-72 hr at 4 $^{\circ}\text{C}$ in a mixture of PBS, 0.5 % Triton X-100 (T8787; Millipore Sigma; PBS-T), and 2 % normal donkey serum (017-000-121; Jackson ImmunoResearch, West Grove, PA, USA) containing primary antibodies (see below). Sections were then washed in PBS before incubation for 90 minutes at room temperature (RT) in PBS-T containing secondary antibodies (see below). Lastly, sections were washed in PBS and mounted on slides with Prolong Gold Antifade Reagent (P36930; ThermoFisher Scientific, Waltham, MA, USA). Mountant was allowed to cure for at least 24 hours prior to storage at 4 $^{\circ}\text{C}$ or imaging. GFP, DiI, and immunofluorescent labeling were imaged using a Zeiss Axioskop 2 microscope (Zeiss, Oberkochen, Germany), an AxioCam CCD camera (426508-9901-000; Zeiss), and NeuroLucida software (MFB Bioscience, Williston, VT, USA). Representative images were acquired using confocal laser scanning microscopy (A1R; Nikon, Melville, USA).

A 1:6 series of the striatum and SN was processed for the immunohistochemical detection of tyrosine hydroxylase (TH; 1:500 mouse anti-TH; MAB318, RRID:AB_2201528, Millipore Sigma, Charalampopoulos et al., 2005; Peng et al., 2005; 1:250 Alexa Fluor 488 donkey anti-mouse IgG; 715-545-152, RRID: AB_2313584, Jackson ImmunoResearch) and expression was

quantified, as described previously (Fan et al., 2012). Immunoreactivity was averaged across three evenly spaced rostral, middle, and caudal sections. Cortical immunoreactivity was then subtracted from striatal immunoreactivity to normalize for background fluorescence. Dopamine depletion was assessed from the immunoreactivity in the vehicle or 6-OHDA-injected hemisphere, expressed as a percentage of immunoreactivity in the contralateral hemisphere (Table 2.1.1). For PV-cre mice, in which PV GPe neurons expressed Arch-GFP, adjacent sections of the GPe were processed for the immunohistochemical detection of PV (1:200 rabbit anti-PV; 195 002, RRID:AB_2156474, Basco et al., 2011; or 1:200 guinea pig anti-PV; 195 004, RRID:AB_2156476, Kotzadimitriou et al., 2018; 1:250 Alexa Fluor 594 donkey anti-rabbit IgG; 711-585-152, RRID:AB_2340621; or 1:250 Alexa Fluor 594 donkey anti-guinea pig IgG; 706-585-148, RRID:AB_2340474; Jackson ImmunoResearch) or FoxP2 (1:500 rabbit anti-FoxP2; MFCD06411813, RRID:AB_1078909, Millipore Sigma, Hernandez et al., 2015; 1:250 Alexa Fluor 594 donkey anti-rabbit IgG; 711-585-152, RRID:AB_2340621, Jackson ImmunoResearch). Sections of the STN from PV-cre and GABRR3-cre mice, the GPe from GABRR3-cre and A2A-cre mice, and the striatum from A2A-cre mice were processed for the immunohistochemical detection of the neuronal markers NeuN (1:200 mouse anti-NeuN; MAB377, RRID:AB_2298772, Millipore Sigma, Aranha et al., 2010; or 1:1,000 rabbit anti-NeuN; AB177487, RRID:AB_2532109, Abcam, Xu et al., 2018; 1:250 Alexa Fluor 594 donkey anti-mouse IgG; 715-585-150; or 1:250 Alexa Fluor 594 donkey anti-rabbit IgG; 711-585-152, Jackson ImmunoResearch) or HuC/D (1:66 mouse anti-HuC/D; A-21271, RRID:AB_221448, ThermoFisher Scientific, Nogueira et al., 2017; 1:250 Alexa Fluor 594 donkey anti-mouse; 715-585-150, Jackson ImmunoResearch) to aid reconstruction of electrode tracks and sites of recording.

Stereological counts of Arch-GFP-, PV-, and FoxP2-expressing GPe cells were determined using the optical dissector method (West et al., 1991) on a 1:4 series of sections. Structures were traced with a 10 X objective (420943-9900-000; Zeiss, Oberkochen, Germany) and imaged using a 40 X oil- (000000-1022-818; Zeiss, Oberkochen, Germany) or 60 X water-immersion (UplanApo 60X/1.2 NA; Olympus, Tokyo, Japan) objectives. Counting frames of 100 x 100 or 90 x 90 μm , and grid sizes of 300 x 300 or 200 x 200 μm , respectively were used. Images were taken at 1 μm intervals for 5 μm beneath a 1 μm guard zone (NeuroLucida system, MFB Bioscience, Williston, VT, USA).

2.6: *In vivo* Electrophysiological Analysis

Due to the impaired movement of 6-OHDA-dopamine-depleted mice, experimenters were not blinded to the experimental group of the mice that they were recording from. Putative single unit activity was discriminated with Plexon Offline Sorter software (Version 3; Plexon. Inc., Dallas, TX; RRID:SCR_000012) using a combination of template matching, principal component analysis, and manual clustering. Spike times were aligned to the peak of the extracellularly recorded action potential and a dead time of 500 μs was utilized during discrimination of units (Maccione et al., 2009; Adamos et al., 2010; Lu et al., 2016). Given that action potential widths varied between ~ 1.0 and 1.5 ms and assuming an absolute refractory period of ~ 1.0 ms, the minimum interspike interval (ISI) of a single neuron's spike train should be ~ 2 ms. A threshold of $< 1\%$ of ISIs < 2 ms was therefore utilized for the designation of putative single units in this study (Mallet et al., 2008a; Mallet et al., 2008b; Sharott et al., 2017). Of the 551 putative single unit spike trains reported here, the percentage of ISIs with durations < 2 ms was 0.0457, 0-0.227%, suggesting that there was minimal contamination by stray units.

All data were visually inspected in Neuroexplorer 4 (Nex Technologies, Colorado Springs, CO; RRID:SCR_001818) and exported to MATLAB 2017b (MathWorks, Natick, MA; RRID:SCR_001622) for analysis. Epochs with consistent, robust cortical SWA or ACT were selected for analysis. During cortical SWA, 30 second epochs were used to assess baseline neuronal activity. During cortical SWA, the impact of optogenetic inhibition was assessed by comparing neuronal activity 5 seconds prior to Arch-GFP stimulation with neuronal activity during 5 seconds of Arch-GFP stimulation. Neurons that were responsive to Arch-GFP stimulation are reported. In areas that received direct optogenetic stimulation of Arch-GFP, neurons were considered to be responsive if their firing rate was rapidly, consistently, and persistently suppressed by at least 2 SD. Although polysynaptic mechanisms cannot be completely excluded, these effects are consistent with direct optogenetic inhibition as the primary cause of firing rate reduction.

In most cases, the activity of downstream/postsynaptic neurons increased when the upstream/presynaptic nucleus was GABAergic (i.e., striatum or GPe) and decreased when the upstream/presynaptic nucleus was glutamatergic (i.e., STN). In a small number of neurons, the opposite response was observed or more subtle changes in firing pattern occurred without a change in firing rate. Therefore, downstream/postsynaptic neurons were deemed to be responsive to optogenetic inhibition of the upstream/presynaptic nucleus if their firing rate or regularity changed by greater than 2 SD during inhibition of the upstream/presynaptic nucleus. Although polysynaptic mechanisms cannot be completely excluded, the typical effects on downstream/postsynaptic activity are consistent with optogenetic inhibition of the presynaptic nucleus as the primary cause.

During cortical ACT, five seconds of neuronal activity prior to and during tail pinch were compared. “Putative PV” GPe neurons were “isolated” from unidentified populations of GPe neurons in A2A-cre and GABRR3-cre mice by restricting analysis of unidentified GPe neurons to those with an in-:antiphase ratio within the interquartile range of optogenetically identified PV GPe neurons in PV-cre mice. Mean firing rates were calculated from the number of spikes divided by epoch length. The coefficient of variation of the interspike interval (CV) was used as a metric of regularity.

To examine the relationship between cortical SWA and neuronal firing, phase histograms were generated in MATLAB: 1) cortical SWA was extracted from the raw EEG signal by applying a bandpass 0.5-1.5 Hz 2nd order Butterworth filter in the forward and reverse directions to avoid phase shifts; 2) the EEG was downsampled to 1 kHz using the MATLAB function “resample”; 3) the instantaneous phase of the EEG was calculated from the Hilbert transform (Le Van Quyen et al., 2001); 4) the empirical cumulative distribution function (MATLAB) was applied to correct for the non-sinusoidal nature of slow cortical oscillations, (Siapas et al., 2005; Mallet et al., 2008b; Abdi et al., 2015) 5) each spike was assigned to a phase of the EEG from 0-360° (0°/360° and 180° corresponding to the peak-active and -inactive components of the EEG, respectively). Each neuron’s spike probability was calculated from (spikes/bin)/(total # of spikes) X 100. Data were binned at 10° in figures, and at 180° for statistical comparisons. Population phase histograms are plotted as median and interquartile range.

The multitaper Fourier transform function (Bokil et al., 2010; McConnell et al., 2012; Brazhnik et al., 2016) was applied using MATLAB to assess spectral power within the 1 kHz

downsampled EEG, GPe and STN LFP (chronux.org; NW = 3, K = 5). 5 s epochs during cortical SWA or ACT were examined to determine total power in the 0.5-1.5 Hz, 10-39.9 Hz, and 40-250 Hz frequency bands respectively. The power within each band of interest was then normalized to the total power from 0-250 Hz to control for variability in signal amplitude between recordings.

2.7: *Ex vivo* electrophysiological recording

Acute brain slices were prepared from PV-cre X Ai9 mice as previously described (Chazalon et al., 2018). Briefly, mice were anesthetized with ketamine/xylazine (100/20 mg/kg, respectively) and perfused transcardially with ice-cold modified artificial cerebrospinal fluid (ACSF), equilibrated with 95% O₂ and 5% CO₂, and containing (in mM): 230 sucrose, 26 NaHCO₃, 2.5 KCl, 1.25 NaH₂PO₄, 0.5 CaCl₂, 10 MgSO₄, and 10 glucose. Brains were rapidly removed and sectioned into 300 µm-thick parasagittal slices with a vibrating blade microtome (VT1200S; Leica Microsystems, Germany). Slices containing the GPe were then left to equilibrate for 1 h (at 35°C) in ACSF of the following composition (in mM): 126 NaCl, 26 NaHCO₃, 2.5 KCl, 1.25 NaH₂PO₄, 2 CaCl₂, 2 MgSO₄, 10 glucose, 1 sodium pyruvate and 4.9 reduced L-glutathione (equilibrated with 95% O₂ and 5% CO₂). Individual brain slices were placed in a recording chamber where they were perfused at 4-5 ml/min with synthetic interstitial fluid (SIF) at 35 °C containing (in mM): 126 NaCl, 3 KCl, 1.25 NaH₂PO₄, 1.6 CaCl₂, 1.5 MgSO₄, 10 glucose and 26 NaHCO₃ (equilibrated with 95 % O₂ and 5 % CO₂). Somatic patch-clamp recordings were obtained under visual guidance (E600FN Eclipse workstation, Nikon, Japan; Nikon Fluor 60 X/1.0 NA) using motorized manipulators (Patchman NP2, Eppendorf, France). PV GPe neurons were identified by visualization of tdTomato under epifluorescence. Autonomous PV GPe

neuron activity was recorded in the presence of the GABA_A receptor (GABA_Azine, 20 μ M), GABA_B receptor (CGP 55845, 1 μ M), AMPA/Kainate receptor (DNQX, 20 μ M), and NMDA receptor (D-APV, 50 μ M) antagonists in the loose-seal configuration of the patch clamp technique in current clamp mode using borosilicate glass pipettes (4-6 M Ω) containing (in mM): 140 NaCl, 23 glucose, 15 HEPES, 3 KCl, 1.5 MgCl₂, 1.6 CaCl₂. pH and osmolarity were adjusted to 7.2 with 1 M NaOH and to 300-310 mOsm, respectively. Electrophysiological recordings were acquired using a computer running Clampex 9.2 software (Molecular Devices, Palo Alto, CA, USA) connected to a Multiclamp 700B amplifier (Molecular Devices) via a Digidata 1320A digitizer (Molecular Devices). Data were low-pass filtered at 4 kHz and sampled at 20 kHz.

2.8: Histological processing for *ex vivo* experiments

PV-cre X Ai9 mice were euthanized with 20 % urethane and transcardially perfused with PBS, followed by 4 % w/v paraformaldehyde in 0.1 M PB, pH 7.4. The brain was then removed and incubated overnight in the same fixative at 4°C, then immersed in PBS containing 20 % w/v sucrose for 24h at 4°C, and stored in this solution at -80°C before being sectioned in the coronal plane at 50 μ m on a cryostat (CM3000; Leica Microsystems Inc.). Sections were then washed in PBS and those containing ‘rostral’, ‘central’, and ‘caudal’ GPe (corresponding approximately to AP -0.2 mm, -0.45 mm, and -0.7 mm from Bregma, respectively (Paxinos and Franklin, 2001) were selected for immunohistochemical detection of GPe markers. Sections were incubated overnight at RT in a mixture of 3 primary antibodies diluted in PBS-T (1:100 goat anti-FoxP2; sc-21069, RRID:AB_2107124, Santa Cruz, Fu et al., 2014; 1:1,000 guinea pig anti-parvalbumin; 195 004, RRID:AB_2156476 , Synaptic Systems, Abbas et al., 2018; 1:1,000 rat anti-red

fluorescent protein 5f8, RRID:AB_2336064, Chromotek). Sections were then washed and incubated for 1 hour at RT in PBS-T containing a mixture of secondary antibodies (1:500 Alexa Fluor 488 donkey anti guinea-pig IgG; A11073, RRID:AB_2534117, Life Technologies; 1:500 Alexa Fluor 647 donkey anti-goat IgG; A21447, RRID:AB_2535864, Life Technologies; 1:500 DyLight 594 donkey anti-rat IgG; NBP1-75661, RRID:AB_11055284, Novus). Finally, sections were washed in PBS, mounted in Vectashield (Vector Laboratories), and imaged on a confocal fluorescence microscope (TCS SP8, Leica Microsystems Inc.). Images were acquired using a 20 X 1.0 NA objective lens in 1.0 μm steps between 2 μm and 17 μm from the upper surface of each section. Colocalization was assessed from maximal z-projection images using the cell counter plug-in of ImageJ.

Sections containing the striatum were processed for the immunohistochemical detection of TH. Sections were first incubated in primary antibody (1:10,000 monoclonal anti-TH; MAB318, RRID:AB_2201528, Millipore Bioscience Research Reagents) in PBS-T overnight at RT. Subsequently, the sections were incubated in a secondary antibody in PBS-T (1:1000 biotinylated horse anti-mouse IgG; BA-2000, RRID:AB_2313581, Vector Laboratories) for 90 min at RT. Finally, sections were incubated in avidin-biotin peroxidase complex (1:500; PK-4002, RRID:AB_2336811, Vector Laboratories) for 60 min at RT and immunoreactivity was revealed using AMEC (SK-4285, RRID:AB_2336519, Vector Laboratories). Sections were then rinsed, mounted on gelatin-coated slides, and coverslipped in VectaMount (Vector Laboratories). At least three sections from each hemisphere containing the striatum were scanned in an Epson expression 10000XL high-resolution scanner. Mean optical density was measured in the top half of the striatum (Mercator; Explora Nova, La Rochelle, France) and values were corrected for

background staining as above. TH immunoreactivity ipsilateral to vehicle or 6-OHDA injection was expressed as a percentage of immunoreactivity in the contralateral hemisphere, as described above (Table 2.1.1).

2.8: Statistical analysis

Statistics were performed using Prism 6 (GraphPad Software, Inc., La Jolla, CA, USA; RRID:SCR_002798) or R (<https://www.r-project.org/>; exactRankTests package; RRID:SCR_001905). Population data are expressed as median and interquartile range and illustrated using box plots (central line: median; box: 25 % - 75 %; whiskers: 10 % - 90 %); outliers were not excluded from analysis. Paired data are illustrated using line plots. It should be noted that some data were excluded from paired analyses that were included in unpaired analyses (e.g. when CV could not be calculated due to an absence of firing); these data are represented in box plots overlying paired line plots. Because no assumptions were made concerning the distribution of population data, non-parametric statistics were used throughout. Paired and unpaired data were compared using the non-parametric Mann-Whitney U (MWU) and Wilcoxon Signed Rank (WSR) tests, respectively, and Fisher's exact test was used for contingency analyses. When applicable, the Holm-Bonferroni correction for multiple comparisons (Holm, 1997) was applied (adjusted p-values are indicated as $p_{h\#}$, where # is the adjustment factor). P values < 0.05 were considered significant. To ensure the proposed research was adequately powered, sample sizes were estimated using the formulae described by Noether (Noether, 1987) assuming 80% power (i.e. the probability of a Type 2 error of 20%) and a two-tailed level of 0.05. For unpaired data (groups X and Y), and probabilities of $X > Y$ (or $X < Y$) being 0.7, 0.8, and 0.9, the estimated sample sizes for each group are 33, 15, and 9, respectively. For paired data

(where X_i and X_j are independent samples from X , reflecting effect size and sign) and the probabilities of $X_i + X_j > 0$ being 0.7, 0.8, and 0.9, the estimated sample sizes are 66, 30, and 17, respectively. Probabilities between 0.7 and 0.9 are representative of our historical, pilot, and actual data. Thus, for all core findings our study was at 80% power to detect probabilities of $X > Y$ (or $X < Y$) and $X_i + X_j > 0$ (for unpaired and paired tests, respectively) between approximately 0.7 and 0.9.

Chapter 3: Results

3.1: During cortical SWA the frequency of D2-SPN activity is greater in 6-OHDA-injected mice

Dopamine negatively modulates both cortico-striatal transmission (Bamford et al., 2004; Higley and Sabatini, 2010) and the intrinsic excitability of D2-SPNs (Gerfen and Surmeier, 2011; Planert et al., 2013). Therefore, we predicted that following the loss of dopamine, cortical SWA-associated D2-SPN activity would be elevated despite the similarity of cortical SWA in vehicle- and 6-OHDA-injected mice (Tables 2.1.2 and 2.1.3). The specificity of Arch-GFP expression in D2-SPNs in A2A-cre mice was confirmed by its presence in the subset of SPNs that project to the GPe (Fig. 3.1.1A-C) but not to the SNr (Fig. 3.1.1D). In regions expressing Arch-GFP, approximately one half of striatal neurons were directly inhibited by activation of Arch-GFP and therefore identified as D2-SPNs (Fig. 3.1.1E and F; vehicle: 55 %, n = 62 of 112; 6-OHDA: 54 %, n = 34 of 63; $p = 1.0000$; Fisher's Exact). Of the neurons that were excluded due to the absence of direct inhibition, 2 % (n = 1 of 50) in vehicle- and 8 % (n = 3 of 28) in 6-OHDA-treated mice were disinhibited during optogenetic stimulation. In both vehicle- and 6-OHDA-injected mice, D2-SPN activity was highly phasic and entrained to the active (positive) component of cortical SWA in the EEG in dopamine-intact and -depleted mice, consistent with direct driving of D2-SPN activity by cortical inputs (Fig. 3.1.1F). The frequency of D2-SPN activity measured during 30 second epochs of cortical SWA was elevated in 6-OHDA-injected mice relative to vehicle-injected controls (Fig. 3.1.1F and Ga; vehicle: rate = 1.75, 0.91-3.55 Hz; n = 62; 6-OHDA: rate = 3.02, 1.53-4.58 Hz; n = 34; $p = 0.02068$; MWU). The median increase was modest in absolute terms (~ 1.27 Hz) but large in relative terms (~ 72.6%). There was also a

significant but slight increase in the, presumably due to the more intense phasic activity (Fig. 3.1.1*Ga* vehicle: CV = 1.47, 1.19-1.77; n = 62; 6-OHDA: CV = 1.65, 1.25-2.18; n = 34; p = 0.04235; MWU), equivalent to a 12% increase in median. The relationship between cortical SWA and D2-SPN firing was further examined through the generation of phase histograms. Firing in phase with cortical SWA was designated as activity within a 180° window centered on 0/360°. Antiphase firing was designated as activity within a 180° window centered on 180°. The ratio of in-:antiphase spike probability in D2-SPNs was not altered by dopamine depletion (Fig. 3.1.1*Ga* and *Gb*; vehicle = 9.81, 3.60-14.4; n = 48; 6-OHDA = 3.91, 2.51-17.0; n = 27; p = 0.4671; MWU). Together these data demonstrate that following the loss of dopamine, the firing rate of D2-SPNs increased but the phase relationship of D2-SPN activity to cortical SWA was not altered. These data in mice are consistent with the activity of putative and identified striatopallidal neuron activity in dopamine intact and -depleted rats during cortical SWA (Mallet et al., 2006; Walters et al., 2007; Zold et al., 2012; Escande et al., 2016; Sharott et al., 2017).

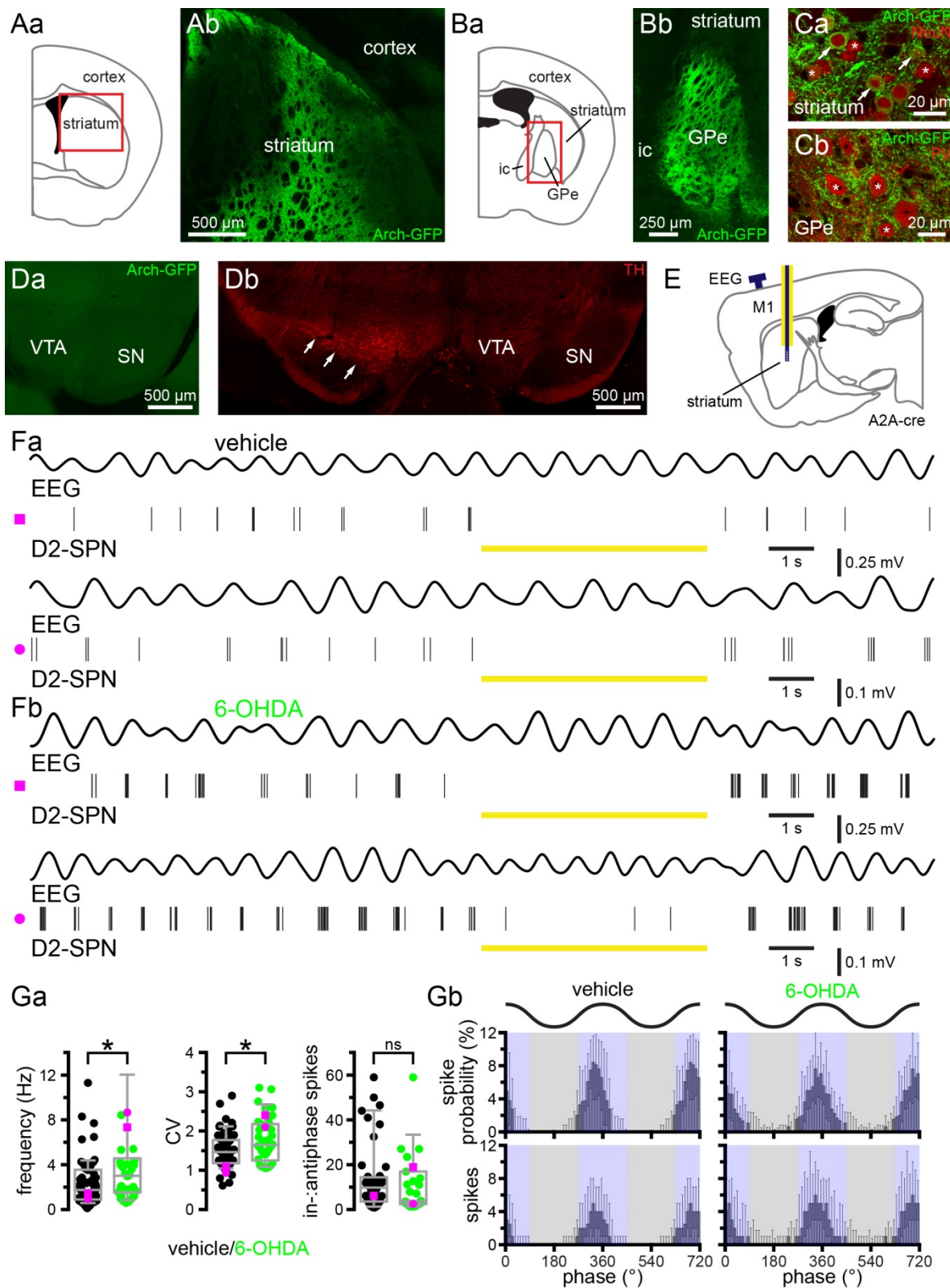


Figure 3.1.1 During cortical SWA the frequency of D2-SPN activity is greater in 6-OHDA-injected mice

A-D, immunohistochemistry was used to verify cre-dependent viral expression of Arch-GFP in D2-SPNs in vehicle- and 6-OHDA-injected A2A-cre mice. *Aa* and *Ba*, schematic representations of areas imaged in *Ab* and *Bb* (red box denotes the imaged subregion; ic, internal capsule). *Ab*, *Bb*, and *C*, expression of Arch-GFP (green) in D2-SPNs in the striatum (*Ab* and *Ca*) and their axon terminals in the GPe (*Bb* and *Cb*). *Ca* and *Cb*, expression of NeuN (red) in the somata of striatal (*Ca*) and GPe (*Cb*) neurons. NeuN-immunoreactive neurons that express or do not express Arch-GFP are denoted by arrows and asterisks, respectively. *Da* and *Db*, absence of Arch-GFP expressing axon terminals (*Da*) and TH-immunoreactive neurons (*Db*) ipsilateral to injections of AAV in the striatum and 6-OHDA in the MFB. TH-immunoreactive substantia nigra (SN) and ventral tegmental area (VTA) neurons (red; arrows) are visible contralateral to the injection of 6-OHDA (*Db*). *E-G*, optogenetically identified D2-SPN firing rate was elevated in 6-OHDA-injected mice relative to vehicle-injected mice. *E*, schematic representation of EEG electrode and optrode placement (dark blue line indicates electrode; yellow line denotes affixed optical fiber; M1, primary motor cortex). *Fa* and *Fb*, representative EEG (upper trace; filtered at 0.5-1.5 Hz) and D2-SPN unit activity (below) from vehicle- (*Fa*) and 6-OHDA-injected (*Fb*) mice. D2-SPNs were identified by their inhibited activity during optogenetic stimulation of Arch-GFP (yellow bar). *G*, the frequency and to a lesser extent the CV of D2-SPN activity were significantly greater in 6-OHDA- versus vehicle-injected mice. However, D2-SPN activity was similarly entrained to the active component of cortical SWA. *Ga*, population box plots, D2-SPN firing rate (left), CV (middle), and in-:antiphase spikes (right); representative examples plotted with magenta symbols; five individual outlier data points were not plotted for legibility (outliers;

6-OHDA frequency: 15.5, 15.4, 30.3 Hz; vehicle in-:antiphase spikes: 193; 6-OHDA in-:antiphase spikes: 91.0). *Gb*, population linear phase histograms illustrate the phase relationship between D2-SPN neuron firing and cortical SWA in vehicle- and 6-OHDA-injected mice. Active (blue) and inactive (gray) components of SWA are denoted. *, $p < 0.05$. ns, not significant.

3.2: In dopamine-depleted mice PV GPe neuron activity is relatively antiphase to cortical SWA

Given the elevation of D2-SPN activity in dopamine-depleted mice and loss of presynaptic D2R-mediated inhibition of striatopallidal GABA release (Migueluez et al., 2012; Lemos et al., 2016), we predicted that D2-SPNs would more effectively pattern postsynaptic prototypic GPe neuron activity in the absence of dopamine. Because D2-SPNs exhibit increased firing in phase with cortical SWA in dopamine-depleted mice, we predicted that the firing of postsynaptic prototypic GPe neurons would be relatively antiphase to cortical SWA. To identify prototypic GPe neurons, the majority of which express PV (Mastro et al., 2014; Abdi et al., 2015; Dodson et al., 2015; Hernandez et al., 2015), Arch-GFP was virally expressed in PV-cre mice (Fig. 3.2.1A-C). Immunohistochemistry confirmed that the majority of Arch-GFP-expressing neurons co-expressed PV (Fig. 3.2.1A; 83, 73-93 %; n = 2 mice). Consistent with their prototypic identity, Arch-GFP was also strongly expressed by axon terminals in the STN (Fig. 3.2.1B). Incomplete immunohistochemical detection of PV was presumably the reason for the absence of PV immunoreactivity in 17 % of Arch-GFP expressing GPe neurons. In contrast, arkypallidal neurons, identified by their immunoreactivity for FoxP2 (Abdi et al., 2015; Dodson et al., 2015; Hernandez et al., 2015), did not co-express Arch-GFP (Fig. 3.2.1Ad; 0, 0-0 %; n = 2 mice). Together these data confirm the selective expression of Arch-GFP in PV GPe neurons and the absence of Arch-GFP expression in arkypallidal FoxP2 GPe neurons. Consistent with the relative abundance of PV GPe neurons, the majority of GPe neurons that were recorded were inhibited by optogenetic activation of Arch-GFP (Fig. 3.2.1C and D; vehicle: 82 %, n = 27 of 33; 6-OHDA: 84 %, n = 27 of 32; p = 1.0000; Fisher's Exact). However, given that recordings were initiated from tetrode locations where at least one GPe neuron was inhibited during optogenetic

activation of Arch-GFP, recordings were likely to be biased toward prototypic neurons. Of those GPe neurons that were not directly inhibited by stimulation, 83 % (n = 5 of 6) in vehicle and 40 % (n = 2 of 5) in 6-OHDA-treated mice were disinhibited, presumably due to inhibition of presynaptic PV GPe neurons.

As for D2-SPNs, PV GPe neuron firing was first recorded during 30 second epochs of robust cortical SWA. In control mice, PV GPe neurons discharged in a tonic, irregular firing pattern during cortical SWA (Fig. 3.2.1*Da* and *Ea*; vehicle: frequency = 16.8, 9.23-30.1 Hz; n = 27; CV = 0.868, 0.554-1.01; n = 27). In dopamine-depleted mice, the rate of discharge of PV GPe neurons was similar but firing was more irregular relative to control (Fig. 3.2.1*Db* and *Ea*; 6-OHDA: frequency = 15.6, 12.5-25.2 Hz; n = 27; p = 0.9280; MWU; CV = 1.29, 0.824-1.59; n = 27; p = 2.163 x 10⁻³; MWU). Comparison of the in-:antiphase spike probability ratio in vehicle- and 6-OHDA-injected mice, revealed a shift in PV GPe neuron phase preference to firing that was more antiphase to cortical SWA (Fig. 3.2.1*E*; SWA: vehicle = 0.801, 0.664-1.18; n = 27; 6-OHDA = 0.675, 0.418-0.883; n = 27; p = 9.16 x 10⁻³; MWU). These data are consistent with studies in dopamine-depleted rats, which demonstrated that juxtacellularly labeled prototypic GPe neurons, defined on the basis of their descending axon collaterals and in some cases their expression of PV, exhibited firing that was relatively antiphase to cortical SWA (Magill et al., 2001; Mallet et al., 2008b; Mallet et al., 2012; Abdi et al., 2015). Past studies focused on prototypic GPe neuron populations that adhered to specific firing characteristics such as phase locking to cortical SWA for analysis (Magill et al., 2001; Mallet et al., 2008b; Mallet et al., 2012; Abdi et al., 2015). Here, we included all optogenetically identified PV GPe neurons and

report more variability in phase preference. Our use of mice versus rats in earlier studies may also contribute to this variability.

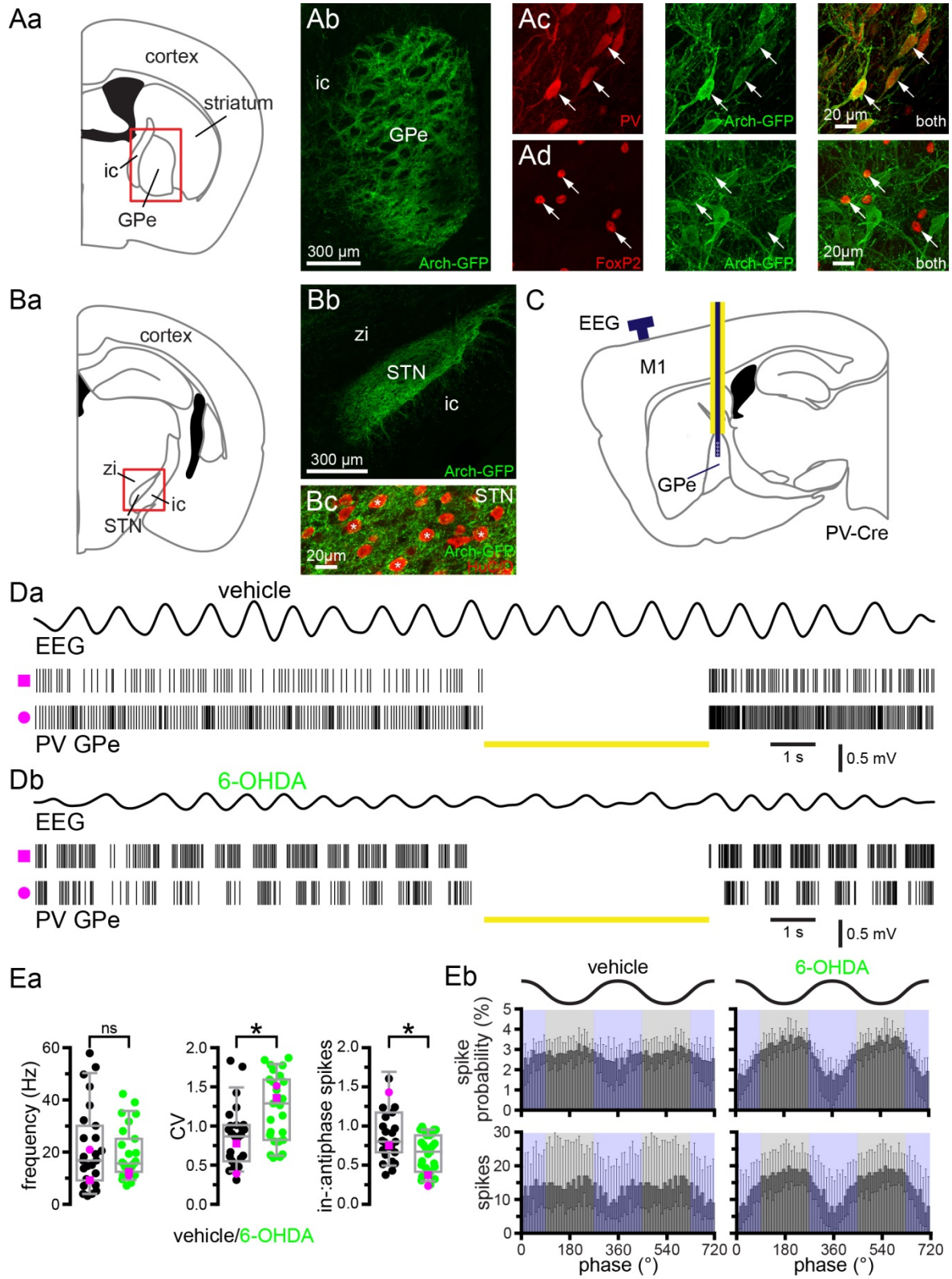


Figure 3.2.1 In 6-OHDA-injected mice PV GPe neuron activity is relatively antiphase to cortical SWA

A and *B*, immunohistochemistry was used to verify the cre-dependent viral expression of Arch-GFP in PV GPe neurons in vehicle- and 6-OHDA-injected PV-cre mice. *Aa* and *Ba*, schematic representations of areas imaged in *Ab* and *Bb* (red box denotes the imaged subregion). *Ab-d*, *Bb*, and *Bc*, expression of Arch-GFP (green) in GPe neurons (*Ab-d*) and their axon terminals in the STN (*Bb*, *Bc*; zi, zona incerta). *Ac*, expression of Arch-GFP in PV-immunoreactive prototypic GPe neurons (red; arrows). *Ad*, absence of Arch-GFP expression in FoxP2-immunoreactive arypallidal GPe neurons (red; arrows). *Bb*, Arch-GFP expression in GPe axon terminals in the STN arising from the injection in *Ab*. *Bc*, Arch-GFP expressing axon terminals in the vicinity of NeuN-immunoreactive STN neurons (red; asterisks). *C*, schematic representation of optrode and EEG electrode placement (dark blue line indicates electrode; yellow line denotes affixed optical fiber). *D*, PV GPe neurons were identified through optogenetic stimulation of Arch-GFP which inhibited their activity (yellow bar). *Da* and *E*, in vehicle-injected dopamine-intact mice PV GPe neuron activity was relatively tonic and not consistently phase-related to cortical SWA. *Db* and *E*, in 6-OHDA-injected, dopamine-depleted mice PV GPe neuron activity was more entrained to the inactive component of cortical SWA. *Ea*, population data, PV GPe neuron firing rate (left), CV (middle), and in-:antiphase spikes (right); example data plotted with magenta symbols; two outlier data points were not plotted for legibility (vehicle in-:antiphase spike probability outliers: 2.05, 6.63). *Eb*, Population linear phase histograms of PV GPe neuron firing relative to cortical SWA in vehicle- and 6-OHDA-injected mice. *, $p < 0.05$. ns, not significant.

3.3: During cortical SWA, D2-SPNs contribute to the antiphase firing of GPe neurons in 6-OHDA-injected mice

To determine whether the relatively antiphase firing of GPe neurons is linked to the increased in-phase activity of D2-SPNs in dopamine-depleted mice, D2-SPNs were optogenetically inhibited for 5 second epochs and the effect on GPe neuron activity was assessed. Use of A2A-cre mice to selectively express Arch-GFP in D2-SPNs precluded optogenetic identification of PV GPe neurons. Although recordings were only initiated where putative disinhibition of GPe neurons was observed during optical stimulation, responsive GPe neurons were relatively rare (46 %, n = 26 of 57), presumably because 1) the zone of optogenetic inhibition versus the size of the striatum was small and 2) the striatopallidal projection is highly topographic in nature (Chang et al., 1981; Wilson and Phelan, 1982; Hedreen and DeLong, 1991; Hazrati and Parent, 1992; Smith et al., 1998), lowering the probability of recording from connected parts of the striatum and GPe. In the majority of responsive GPe neurons D2-SPN inhibition elevated the frequency (Fig. 3.3.1A and Ba; 6-OHDA: 85 %, n = 22 of 26; laser off = 17.9, 11.3-29.4 Hz; laser on = 23.0, 15.9-34.0 Hz; n = 26; $p = 1.013 \times 10^{-6}$; WSR) and regularity (Fig. 3.3.1A and Ba; 6-OHDA: 92 %, n = 23 of 25; laser off CV = 1.10, 0.898-1.27; laser on CV = 0.701, 0.561-0.817; n = 25; $p = 2.98 \times 10^{-7}$; WSR) of their firing. Furthermore, inhibition of D2-SPNs reduced antiphase GPe activity, as indicated by an increase in in-:antiphase spike probability (Fig. 3.3.1Ba and Bb; 6-OHDA: 64 %, n = 16 of 25; laser off = 0.694, 0.567-1.07; laser on = 0.897, 0.791-1.02; n = 25; $p = 0.04826$; WSR).

To more selectively examine the impact of D2-SPN input on PV GPe neurons, putative PV GPe neuron activity was isolated by analyzing neurons with in-:antiphase spike probability ratios

falling within the IQR of identified PV GPe (putative PV GPe) neurons in PV-cre mice. In response to optogenetic inhibition of D2-SPNs, putative PV GPe neurons in A2A-cre mice were uniformly disinhibited, (Fig. 3.3.1Ca; 6-OHDA: 100 %, n = 14 of 14; laser off = 24.3, 16.3-34.2 Hz; laser on = 30, 20.5-40.9 Hz; n = 14; p = 1.221×10^{-4} ; WSR). In addition, their firing decreased in irregularity (Fig. 3.3.1Ca; 6-OHDA: 93 %, n = 13 of 14; laser off CV = 1.24, 0.967-1.37; laser on CV = 0.752, 0.536-0.870; n = 14; p = 2.441×10^{-4} ; WSR) and became less antiphase (Fig. 3.3.1C; 6-OHDA: 93 %, n = 13 of 14; in-:antiphase spike probability: laser off = 0.638, 0.574-0.721; laser on = 0.813, 0.76-102; n = 14; p = 2.441×10^{-4} ; WSR). Thus, optogenetic inhibition of D2-SPNs reduced antiphase discharge and normalized the pattern of unidentified GPe neuron activity in dopamine-depleted mice. These effects were more uniform in the putative PV GPe subset of GPe neurons. Together, these data demonstrate that during cortical SWA, D2-SPN activity contributes to the abnormally antiphase firing of GPe neurons in dopamine-depleted mice.

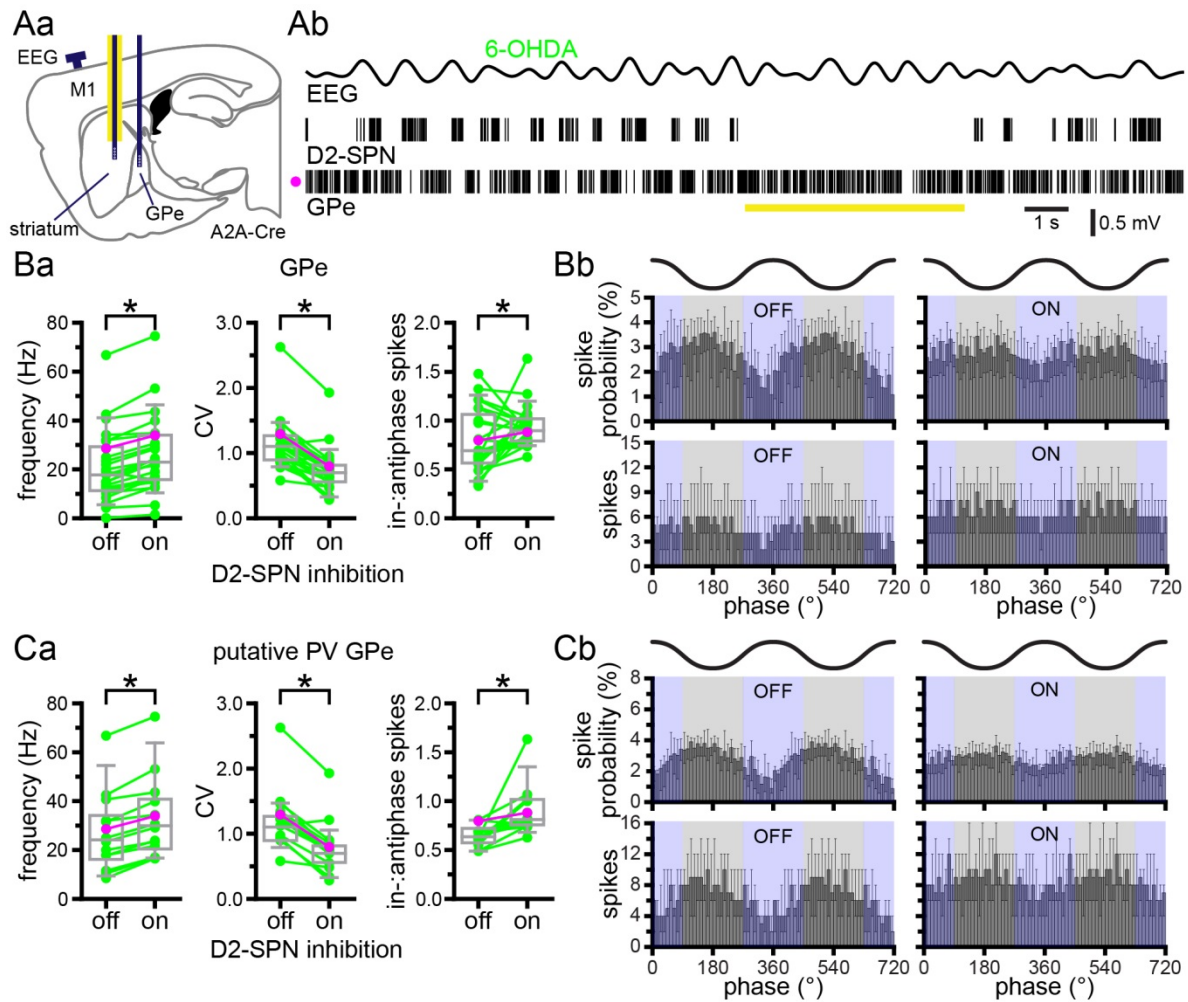


Figure 3.3.1 Optogenetic inhibition of D2-SPNs reduces antiphase GPe activity in 6-OHDA-injected mice

A-C, optogenetic inhibition of D2-SPNs in 6-OHDA-injected A2A-cre mice increased the frequency and decreased the variability (CV) of firing, and increased the in-:antiphase spike probability of unidentified (*B*) and putative PV GPe neurons (*C*). *A*, schematic representation of optrode and electrode placement (*Aa*, dark blue line indicates electrode; yellow line denotes affixed optical fiber) and representative example (*Ab*). *Ba* and *Ca*, population firing rate (left), CV (middle), and in-:antiphase spike probability (right) for unidentified (*Ba*) and putative PV

(*Ca*) GPe neurons; example data plotted in magenta. *Bb* and *Cb*, population linear phase histograms for unidentified (*Bb*) and putative PV (*Cb*) GPe neurons (*C*). *, $p < 0.05$.

3.4: Following loss of dopamine the autonomous firing of PV GPe neurons is significantly elevated

Loss of autonomous activity in GPe neurons has been suggested to contribute to their abnormally phasic activity *in vivo* following dopamine depletion (Chan et al., 2011). However, this work was carried out before the more recent discovery of multiple GPe neuron subtypes. Therefore, the autonomous firing of PV GPe neurons was compared in *ex vivo* brain slices derived from vehicle- and 6-OHDA-injected mice. In order to identify PV GPe neurons for patch clamp recording, tdTomato was conditionally expressed in PV neurons by crossing PV-cre mice with Ai9 reporter mice in which a loxP-flanked STOP cassette prevents transcription of downstream tdTomato. Selective expression of tdTomato in PV GPe neurons was first confirmed using immunohistochemistry for PV (Fig. 3.4.1A and B). Of neurons expressing tdTomato, PV, or both markers: 1) 73, 66-78 % co-expressed tdTomato and PV (n = 3 mice) 2) 9, 4-14 % expressed tdtomato but were not immunoreactive for PV (n = 3 mice), most likely due to less than 100% efficiency of immunodetection 3) 18, 18-20 % (n = 3 mice) of neurons did not express tdTomato but were PV-immunoreactive, presumably due to < 100 % efficiency of cre-mediated excision of the loxP-flanked STOP cassette. Less than 1 % of tdTomato expressing GPe neurons co-expressed the arkypallidal neuron marker FoxP2, consistent with previous reports (Abdi et al., 2015; Hernandez et al., 2015; data not shown). Together, these data suggest that tdTomato expression in this mouse line is a reliable marker of prototypic, PV GPe neurons. Cell-attached, current clamp recordings of GPe tdTomato-expressing neurons in *ex vivo* brain slices were conducted in the presence of AMPA, NMDA, GABA_A, and GABA_B receptor antagonists in order to measure their autonomous activity. As described previously, PV GPe neurons discharged regularly and at high frequency in brain slices derived from dopamine-intact mice

(Fig. 3.4.1C and D; vehicle: frequency = 35.1, 26.8-44.0 Hz; CV = 0.13, 0.10-0.23; n = 89) (Mastro et al., 2014; Abdi et al., 2015; Dodson et al., 2015; Hernandez et al., 2015). The autonomous firing of PV GPe neurons in slices from 6-OHDA-injected mice was not only retained but significantly elevated compared to firing of PV GPe neurons in vehicle-injected mice (Fig. 3.4.1C and D; 6-OHDA: frequency = 41.7, 34.0-50.2 Hz; CV = 0.12, 0.08-0.20; n = 98; frequency, $p = 5.35 \times 10^{-4}$; CV, $p = 0.1336$; WSR). Together these data suggest that the abnormally phasic pattern of PV GPe neuron firing in dopamine-depleted mice *in vivo* is not caused by loss of autonomous firing. In fact, autonomous firing was significantly up-regulated following the loss of dopamine, presumably through engagement of homeostatic compensatory mechanisms that were triggered by elevated striatopallidal transmission.

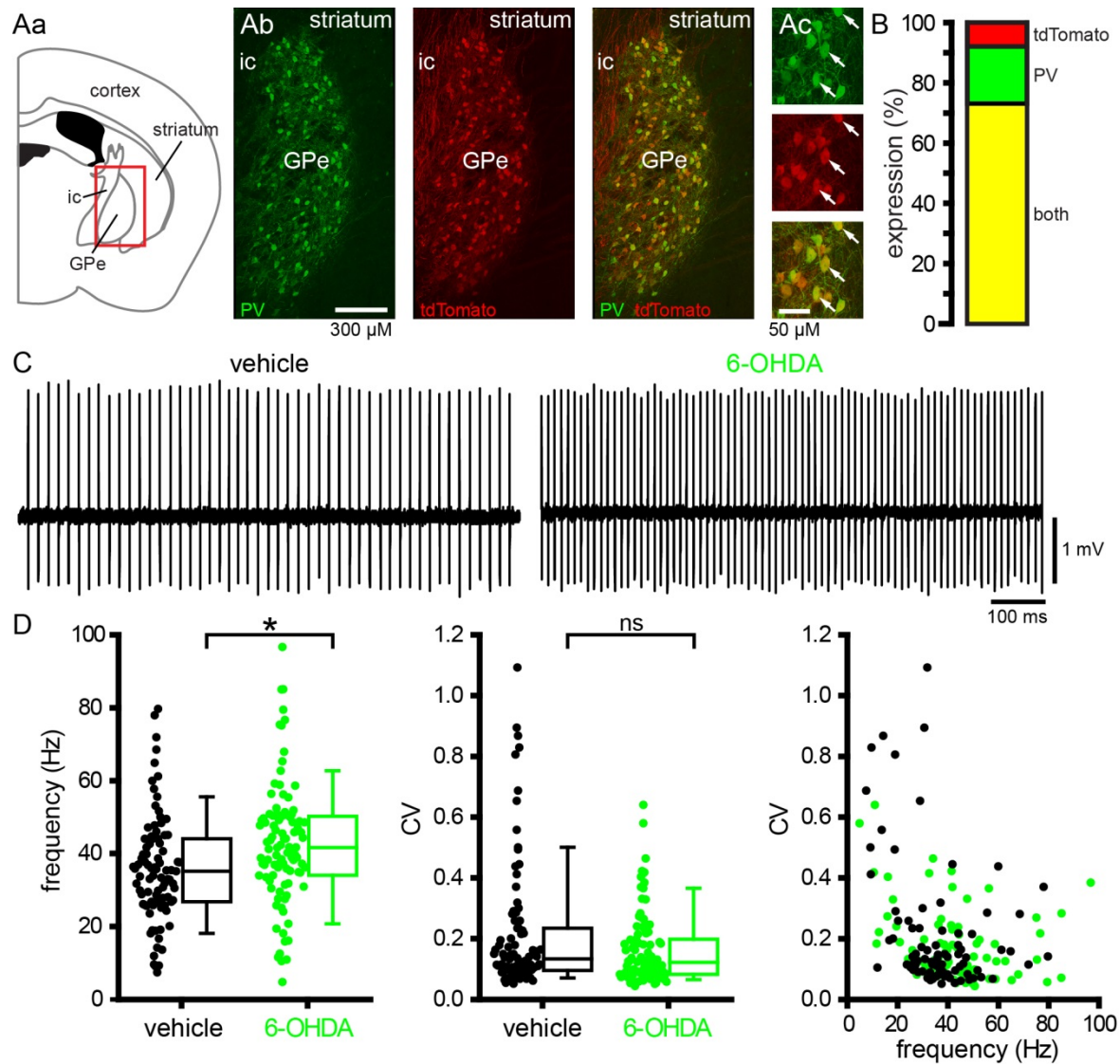


Figure 3.4.1 In 6-OHDA-injected mice the frequency of autonomous PV GPe neuron activity *ex vivo* is elevated

A and *B*, in PV-cre X Ai9 mice the majority of GPe neurons that expressed tdTomato (red) or were immunohistochemically labeled for PV (green), co-expressed both proteins (yellow), as evinced by a representative coronal section through the GPe (*Aa*, schematic representation of the area imaged in *Ab*; *Ac*, upper panel, PV; middle panel, tdTomato; lower panel, both) and quantitative population data (*B*). *C* and *D*, the autonomous activity of tdTomato-expressing GPe

neurons recorded in the loose-seal, cell-attached configuration was not disrupted in 6-OHDA-injected mice relative to activity in control mice. Indeed, the frequency of autonomous firing was significantly greater in 6-OHDA-injected dopamine-depleted mice compared to that in control mice. *C*, representative examples. *D*, population data. *, $p < 0.05$. ns, not significant.

3.5: The STN opposes rather than facilitates antiphase GPe neuron activity

The GPe-STN network has been proposed to be a central pattern generator of abnormal oscillatory activity in PD (Plenz and Kital, 1999; Holgado et al., 2010; Moran et al., 2011). In dopamine-depleted mice, if the STN contributes to the abnormal antiphase activity of the GPe during cortical SWA, optogenetic inhibition of the STN should regularize GPe activity. Thus, we compared the responses of GPe neurons to optogenetic inhibition of the STN for 5 seconds in vehicle- and 6-OHDA-injected GABRR3-cre mice (Table 2.1.1) during cortical SWA. Confocal imaging confirmed the robust, selective, cre-dependent expression of Arch-GFP in STN neurons (Fig. 3.5.1A and Ca) and their axon terminals in the GPe (Fig. 3.5.1B and Cb). However, the use of this cre-driver line to virally express Arch-GFP in the STN precluded optogenetic identification of PV GPe neurons. The proportion of GPe neurons that responded to optogenetic inhibition of the STN was not significantly different in vehicle- and 6-OHDA-injected mice (vehicle: 62 % responsive, n = 23 of 37; 6-OHDA 70 % responsive, n = 21 of 30; p = 0.6076; Fisher's Exact). Optogenetic inhibition of STN neurons reduced GPe neuron activity in all responsive neurons in both vehicle- and 6-OHDA-injected mice (Figs. 3.5.1D, 3.5.2A and Ba; vehicle: laser off = 14.3, 7.60-21.5 Hz; laser on = 7.90, 4.90-12.6 Hz; n = 23; $p_{h4} = 9.54 \times 10^{-7}$; WSR; 6-OHDA: laser off = 17.8, 13.1-28.3 Hz; laser on = 15.6, 7.50-23.2 Hz; n = 21; $p_{h3} = 8.58 \times 10^{-6}$; WSR). The firing rate of GPe neurons in vehicle-injected mice was not significantly different to those in 6-OHDA-injected mice (Figs. 3.5.1D, 3.5.2A and 3.5.2Ba; laser off: $p_{h1} = 0.05722$; MWU); however, during optogenetic inhibition of the STN, GPe neuron firing rates were relatively elevated in 6-OHDA mice (Figs. 3.5.1D, 3.5.2A and 3.5.2Ba; laser on: $p_{h2} = 0.02696$; MWU).

The firing of unidentified GPe neurons in vehicle- and 6-OHDA-injected mice prior to and during optogenetic inhibition of the STN was significantly more irregular in 6-OHDA-injected mice (Figs. 3.5.1D and 3.5.2Ba; vehicle: laser off CV = 0.606, 0.413-0.717; n = 23; 6-OHDA: laser off CV = 1.03, 0.723-1.27, n = 21; $p_{h4} = 2.502 \times 10^{-3}$; MWU; vehicle: laser on CV = 0.737, 0.436-0.973; n = 22; 6-OHDA: laser on CV = 1.20, 0.903-1.37; n = 21; $p_{h3} = 6.951 \times 10^{-3}$; MWU). During optogenetic inhibition of STN neurons, the regularity of firing of responsive GPe neurons decreased in vehicle-injected mice but was not altered in 6-OHDA-injected mice (Figs. 3.5.1D and 3.5.2Ba; vehicle: laser off CV = 0.581, 0.410-0.711; n = 22; vehicle: laser on CV = 0.737, 0.436-0.973; n = 22; $p_{h2} = 9.37 \times 10^{-3}$; WSR; 6-OHDA: laser off CV = 1.03, 0.723-1.27; n = 21; 6-OHDA: laser on CV = 1.20, 0.903-1.37; n = 21; $p_{h1} = 0.1281$; WSR). During optogenetic inhibition of the STN, the in-:antiphase spike probability of GPe neurons decreased in 6-OHDA- but was unaltered in vehicle-injected mice (Fig. 3.5.2B; vehicle: laser off = 1.18, 0.908-1.36; laser on = 1.11, 0.571-1.43; n = 22; $p_{h2} = 1.000$; WSR; 6-OHDA: laser off = 1.02, 0.799-1.55; laser on = 0.781, 0.641-1.02; n = 21; $p_{h4} = 0.01143$; WSR). Unidentified GPe neurons in dopamine-depleted GABRR3-cre mice were less antiphasic than optogenetically identified PV GPe neurons in dopamine-depleted PV-cre mice. The reason for this difference could be inclusion of arkypallidal GPe neurons thought to fire in phase with cortical SWA following dopamine depletion and perhaps also non-PV-expressing prototypic GPe neurons, whose phase preference has not been well characterized (Mallet et al., 2012; Abdi et al., 2015).

To examine the impact of STN inhibition on PV GPe neuron firing, putative PV GPe neurons in 6-OHDA-injected mice were isolated from the unidentified population as for unidentified GPe neurons in A2A-cre mice on the basis of their in-:antiphase spike probability. The firing rate of

all putative PV GPe neurons decreased during optogenetic inhibition of the STN (Fig. 7Ca; 6-OHDA: laser off = 26.2, 20.3-33.9 Hz; laser on = 19.4, 15.3-27.9 Hz; $n = 7$; $p = 0.01562$; WSR). Unlike the unidentified population of GPe neurons, the irregularity of putative PV GPe neurons was elevated by optogenetic inhibition of the STN (Fig. 3.5.2Ca; 6-OHDA: laser off CV = 0.815, 0.509-1.3; laser on CV = 1.17, 1.03-1.93; $n = 7$; $p = 0.01562$; WSR). Lastly, all putative PV GPe neurons became more antiphase during optogenetic inhibition of the STN as evinced by a significant decrease in in-:antiphase spike probability (Fig. 3.5.2C; 6-OHDA: laser off = 0.795, 0.670-0.811; laser on = 0.731, 0.280-0.781; $n = 7$; $p = 0.01562$; WSR). Overall, STN silencing enhanced antiphase firing in unidentified and putative GPe neurons in dopamine-depleted mice, arguing that STN-GPe transmission opposes rather than facilitates the abnormal patterning of GPe neurons during cortical SWA.

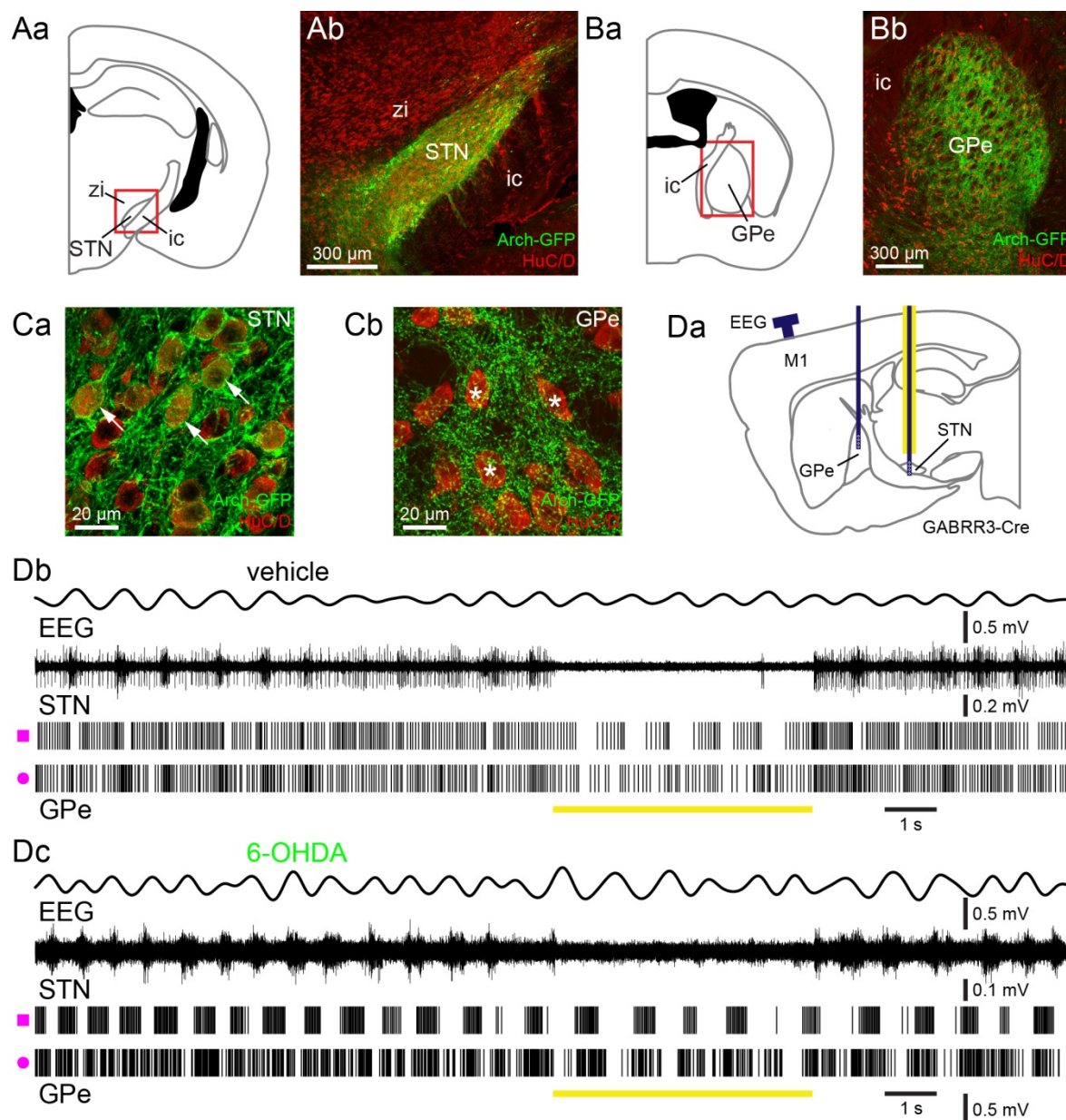


Figure 3.5.1 Effect of optogenetic inhibition of the STN on GPe activity

A-C, histological verification of cre-dependent expression of Arch-GFP in STN-GPe neurons in GABRR3-cre mice. *Aa* and *Ba*, schematic representations of areas imaged in *Ab* and *Bb*, respectively (red box denotes the imaged subregion). *Ab*, *Bb*, and *C*, coronal sections illustrating expression of Arch-GFP (green) in STN neuron somata (*Ab* and *Ca*; arrows) and their axon terminals in the GPe (*Bb* and *Cb*). *Ca*, expression of Arch-GFP in HuC/D-immunoreactive (red)

STN neurons. *Cb*, Arch-GFP expressing STN axon terminals in the vicinity of HuC/D-immunoreactive (red; asterisks) GPe neurons. *D*, schematic representation of optrode and electrode placement (*Da*; dark blue line indicates electrode; yellow line denotes affixed optical fiber) and representative examples from vehicle- (*Db*) and 6-OHDA-injected (*Dc*) mice. Note that multi-unit STN activity is illustrated due to the greater difficulty of spike sorting individual STN units when recorded with an optrode versus a silicon tetrode without a fiber optic.

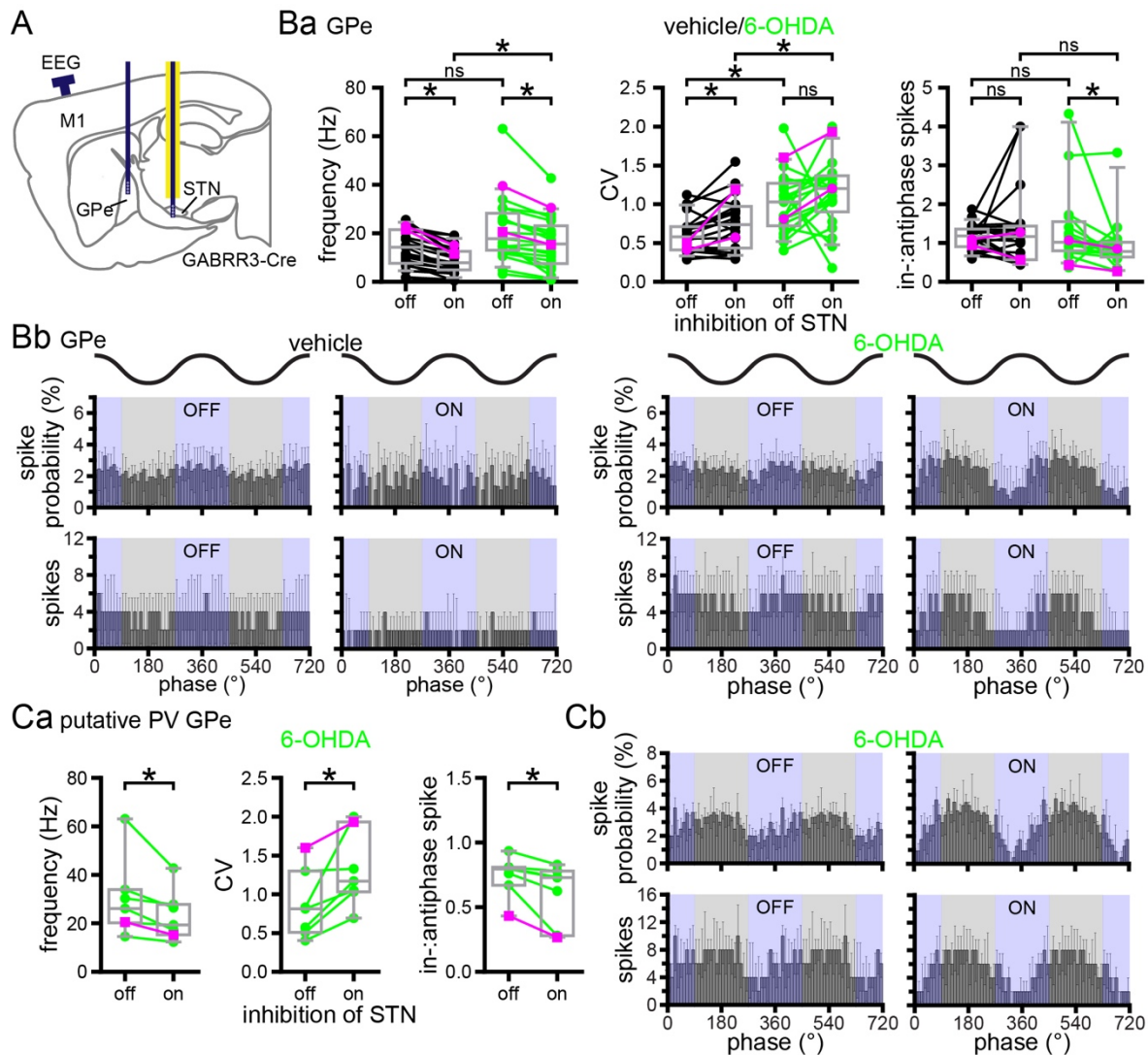


Figure 3.5.2 Optogenetic inhibition of STN neurons decreases the firing rate of unidentified and putative PV GPe neurons and increases their antiphase activity in 6-OHDA-injected mice

A-C, optogenetic inhibition of STN neurons in vehicle-injected GABRR3-cre mice reduced the firing frequency and firing regularity of unidentified GPe neurons (*B*). Inhibition of the STN also reduced the firing frequency and in-antiphase spike probability of unidentified (*B*) and putative PV GPe (*C*) neurons in 6-OHDA-injected mice. *A*, schematic representation of optrode and electrode placement (*A*; dark blue line indicates electrode; yellow line denotes affixed optical

fiber). *Ba* and *Ca*, population data of unidentified (*Ba*) and putative PV (*Ca*) GPe neurons; firing rate (left), CV (middle), and in-:antiphase spike probability (right); example data from Fig. 3.5.1D plotted in magenta. Note an extreme outlier was excluded from the 6-OHDA-injected mouse in-:antiphase plot for clarity (*Ba*; in- to antiphase spike probability ratio: laser off = 18.5, laser on = 7.0). *Bb* and *Cb*, linear phase histograms of unidentified (*Bb*) and putative PV (*Cb*) GPe neuron activity prior to and during optogenetic inhibition of STN neurons. *, $p < 0.05$. ns, not significant.

3.6: Dopamine depletion reduces phase locking of STN neuron firing to cortical SWA

Parkinsonian circuit activity in humans (Sharott et al., 2014), monkeys (Soares et al., 2004; Deffains et al., 2016), and rats (Magill et al., 2001; Ni et al., 2001; Walters et al., 2007; Mallet et al., 2008b; Ryu et al., 2011; Tachibana et al., 2011; Delaville et al., 2015) is typically associated with alterations in STN activity, including relative entrainment to cortical rhythmic activity, increased phasic or burst firing, and overall hyperactivity. Thus, in urethane-anesthetized dopamine-depleted mice, we predicted similar changes in the rate and pattern of STN activity as those reported in equivalent rat studies. To assess the impact of dopamine depletion on the rate and pattern of STN activity, 30 s epochs of firing during robust cortical SWA were compared in vehicle- and 6-OHDA-injected PV-cre mice (Table 2.1.1). Similar proportions of STN neurons were responsive to optogenetic inhibition of PV GPe neurons in vehicle and 6-OHDA treated mice (vehicle: 82 %, n = 18 of 22; 6-OHDA: 84 %, n = 21 of 25; p = 1.000; Fisher's Exact). Dopamine depletion did not alter the firing rate (Fig. 3.6.1A, and B*a*; SWA: vehicle = 9.38, 5.90-16.4 Hz; n = 18; 6-OHDA = 11.7, 8.17-13.3 Hz; n = 21; p = 0.7122; MWU) or CV (SWA: vehicle = 1.3, 0.979-1.64; n = 18; 6-OHDA = 1.35, 1.15-1.68; n = 21; p = 0.494; MWU) of responsive STN neurons. However, there was a significant reduction in in-antiphase spike probability following dopamine depletion (Fig. 3.6.1B; SWA: vehicle = 3.45, 1.92-6.54; n = 18; 6-OHDA = 1.69, 0.992-3.16; n = 21; p = 0.0148; MWU). These findings are in contrast to what has been reported in dopamine-depleted rats (Magill et al., 2001; Mallet et al., 2008a; Mallet et al., 2008b) and unexpected given the emergence of phase-offset prototypic GPe neuron activity, but are consistent with downregulation of cortico-STN transmission strength in parkinsonian rats (Kita and Kita, 2011b; Wang et al., 2018), mice (Chu et al., 2017), and non-human primates

(Mathai et al., 2015) and downregulation of intrinsic excitability in rats and mice (Zhu et al., 2002; Wilson et al., 2006; McIver et al., 2019).

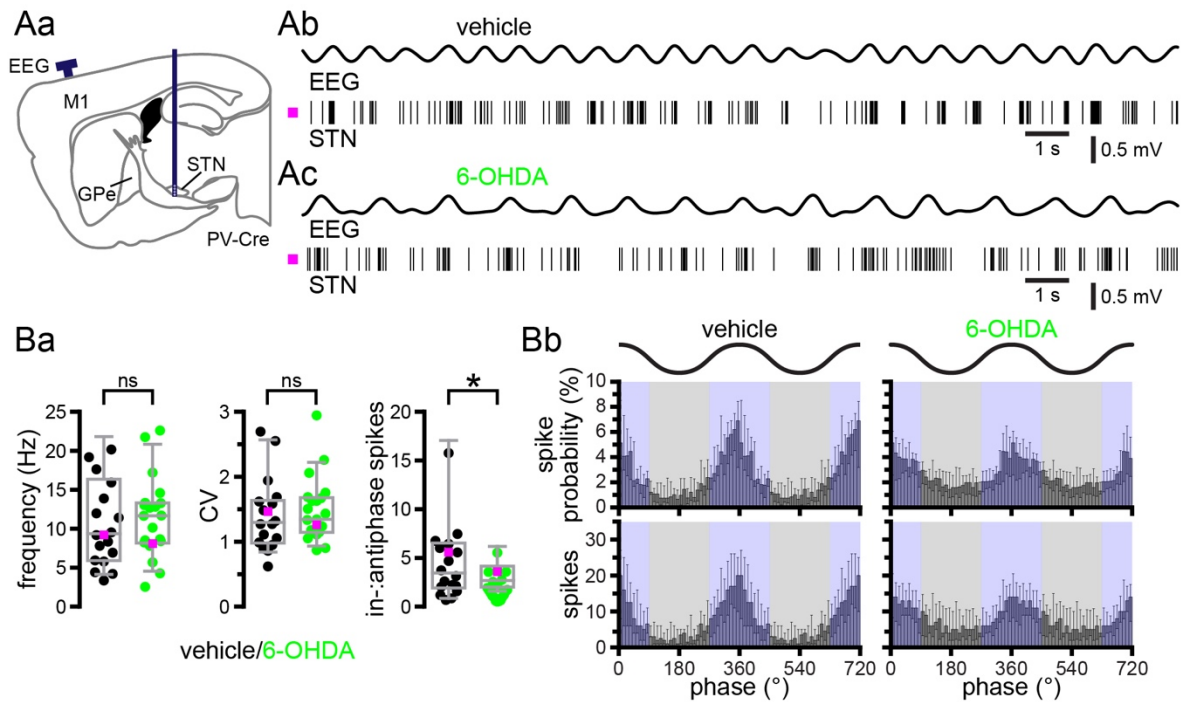


Figure 3.6.1 In 6-OHDA-injected mice phase locking of STN firing to cortical SWA is reduced

A and *B*, although STN neuron firing rate and CV were unaffected by dopamine depletion, there was a significant reduction in in-:antiphase spike probability. *A*, schematic representation of electrode placement (*Aa*; dark blue line indicates electrode) mice and representative examples from vehicle- (*Ab*) and 6-OHDA- (*Ac*) injected PV-cre mice. *Ba*, population firing rate (left), CV (middle), and in-:antiphase spike probability (right); example data plotted in magenta; three individual outlier data points were not plotted for legibility (vehicle frequency outlier: 36.7 Hz; vehicle in-:antiphase spike probability outlier: 28.7; 6-OHDA in-:antiphase spike probability outlier: 50.2). (*Bb*) Population linear phase histograms. *, $p < 0.05$. ns, not significant.

3.7: PV GPe neuron activity enhances STN neuron entrainment to cortical SWA in control- and dopamine-depleted mice

To determine how alterations in the firing pattern, and intrinsic and synaptic properties of prototypic GPe neurons following the loss of dopamine (Fan et al., 2012; Mallet et al., 2012; Abdi et al., 2015; Chu et al., 2015; this study) affect their regulation of STN activity *in vivo*, the effects of optogenetically inhibiting Arch-GFP expressing PV GPe neurons for 5 seconds on STN neuron firing in control and dopamine-depleted mice (Table 2.1.1) were compared. The majority of responsive STN neurons were disinhibited during optogenetic inhibition of PV GPe neurons (vehicle: 72 %, n = 13 of 18; 6-OHDA: 100 %, n = 21 of 21, p = 0.6356; Fisher's Exact). Inhibition of a minority of responsive STN neurons during PV GPe neuron silencing in vehicle-injected mice may reflect disinhibition of GPe-STN neurons due to reduced lateral inhibition in the GPe (11 %, n = 2 of 18). The failure of a subset of STN neurons to respond to PV GPe neuron inhibition presumably reflects a failure to inhibit GPe neurons that were presynaptic to recorded STN neurons (vehicle: 18 %, n = 4 of 22; 6-OHDA: 16 %, n = 4 of 25). Given that STN activity was not recorded at sites where optogenetic inhibition of PV GPe neurons failed to elicit a response from at least one STN neuron, the proportion of STN neurons that did not respond to optical stimulation is likely to be higher than that reported here. During optogenetic inhibition of PV GPe neurons, the rate and regularity of STN firing increased in both vehicle- and 6-OHDA-injected mice consistent with disinhibition of STN neurons (Fig. 3.7.1A and B*a*; vehicle: laser off = 11.9, 6.58-16.6 Hz; laser on = 15, 8.88-22.7 Hz; n = 18; $p_{h3} = 8.424 \times 10^{-3}$; WSR; laser off CV = 1.38, 1.04-1.82; laser on CV = 0.891, 0.704-0.968; n = 17; $p_{h3} = 6.27 \times 10^{-3}$; WSR; 6-OHDA: laser off = 10.3, 7.30-13.7 Hz; laser on = 18.3, 12.3-29.9 Hz; n = 21; $p_{h4} = 3.815 \times 10^{-6}$; WSR; laser off CV = 1.22, 0.985-1.47; laser on CV = 0.727, 0.538-0.872; n = 21;

$p_{h4} = 7.628 \times 10^{-6}$; WSR). The firing rate of responsive STN neurons was not significantly different in dopamine-intact and -depleted mice in the absence of or during optogenetic inhibition of PV GPe neurons (Fig. 3.7.1A and Ba; laser off: $p_{h1} = 0.4990$; MWU; laser on: $p_{h2} = 0.4464$; MWU). Although the CV of STN neuron firing was not altered by dopamine depletion alone, it was relatively reduced in 6-OHDA-injected mice during optogenetic inhibition of PV GPe neurons (Fig. 3.7.1A and Ba; vehicle: laser off CV = 1.36, 0.936-1.79, $n = 18$; 6-OHDA laser off CV = 1.22, 0.985-1.47; $n = 21$; $p_{h1} = 0.770$ MWU; vehicle: laser on CV = 0.891, 0.704-0.968; $n = 17$; 6-OHDA: laser on CV = 0.727, 0.538-0.872; $n = 21$; $p_{h2} = 0.02074$; MWU).

Inhibition of PV GPe neurons in vehicle- and 6-OHDA-injected mice also reduced STN in-:antiphase spike probability (Fig. 3.7.1B; vehicle: laser off = 4.05, 2.02-7.75; laser on = 1.45, 1.19-1.69; $n = 16$; $p_{h4} = 1.709 \times 10^{-3}$; WSR; 6-OHDA: laser off = 1.64, 1.13-2.80; laser on = 1.17, 0.986-1.50; $n = 21$; $p_{h3} = 6.453 \times 10^{-3}$; WSR). In 6-OHDA-injected mice, STN neurons also exhibited a reduced in-:antiphase spike probability relative to vehicle-injected controls both before and during optogenetic inhibition of PV GPe neurons (Fig. 3.7.1B; vehicle: laser off = 3.8, 1.98-7.50; $n = 17$; 6-OHDA: laser off = 1.64, 1.13-2.80; $n = 21$; $p_{h2} = 0.03024$; MWU; vehicle: laser on = 1.46, 1.22-1.70; $n = 17$; 6-OHDA: laser on = 1.17, 0.986-1.50; $n = 21$; $p_{h1} = 0.04414$; MWU). The reduced in-:antiphase spike probability of STN neurons in 6-OHDA mice is consistent with the downregulation of cortico-STN transmission strength in parkinsonian rats (Kita and Kita, 2011b; Wang et al., 2018), mice (Chu et al., 2017), and non-human primates (Mathai et al., 2015). The additional decrease in in-:antiphase STN activity that occurred during optogenetic inhibition of PV GPe neurons in 6-OHDA-injected mice may reflect a reduction in post-inhibitory rebound neuron firing in the STN (Bevan et al., 2002; Baufreton et al., 2005;

Hallworth and Bevan, 2005) when phase-offset inhibition from the GPe is suppressed (Mallet et al., 2008b; this study; Mallet et al., 2012). Interestingly, optogenetic inhibition of PV GPe neurons also significantly reduced in-:antiphase STN activity in dopamine-intact mice, arguing GPe-STN inhibition also enhances in-:antiphase STN activity under normal conditions, despite the fact that inhibition was less antiphase to cortical SWA. Together, these data argue that prototypic PV GPe neurons powerfully regulate the frequency and pattern of postsynaptic STN activity in both dopamine-intact and -depleted mice but their relative effects are difficult to decipher, presumably in part due to adaptive alterations in the intrinsic and synaptic properties of STN neurons (Chu et al., 2015; Mathai et al., 2015; Chu et al., 2017; Wang et al., 2018; McIver et al., 2019).

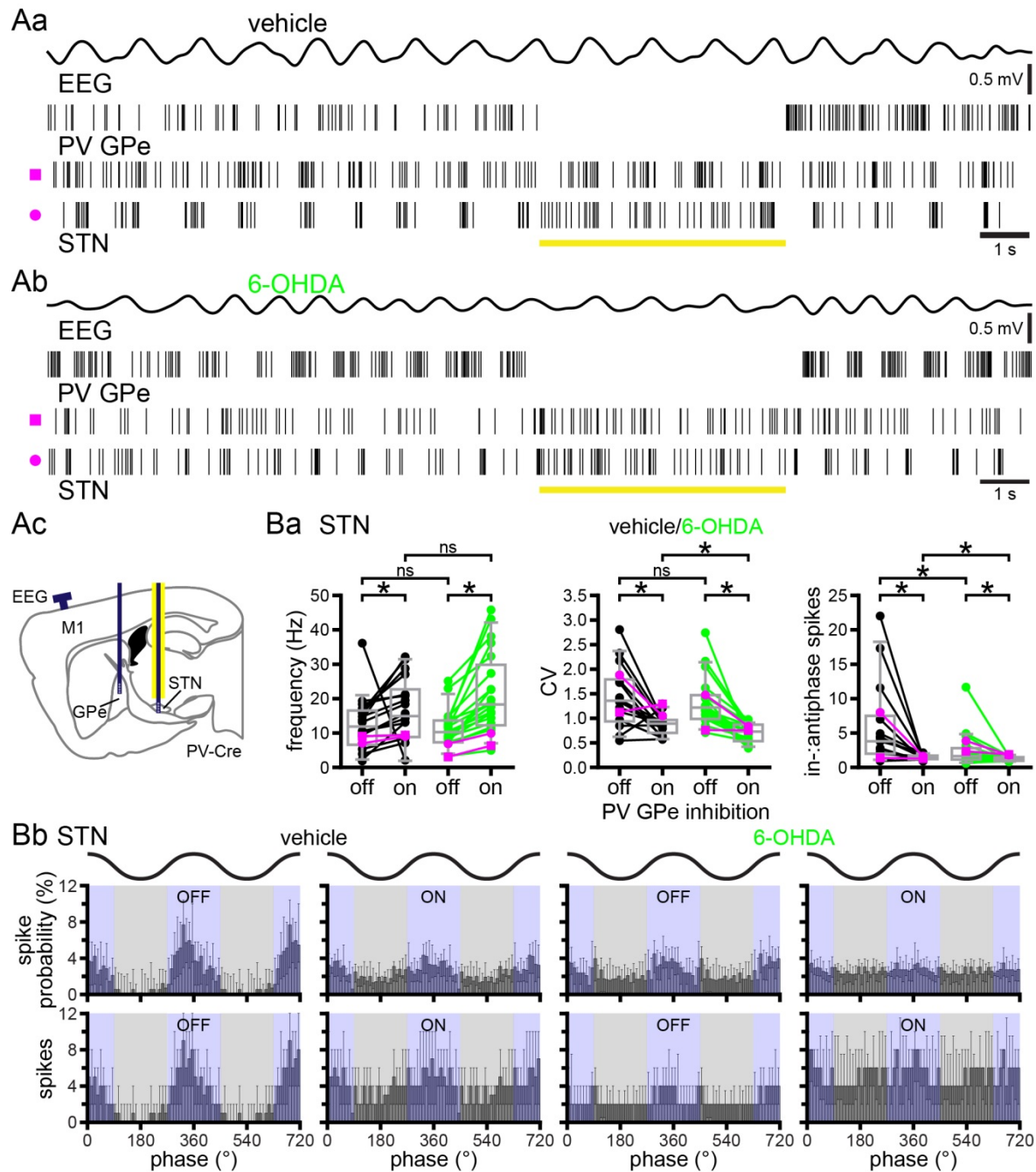


Figure 3.7.1 Optogenetic inhibition of PV GPe neurons disinhibits STN neurons and reduces their phase locking to cortical SWA in both vehicle- and 6-OHDA-injected mice. *A* and *B*, optogenetic inhibition of PV GPe neurons increased the frequency and regularity of STN activity and reduced the in-antiphase spike probability of STN neurons (*B*) in vehicle- (*Aa*)

and 6-OHDA- (*Ab*) injected PV-cre mice. *A*, representative examples (*Aa* and *Ab*) and schematic representation of optrode and electrode placement (*Ac*; dark blue line indicates electrode; yellow line denotes affixed optical fiber). *Ba*, Population data; firing rate (left), CV (middle), and in-antiphase spikes (right); example data plotted in magenta symbols. *Bb*, Population linear phase histograms of STN activity relative to cortical SWA in vehicle- (left) and 6-OHDA-injected (right) mice prior to and during optogenetic inhibition of PV GPe neurons. * $p < 0.05$. ns, not significant.

3.8: Loss of dopamine profoundly alters the responses of D2-SPNs and prototypic PV GPe neurons to cortical ACT, whereas STN activity is relatively unaffected

Dopamine depletion profoundly alters the response of the basal ganglia to pinch-evoked cortical ACT in rats (Magill et al., 2001; Mallet et al., 2008a; Mallet et al., 2008b; Mallet et al., 2012; Abdi et al., 2015; Sharott et al., 2017). Consistent with elevated striatopallidal transmission, rat D2-SPNs were hyperactive, GPe neurons were hypoactive, and STN neurons were hyperactive in 6-OHDA-injected rats during this brain state (Magill et al., 2001; Mallet et al., 2008a; Mallet et al., 2008b; Mallet et al., 2012; Abdi et al., 2015; Sharott et al., 2017). In addition, tail pinch-evoked sustained periods of cortical ACT, which were associated with exaggerated beta band activity in dopamine-depleted rats (Mallet et al., 2008b; Mallet et al., 2012). To determine whether parkinsonian mice exhibit similar alterations, we compared the activities of D2-SPNs, PV GPe neurons, and STN neurons in vehicle- and 6-OHDA-injected mice during and following 5-second tail pinch-evoked cortical ACT (Magill et al., 2001). However, prolonged periods of cortical ACT could not be induced in mice without clear signs of inadequate anesthesia. Therefore, our study was restricted to the tail-pinch period. The failure to elicit prolonged cortical ACT may explain the absence of exaggerated beta band activity in dopamine-depleted mice (Tables 2.1.2 and 2.1.3). That said, exaggerated beta band activity has been rarely reported in the cortex or basal ganglia of awake dopamine-depleted mice, arguing that this activity pattern is simply less prominent in this model (Lobb and Jaeger, 2015; Willard et al., 2019). Prior to tail pinch, the firing rate of D2-SPNs during cortical SWA was elevated in 6-OHDA- versus vehicle-injected mice, as described above (Fig. 3.8.1A; vehicle: SWA = 2.5, 1.60-3.40 Hz; n = 34; 6-OHDA: SWA = 3.4, 2.10-7.80; n = 21; $p_{h2} = 0.02476$; MWU). In response to cortical ACT, the firing rate of D2-SPNs in vehicle-injected mice decreased (Fig. 3.8.1A; vehicle: ACT = 0.300,

0.00-1.35 Hz; $n = 34$; $p_{h3} = 1.751 \times 10^{-3}$; WSR), whereas in 6-OHDA-injected mice, D2-SPNs maintained their elevated rate of firing (Fig. 3.8.1A; 6-OHDA: ACT = 4.00, 2.10-9.60 Hz; $n = 21$; $p_{h1} = 0.5578$; WSR). As a result, the median firing rate of D2-SPNs during tail pinch-evoked cortical ACT was approximately 13 times greater in dopamine-depleted mice (MWU; $p_{h4} = 2.656 \times 10^{-4}$). In addition, the spiking of D2-SPNs was relatively sustained during cortical ACT compared to cortical SWA-associated firing, as evinced by a reduction in CV in both control and dopamine-depleted mice (vehicle: SWA = 1.53, 1.21-1.78; ACT = 0.935, 0.229-1.29; $n = 17$; $p = 0.0147$; WSR; 6-OHDA: SWA = 1.87, 1.35-2.45; ACT = 0.955, 0.737-1.16; $n = 18$; $p = 0.0001$; WSR). These data are consistent with a recent study in rats (Sharott et al., 2017) in which the firing of D2-SPNs was elevated in dopamine-depleted rats during prolonged cortical ACT.

Because D2-SPNs were relatively active in 6-OHDA-injected mice during cortical ACT, we hypothesized that the firing of downstream PV GPe neurons would be suppressed. Indeed, dopamine depletion profoundly altered the response of optogenetically identified PV GPe neurons to cortical ACT, consistent with earlier studies in rats (Fig. 3.8.1B) (Magill et al., 2001; Mallet et al., 2008a; Mallet et al., 2012; Abdi et al., 2015). In vehicle-injected mice, the firing of PV GPe neurons increased during cortical ACT (Fig. 3.8.1B ; vehicle: SWA = 15.8, 9.00-42.0 Hz; ACT = 27.2, 18.6-41.0 Hz; $n = 23$; $p_{h2} = 0.02512$; WSR), whereas firing decreased in 6-OHDA-injected mice (Fig. 3.8.1B; 6-OHDA: SWA = 15.6, 12.4-19.0 Hz; ACT = 1.8, 0.20-16.0 Hz; $n = 15$; $p_{h3} = 3.48 \times 10^{-3}$; WSR). As a result, the frequency of PV GPe neuron firing during cortical ACT was considerably lower in dopamine-depleted mice; the median firing rate of PV-GPe neurons in 6-OHDA-injected mice was only 7% of that in vehicle-injected mice (Fig. 3.8.1B; ACT: $p_{h4} = 1.31 \times 10^{-5}$; MWU)

Despite the hugely different firing rates of presynaptic PV GPe neurons, the frequency of downstream STN neuron activity 1) increased during tail pinch-evoked cortical ACT in both vehicle- and 6-OHDA-injected mice; 2) the firing rates of STN neurons during cortical ACT were similar in dopamine-intact and -depleted mice (Fig. 3.8.1C; vehicle: SWA = 13.8, 10.0-17.8 Hz; ACT = 18.8, 12.2-23.0; n = 15; $p_{h3} = 0.03552$; WSR; 6-OHDA: SWA = 9.60, 6.70-13.3 Hz; ACT = 15.6, 8.6-18.3 Hz; n = 13; $p_{h4} = 0.0371$; WSR) (SWA: $p_{h2} = 0.1407$; MWU; ACT: $p_{h1} = 0.1589$; MWU). These data are in contrast to studies in rats (Magill et al., 2001; Mallet et al., 2008a; Mallet et al., 2012). Thus, in dopamine-depleted mice, the activity of STN neurons during cortical ACT does not reflect the hypoactivity of upstream prototypic PV GPe neurons, presumably due to adaptive changes triggered by the loss of dopamine (Fan et al., 2012; Chu et al., 2015; Mathai et al., 2015; Chu et al., 2017; Wang et al., 2018; McIver et al., 2019).

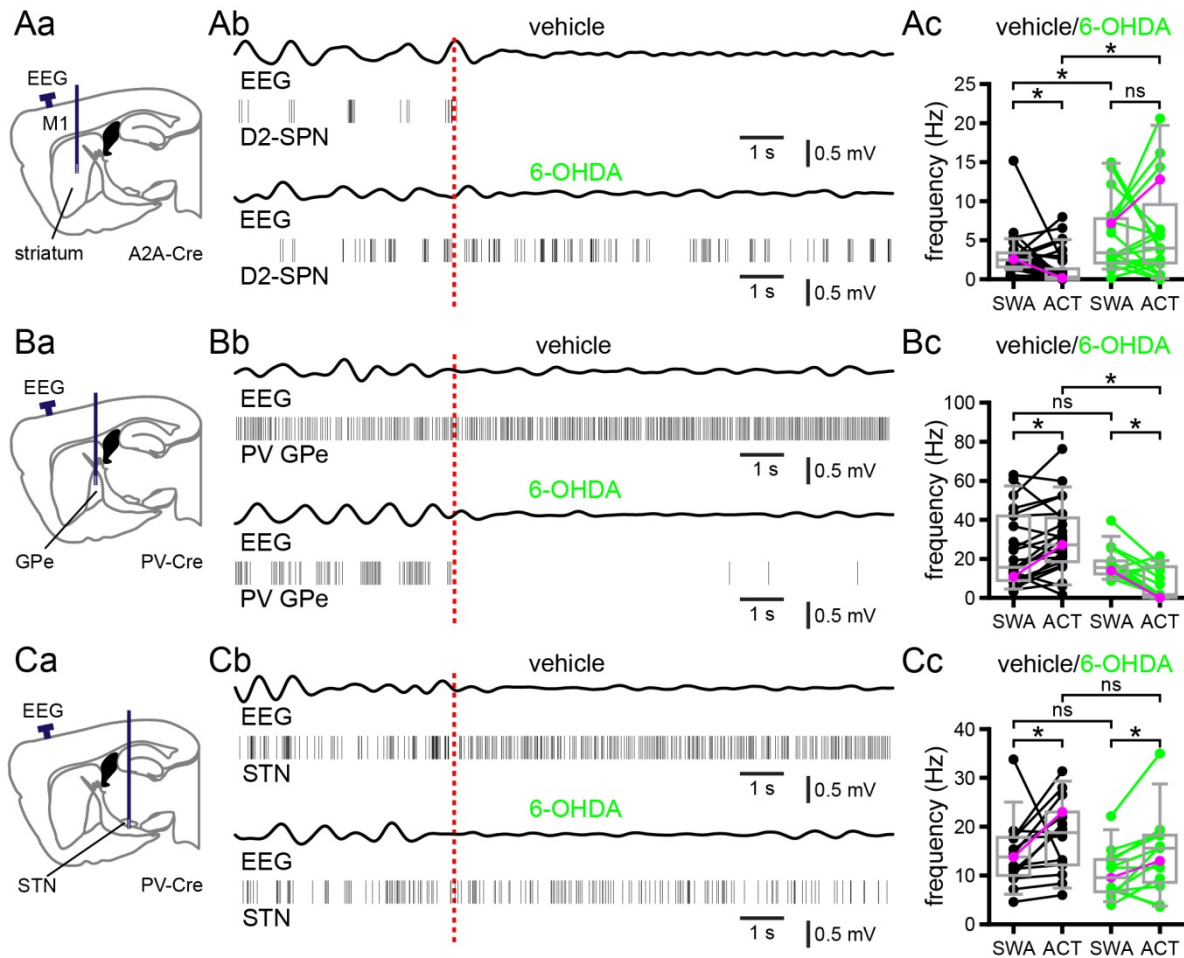


Figure 3.8.1 Effects of tail pinch-evoked cortical ACT on D2-SPNs, PV GPe neurons, and STN neurons in vehicle- and 6-OHDA injected mice

A, in vehicle-injected, dopamine-intact A2A-cre mice D2-SPN activity decreased during cortical ACT relative to cortical SWA. In 6-OHDA-injected, dopamine-depleted mice D2-SPN activity was similar during cortical SWA and ACT. Thus, the firing rate of D2-SPNs during cortical ACT was greater in 6-OHDA-injected mice. *B*, in vehicle-injected dopamine-intact PV-cre mice PV GPe neuron activity increased during cortical ACT, relative to cortical SWA. In 6-OHDA-injected, dopamine-depleted PV-cre mice, PV GPe neuron activity was suppressed during cortical ACT. *C*, STN neuron activity significantly increased during cortical ACT relative to SWA in both vehicle- and 6-OHDA-injected mice. The rate of STN activity during cortical ACT

was similar in dopamine-intact and -depleted mice. *Aa*, *Ba*, and *Ca*, schematic representations of electrode placement (dark blue line indicates electrode). *Ab*, *Bb*, and *Cb*, representative examples of neuronal activity in D2-SPNs (*Ab*), PV GPe neurons (*Bb*), and STN neurons (*Cb*) in vehicle- (top) and 6-OHDA-injected (bottom) mice; onset of tail pinch denoted by dashed red line. *Ac*, *Bc*, and *Cc*, population firing rate data; examples plotted in magenta. *, $p < 0.05$; ns, not significant.

Chapter 4: Discussion

4.1: Experimental findings in brief

Our goal was to acquire novel mouse data about the effects of dopamine depletion on D2-SPN, GPe and STN neuron activity and to optogenetically inhibit nodes of the indirect pathway to determine which were important for the propagation of abnormal activity patterns in the dopamine-depleted state. D2-SPN firing rate was elevated, PV GPe neuron firing rate was unaltered, and STN neurons were spared rate changes during cortical SWA in dopamine-depleted compared to -intact mice. However, PV GPe neurons developed a phenotype similar to that shown in rats whereby PV GPe neurons paused during the active phase of cortical SWA (Mallet et al., 2012; Abdi et al., 2015). STN neurons in dopamine-depleted mice did not burst excessively and in fact, showed reduced phase locking to cortical SWA which was further reduced during optogenetic inhibition of PV GPe neurons. STN, for its part in pathological patterning of GPe activity, appears to counteract antiphase entrainment of GPe neurons to cortical SWA which takes place despite elevated autonomous firing of PV GPe neurons in the dopamine depleted state. Cortical ACT, achieved by tail-pinch, revealed that D2-SPN firing rate in dopamine-intact mice is reduced by cortical desynchronization; however, following dopamine depletion, D2-SPNs maintained elevated firing rates during cortical ACT but in a more evenly temporally distributed manner. Correspondingly, GPe neuron firing was elevated during ACT in dopamine-intact mice and suppressed in dopamine-depleted mice. Unintuitively, STN neuron firing was elevated during ACT in both dopamine-intact and -depleted mice without detectable difference due to dopamine depletion; this suggests that the diminished strength of the

hyperdirect pathway and loss of autonomous activity in STN neurons balanced the silencing of PV GPe neurons (and therefore STN disinhibition) during ACT in dopamine-depleted mice.

4.2: Implications of D2-SPN hyperactivity

The finding that D2-SPNs fire significantly faster in dopamine depleted mice compared to controls is somewhat unsurprising because other groups have found similar results in anesthetized rats during SWA and ACT (Sharott et al., 2017), in anesthetized mice in response to electrical stimulation of cortex (Escande et al., 2016), and in awake immobile mice (Parker et al., 2018; Ryan et al., 2018). However, our findings constitute a useful contribution to the scientific literature by way of comparison to prior studies in rats using nearly identical anesthetic regimens and confirming similarities in rate and pattern modulation across species and brain states. The finding that D2-SPN activity is suppressed by cortical ACT in dopamine-intact mice but retain elevated firing following dopamine depletion is of particular interest because it corresponds with the recent finding that more D2-SPNs are recruited to activity following dopamine depletion in awake-behaving mice (Maltese et al., 2019). How this alteration bears on behavioral output is a matter of speculation; there are various models of how striatal activity influences motor output and all are controversial at present. The idea of ‘center-surround’ or ‘winner-take-all’ action selection models have been around for a long time (Groves, 1983; Mink and Thach, 1993) but evidence that D1- and D2-SPNs are sufficiently interconnected to support such a model has been slow to develop. Still, there is evidence that lateral inhibition among SPNs, although perhaps too sparse to be represented on the level of individual neurons controlling a local circuit on their own, could feasibly support the selection of ensemble activity by a process of sparse D2-SPN-biased lateral inhibition (Burke et al., 2017) likely supported by striatal microcircuitry (Tepper et

al., 2018; Assous and Tepper, 2019) and influenced by arky pallidal and a subset of PV GPe neurons as well (Bevan et al., 1998; Mallet et al., 2016). In dopamine-intact mice, D2-SPNs have been shown to have more inhibitory influence over D1-SPNs than vice versa (Taverna et al., 2008; Planert et al., 2010), though following dopamine depletion collateral inhibition is reduced (Taverna et al., 2008) it may be counterbalanced *in vivo* by the absence of D2R-mediated suppression of D2-SPN lateral inhibition (Dobbs et al., 2016; Lemos et al., 2016). In the dopamine-depleted state, where D2-SPNs are firing more (Sharott et al., 2017; Parker et al., 2018; Ryan et al., 2018; this study), more D2-SPNs are firing (Maltese et al., 2019), and D2-SPN lateral inhibition may yet be dominant (Taverna et al., 2008; Planert et al., 2010), the capacity of D1-SPNs to participate in functional units of action selection in the parkinsonian striatum may indeed be greatly diminished (Burke et al., 2017).

In dopamine-intact animals, D1- and D2-SPNs are coactive during the implementation of behavioral sequences (Cui et al., 2013; Markowitz et al., 2018; Parker et al., 2018). Following dopamine depletion, the propensity for higher firing rates (Escande et al., 2016; Sharott et al., 2017; Parker et al., 2018; Ryan et al., 2018) and additional neuron recruitment (Maltese et al., 2019) suggests that outsized influence of D2-SPN activity in the dopamine-depleted state may underly features of abnormal behavior. That said, optogenetic, electrical, and chemogenetic stimulation of downstream basal ganglia structures have been shown to ameliorate certain motor deficits in parkinsonian mice and rats (Jouve et al., 2010; Li et al., 2012; Chu et al., 2017; Assaf and Schiller, 2019; McIver et al., 2019; Schor and Nelson, 2019) indicating that it may be interference with the transmission of abnormal activity patterns representative of damaged action selection at the level of striatum from which therapeutic effects are derived, rather than

normalization of circuit activity (Chiken and Nambu, 2016; Pan et al., 2016; Guridi and Alegre, 2017).

4.3: Excessive patterning of prototypic GPe neurons

Initially thought of as a relay station in the indirect pathway connecting striatum to STN and composed of homogenous cells (Albin et al., 1989; Wichmann and DeLong, 1996; Abdi et al., 2015), GPe turns out to be significantly more complex and likely to play a more active role basal ganglia function and dysfunction than initially proposed. For one, GPe neurons are not homogenous. At this point and time, there are two primary cell types in GPe, prototypic GPe neurons which project downstream to STN and arkypallidal GPe neurons which project exclusively back up to striatum (Mallet et al., 2012; Abdi et al., 2015; Dodson et al., 2015). Of course, prototypic GPe neurons also project to the output nuclei (Smith et al., 1998) and a small subset of all PV GPe neurons project back to striatum and synapse on PV-expressing interneurons (Bevan et al., 1998). There are also additional subtypes that can be identified by differential gene expression of prototypic (Lhx6, Nkx2-1, PV, ER81), arkypallidal (FoxP2, Meis2, PPE), or mixed (Npas1) genetic cell type markers though the functional significance of these subtypes is largely yet unknown (Mastro et al., 2014; Abdi et al., 2015; Dodson et al., 2015; Abecassis et al., 2020).

The classic model contends that GPe receives input from D2-SPNs and STN neurons (Albin et al., 1989; DeLong, 1990). However, this ignores bridging collaterals of D1-SPNs that also innervate GPe as well as dopaminergic inputs; how bridging collaterals contribute to neural activity underlying behavior or whether or not dopaminergic modulation in GPe has presynaptic

effects on all striatopallidal and subthalamopallidal transmission, GPe neurons directly, or both is poorly understood (Rommelfanger and Wichmann, 2010; Cazorla et al., 2014; Lemos et al., 2016; Blesa et al., 2017). Being tonically active *in* and *ex vivo*, prototypic GPe neurons broadly inhibit downstream structures when animals are inactive (Dodson et al., 2015; Hernandez et al., 2015). How striatopallidal inputs may differentially impact prototypic and arkypallidal neurons is still being worked out, although early evidence points to innervation of primarily prototypic GPe neurons (Cui et al., 2019). In dopamine-intact animals, even synchronous cortical activity that produces reliable bursting activity in SPNs is often unable to produce meaningful pauses in prototypic GPe neurons (Magill et al., 2001; Mallet et al., 2008b; Mallet et al., 2012; Zold et al., 2012; Abdi et al., 2015; this study) but following dopamine depletion the majority develop robust pauses in activity detectable in rats (Magill et al., 2001; Mallet et al., 2008b; Mallet et al., 2012; Abdi et al., 2015; Dodson et al., 2015) and since the present study also in mice, although we detected more variability in phase locking to cortical SWA than in prior rat studies.

It might be the case, for instance, that enhanced transmission properties of D2-SPNs following dopamine depletion induce a homeostatic response in PV GPe neurons leading to the increased autonomous activity we observed *ex vivo*. Interestingly, this does not spare PV GPe neurons from their enhanced pausing phenotype but does maintain normal firing rates despite pauses. It would be informative to know if PV GPe neuron autonomous firing is elevated in dopamine depleted rats. If this plasticity is specific to mice, it might account for the greater variability we observed in phase locking of PV GPe neuron activity.

What factors are responsible for the widespread pausing phenotype of prototypic GPe neurons following dopamine depletion is of critical importance to understand abnormal basal ganglia activity. Here we show that inhibiting D2-SPN firing at the level of the striatum is sufficient to largely alleviate this form of abnormal patterning, but whether the recruitment of additional D2-SPNs to fire, enhanced transmission properties, or lack of presynaptic D2 dopamine receptor stimulation in D2-SPN-GPe terminals in the dopamine-depleted state underly this effect remain open questions. Additionally, what role collateral inhibition may play in shaping information flow through prototypic or arkypallidal GPe neurons is only just beginning to be explored. For instance, whether or not collateral inhibition is strengthened or weakened between or within GPe neuron subtypes following dopamine depletion is unknown. Due to the expansive architecture of arkypallidal input to striatum and potential for widespread inhibitory entrainment of prototypic GPe neurons following dopamine depletion, widespread synchronous lateral disinhibition of arkypallidal neurons could have profound effects on striatal activity especially when the potential for coincident (or just barely subsequent) disinhibition of STN-GPe neurons is taken into account. Anecdotal evidence from our recordings suggests that STN and PV GPe neurons coordinate the activity of putative arkypallidal GPe neurons (those neurons firing in-phase with cortical SWA; Mallet et al., 2012) at least in dopamine-depleted mice where there is some basis for arkypallidal identification by firing pattern; optogenetic inhibition of PV GPe neurons can disinhibit these neurons producing more tonic firing during prolonged PV GPe neuron inhibition; optogenetically suppressing STN activity can reduce their firing rate during the active component of cortical SWA in some cases rendering them nearly silent for the duration of STN inhibition.

4.4: Patterning of STN neuron activity

In some ways, our STN results were the most surprising. There are few metrics of abnormal basal ganglia activity that are consistent signatures of parkinsonism across PD models, but of them all, STN hyperactivity and/or increased burstiness are among the most reliably cited in monkey and rat studies (Bergman et al., 1994; Magill et al., 2001; Soares et al., 2004; Walters et al., 2007; Mallet et al., 2008b; Sanders et al., 2013; Sharott et al., 2014). Additionally, it has been suggested that enhanced hyperdirect pathway activity contributes to hyperactivity and oscillatory entrainment of the basal ganglia in PD and its models (Moran et al., 2011; Tachibana et al., 2011; Pavlides et al., 2015). In both dopamine-intact and -depleted mice, we observed that STN neurons fired at approximately the same rate but that their phase locking to cortical SWA was reduced following dopamine depletion. Some recent findings in mice, rats, and monkeys seem to make sense of this in that it has been shown that the hyperdirect pathway degenerates significantly following dopamine depletion (Mathai et al., 2015; Chu et al., 2017; Wang et al., 2018) and at least in mice and rats, STN neurons lose their autonomous activity (Zhu et al., 2002; McIver et al., 2019). In our experiments, optogenetic inhibition of PV GPe neurons greatly reduced the remaining phase locking of STN neurons in dopamine depleted mice well below what was observed under similar conditions in dopamine-intact mice. The phase locking that remained in dopamine-intact mice during PV GPe neuron inhibition may well represent intact hyperdirect input to STN. The enhanced dependence on GPe input for phase locked activity in STN may be due to the combination of loss of hyperdirect input and the proliferation of GPe-STN synapses in the dopamine depleted state (Fan et al., 2012; Atherton et al., 2013). Together, these observations may also account for the lack of excessive STN activity during cortical ACT

in dopamine-depleted mice which mirrors the results from the few STN recordings performed in awake rats (Delaville et al., 2015).

Cortically driven STN activity is associated with the cessation of ongoing actions, stalling of planned actions, and may also be involved in conflict resolution between planned actions (Baunez et al., 1995; Nambu et al., 2002; Aron and Poldrack, 2006; Isoda and Hikosaka, 2008; Engel and Fries, 2010; Schmidt et al., 2013; Jahanshahi et al., 2015; Zavala et al., 2015). Electrical stimulation (Schor and Nelson, 2019), optogenetic excitation of STN neurons or cortico-STN terminals (Gradinaru et al., 2009; Sanders and Jaeger, 2016), and chemogenetic restoration of STN autonomous activity (McIver et al., 2019) all ameliorate akinetic features of parkinsonism in dopamine-depleted mice. Further, STN-localized knockout of NMDAR expression prior to dopamine depletion prevents GPe-STN synapse proliferation (Chu et al., 2015), hyperdirect pathway degeneration (Chu et al., 2017), loss of autonomous STN activity (McIver et al., 2019), and ameliorated akinetic motor symptoms (Chu et al., 2017). Taken together these findings suggest that maintained STN autonomous activity and corticosubthalamic input in the presence of unaugmented pallidosubthalamic transmission is sufficient to overcome the upstream effects of profound dopamine depletion that otherwise result in akinesia. These factors also have in common that they are likely to reduce the phase offset of GPe and STN that likely lead to abnormal patterning in the output nuclei. Counterintuitively, recordings in rats suggest that STN activity becomes more coherent with motor cortical activity during movement only following dopamine depletion (Delaville et al., 2015); however, these recordings were performed during forced walking and whether or not this phenomenon can be observed in mice is unknown.

4.5: STN's role in GPe patterning

GPe-STN interactions have been proposed to underly, amplify, or otherwise contribute to abnormal entrainment of basal ganglia oscillatory activity (Moran et al., 2011; Tachibana et al., 2011; Shouno et al., 2017). Prior experiments in monkeys and rats (Kita and Kita, 2011a; Tachibana et al., 2011) have approached the issue using pharmacological agents injected intracerebrally. Depending on the time points recorded post-injection, a variety of results can be achieved through manipulations of this kind as well as having non-specific effects. Here we tested STN neurons' contribution to GPe activity patterning in mice during cortical SWA using optogenetic inhibition. We found that inhibiting STN neurons in dopamine-depleted mice (and occasionally in dopamine-intact mice) induced or exaggerated antiphase firing of GPe neurons relative to cortical SWA. This suggests that STN opposes rather than facilitates antiphase patterning of GPe neurons during cortical SWA. In dopamine-intact mice, the interaction of striatopallidal inhibition colliding with cortically or autonomously driven STN input at the level of GPe likely serves an active function in action selection. However, in the dopamine-depleted state where somatotopic specificity in the basal ganglia is degraded (Bergman et al., 1994; Cho et al., 2002; Pessiglione et al., 2005; Leblois et al., 2006; Mallet et al., 2008b; Nambu, 2011; Ketzef et al., 2017) and activity is more homogenous within structures the fine-scale nature of these interactions may be stunted. Whether STN's corrective influence on striatopallidal entrainment applies in higher frequency contexts would be of great interest because this empirical finding runs counter to prior modeling predictions and theories of basal ganglia dysfunction following dopamine depletion (Moran et al., 2011; Tachibana et al., 2011; Pavlides et al., 2015; Shouno et al., 2017). Further, how convergent STN and GPe inputs contribute to

excessive patterning known to take place at the level of the output nuclei (Smith et al., 1998; Willard et al., 2019) remains an unanswered question. Because each of these structures has multiple projection targets, the recent advent of somatically and synaptically targeted optical methods of inhibition (Shu et al., 2011; Lin et al., 2013; Hermann et al., 2015; Mahn et al., 2018) with more reversible and temporally sensitive options on the horizon open the door to more meaningful interrogation of network interactions.

4.6: Concluding remarks

The work presented here represents another example of deviation from the rate model of basal ganglia function in that the rate changes of upstream structures are not uniformly imprinted on downstream structures. Rather, the configuration of circuit elements that follows dopamine depletion imparts excessive firing of D2-SPNs and aberrant patterning of PV GPe neurons that have been shown by others to be transmitted to the output nuclei (Lobb and Jaeger, 2015; Willard et al., 2019). Further, homeostatic alterations to STN neuron activity following dopamine depletion (Fan et al., 2012; Chu et al., 2017; McIver et al., 2019) may reduce the efficacy of cortico-STN-GPe input to resist these phasic patterning changes. The work presented here, tests several predictions of basal ganglia function, in some cases validating, and other cases deviating from prior studies and should serve as a bridge connecting the rich field of rat studies and current and future mouse-based experiments.

The anesthetized paradigm applied here may continue to be useful to interrogate linear information transmission from cortically generated slow oscillations throughout defined circuitry and provide some measure of transmission strength in dopamine-intact and -depleted states, but

this cannot be taken to map cleanly onto awake-behaving contexts in large part due to a fundamental lack of information about exactly what the basal ganglia are for and exactly what each component's contributions are. To make the transition to analyzing basal ganglia circuit activity's contribution to action selection and initiation, we must dispense with the assumption of an order of operations originating in the cortex and propagating linearly through the circuit. GPe and STN project to cortex (Degos et al., 2008; Koshimizu et al., 2013; Saunders et al., 2015); brainstem motor areas project to every nucleus of the basal ganglia (transmitting both glutamate and acetylcholine) (Mena-Segovia et al., 2004; Dautan et al., 2014; Mena-Segovia, 2016); thalamic feedback accounts for a significant portion of glutamatergic input to striatum and may also contribute to D1-/D2-SPN imbalance following dopamine depletion (Parker et al., 2016; Tanimura et al., 2019); there are striatonigralstriatal loops theorized to spiral from medial to lateral striatum/SN (Haber et al., 2000). The idea that cortico-basal ganglia-thalamocortical loops predominate action selection and have a role in action initiation need to be revisited and proven conclusively. The variability in the response of cortical and nigral neurons to even synchronous activation of direct or indirect pathways (Freeze et al., 2013; Oldenburg and Sabatini, 2015) validates this mode of thinking. What can be stated with relative safety is that there is a tremendous amount of variability in single neuron responses to various behaviors/tasks in normal animals and activity becomes more homogenous following dopamine depletion; effective therapies decorrelate activity in a network that has deteriorated into more stereotyped widespread patterns that lead to movement disorders; we are only beginning to have the tools to approach an understanding of the basal ganglia.

References

- Abbas AI, Sundiang MJM, Henoch B, Morton MP, Bolkan SS, Park AJ, Harris AZ, Kellendonk C, Gordon JA (2018) Somatostatin interneurons facilitate hippocampal-prefrontal synchrony and prefrontal spatial encoding. *Neuron* 100:926-939.
- Abdi A, Mallet N, Mohamed FY, Sharott A, Dodson PD, Nakamura KC, Suri S, Avery SV, Larvin JT, Garas FN, Garas SN, Vinciati F, Morin S, Bezard E, Baufreton J, Magill PJ (2015) Prototypic and arkypallidal neurons in the dopamine-intact external globus pallidus. *J Neurosci* 35:6667-6688.
- Abecassis ZA, Berceau BL, Win PH, Garcia D, Xenias HS, Cui Q, Pamukcu A, Cherian S, Hernandez VM, Chon U, Lim BK, Kim Y, Justice NJ, Awatramani R, Hooks BM, Gerfen CR, Boca SM, Chan CS (2020) Npas1(+)-Nkx2.1(+) neurons are an integral part of the cortico-pallido-cortical loop. *J Neurosci* 40:743-768.
- Adamos DA, Laskaris NA, Kosmidis EK, Theophilidis G (2010) NASS: an empirical approach to spike sorting with overlap resolution based on a hybrid noise-assisted methodology. *J Neurosci Methods* 190:129-142.
- Albin RL, Young AB, Penney JB (1989) The functional anatomy of basal ganglia disorders. *Trends Neurosci* 12:366-375.
- Alexander GE, Crutcher MD (1990) Functional architecture of basal ganglia circuits: neural substrates of parallel processing. *Trends Neurosci* 13:266-271.
- Aranha MM, Santos DM, Xavier JM, Low WC, Steer CJ, Sola S, Rodrigues CM (2010) Apoptosis-associated microRNAs are modulated in mouse, rat and human neural differentiation. *BMC Genomics* 11:514.

- Aron AR, Poldrack RA (2006) Cortical and subcortical contributions to stop signal response inhibition: role of the subthalamic nucleus. *J Neurosci* 26:2424-2433.
- Assaf F, Schiller Y (2019) A chemogenetic approach for treating experimental Parkinson's disease. *Mov Disord* 34:469-479.
- Assous M, Tepper JM (2019) Excitatory extrinsic afferents to striatal interneurons and interactions with striatal microcircuitry. *Eur J Neurosci* 49:593-603.
- Atherton JF, Menard A, Urbain N, Bevan MD (2013) Short-term depression of external globus pallidus-subthalamic nucleus synaptic transmission and implications for patterning subthalamic activity. *J Neurosci* 33:7130-7144.
- Averbeck BB, Lehman J, Jacobson M, Haber SN (2014) Estimates of projection overlap and zones of convergence within frontal-striatal circuits. *J Neurosci* 34:9497-9505.
- Ballion B, Frenois F, Zold CL, Chetrit J, Murer MG, Gonon F (2009) D2 receptor stimulation, but not D1, restores striatal equilibrium in a rat model of parkinsonism. *Neurobiol Dis* 35:376-384.
- Bamford NS, Zhang H, Schmitz Y, Wu NP, Cepeda C, Levine MS, Schmauss C, Zakharenko SS, Zablow L, Sulzer D (2004) Heterosynaptic dopamine neurotransmission selects sets of corticostriatal terminals. *Neuron* 42:653-663.
- Basco D, Nicchia GP, D'Alessandro A, Zolla L, Svelto M, Frigeri A (2011) Absence of aquaporin-4 in skeletal muscle alters proteins involved in bioenergetic pathways and calcium handling. *PLoS One* 6:e19225.
- Baufreton J, Atherton JF, Surmeier DJ, Bevan MD (2005) Enhancement of excitatory synaptic integration by GABAergic inhibition in the subthalamic nucleus. *J Neurosci* 25:8505-8517.

- Baunez C, Nieoullon A, Amalric M (1995) In a rat model of parkinsonism, lesions of the subthalamic nucleus reverse increases of reaction time but induce a dramatic premature responding deficit. *J Neurosci* 15:6531-6541.
- Bergman H, Wichmann T, Karmon B, DeLong MR (1994) The primate subthalamic nucleus. II. Neuronal activity in the MPTP model of parkinsonism. *J Neurophysiol* 72:507-520.
- Bevan MD, Booth PAC, Eaton SA, Bolam JP (1998) Selective innervation of neostriatal interneurons by a subclass of neuron in the globus pallidus of the rat. *J Neurosci* 18:9438-9452.
- Bevan MD, Magill PJ, Terman D, Bolam JP, Wilson CJ (2002) Move to the rhythm: oscillations in the subthalamic nucleus-external globus pallidus network. *Trends Neurosci* 25:525-531.
- Blesa J, Trigo-Damas I, Dileone M, Del Rey NL, Hernandez LF, Obeso JA (2017) Compensatory mechanisms in Parkinson's disease: Circuits adaptations and role in disease modification. *Exp Neurol* 298:148-161.
- Bokil H, Andrews P, Kulkarni JE, Mehta S, Mitra PP (2010) Chronux: A platform for analyzing neural signals. *J Neurosci Methods* 192:146-151.
- Bolam JP, Ellender TJ (2016) Histamine and the striatum. *Neuropharmacology* 106:74-84.
- Brazhnik E, Novikov N, McCoy AJ, Cruz AV, Walters JR (2014) Functional correlates of exaggerated oscillatory activity in basal ganglia output in hemiparkinsonian rats. *Exp Neurol* 261:563-577.
- Brazhnik E, McCoy AJ, Novikov N, Hatch CE, Walters JR (2016) Ventral medial thalamic nucleus promotes synchronization of increased high beta oscillatory activity in the basal ganglia-thalamocortical network of the hemiparkinsonian rat. *J Neurosci* 36:4196-4208.

- Brown P, Oliviero A, Mazzone P, Insola A, Tonali P, Di Lazzaro V (2001) Dopamine dependency of oscillations between subthalamic nucleus and pallidum in Parkinson's disease. *J Neurosci* 21:1033-1038.
- Burke DA, Rotstein HG, Alvarez VA (2017) Striatal local circuitry: a new framework for lateral inhibition. *Neuron* 96:267-284.
- Cazorla M, de Carvalho FD, Chohan MO, Shegda M, Chuhma N, Rayport S, Ahmari SE, Moore H, Kellendonk C (2014) Dopamine D2 receptors regulate the anatomical and functional balance of basal ganglia circuitry. *Neuron* 81:153-164.
- Chan CS, Glajch KE, Gertler TS, Guzman JN, Mercer JN, Lewis AS, Goldberg AB, Tkatch T, Shigemoto R, Fleming SM, Chetkovich DM, Osten P, Kita H, Surmeier DJ (2011) HCN channelopathy in external globus pallidus neurons in models of parkinson's disease. *Nat Neurosci* 14:85-94.
- Chang HT, Wilson CJ, Kitai ST (1981) Single neostriatal efferent axons in the globus pallidus: a light and electron microscopic study. *Science* 213:915-918.
- Charalampopoulos I, Dermitzaki E, Vardouli L, Tsatsanis C, Stournaras C, Margioris AN, Gravanis A (2005) Dehydroepiandrosterone sulfate and allopregnanolone directly stimulate catecholamine production via induction of tyrosine hydroxylase and secretion by affecting actin polymerization. *Endocrinology* 146:3309-3318.
- Chazalon M, Paredes-Rodriguez E, Morin S, Martinez A, Cristovao-Ferreira S, Vaz S, Sebastiao A, Panatier A, Boue-Grabot E, Miguelez C, Baufreton J (2018) GAT-3 dysfunction generates tonic inhibition in external globus pallidus neurons in parkinsonian rodents. *Cell Rep* 23:1678-1690.

- Chiken S, Nambu A (2016) Mechanism of Deep Brain Stimulation: Inhibition, Excitation, or Disruption? *Neuroscientist* 22:313-322.
- Cho J, Duke D, Manzino L, Sonsalla PK, West MO (2002) Dopamine depletion causes fragmented clustering of neurons in the sensorimotor striatum: evidence of lasting reorganization of corticostriatal input. *J Comp Neurol* 452:24-37.
- Chow BY, Han X, Dobry AS, Qian X, Chuong AS, Li M, Henninger MA, Belfort GM, Lin Y, Monahan PE, Boyden ES (2010) High-performance genetically targetable optical neural silencing by light-driven proton pumps. *Nature* 463:98-102.
- Chu HY, Atherton JF, Wokosin D, Surmeier DJ, Bevan MD (2015) Heterosynaptic regulation of external globus pallidus inputs to the subthalamic nucleus by the motor cortex. *Neuron* 85:364-376.
- Chu HY, McIver EL, Kovaleski RF, Atherton JF, Bevan MD (2017) Loss of hyperdirect pathway cortico-subthalamic inputs following degeneration of midbrain dopamine neurons. *Neuron* 95:1306-1318.e1305.
- Cui G, Jun SB, Jin X, Pham MD, Vogel SS, Lovinger DM, Costa RM (2013) Concurrent activation of striatal direct and indirect pathways during action initiation. *Nature* 494:238-242.
- Cui Q, Du X, Lilascharoen V, Pamukcu A, Garcia D, Berceau B, Hong D, Chalasani V, Lim B, Chan S Dorsolateral striatum regulates movement oppositely to dorsomedial striatum via complex striatopallidal subcircuitries. Program No. 667.21. 2019 Neuroscience Meeting Planner Chicago, IL: Society for Neuroscience, 2019 Online.

- Dautan D, Huerta-Ocampo I, Witten IB, Deisseroth K, Bolam JP, Gerdjikov T, Mena-Segovia J (2014) A major external source of cholinergic innervation of the striatum and nucleus accumbens originates in the brainstem. *J Neurosci* 34:4509-4518.
- Deffains M, Iskhakova L, Katabi S, Haber SN, Israel Z, Bergman H (2016) Subthalamic, not striatal, activity correlates with basal ganglia downstream activity in normal and parkinsonian monkeys. *Elife* 5:e16443.
- Degos B, Deniau JM, Le Cam J, Mailly P, Maurice N (2008) Evidence for a direct subthalamo-cortical loop circuit in the rat. *Eur J Neurosci* 27:2599-2610.
- Delaville C, McCoy AJ, Gerber CM, Cruz AV, Walters JR (2015) Subthalamic Nucleus Activity in the Awake Hemiparkinsonian Rat: Relationships with Motor and Cognitive Networks. *J Neurosci* 35:6918-6930.
- DeLong MR (1990) Primate models of movement disorders of basal ganglia origin. *Trends Neurosci* 13:281-285.
- Deng YP, Lei WL, Reiner A (2006) Differential perikaryal localization in rats of D1 and D2 dopamine receptors on striatal projection neuron types identified by retrograde labeling. *J Chem Neuroanat* 32:101-116.
- Devergnas A, Pittard D, Bliwise D, Wichmann T (2014) Relationship between oscillatory activity in the cortico-basal ganglia network and parkinsonism in MPTP-treated monkeys. *Neurobiol Dis* 68:156-166.
- Dobbs LK, Kaplan AR, Lemos JC, Matsui A, Rubinstein M, Alvarez VA (2016) Dopamine Regulation of Lateral Inhibition between Striatal Neurons Gates the Stimulant Actions of Cocaine. *Neuron* 90:1100-1113.

- Dodson PD, Larvin JT, Duffell JM, Garas FN, Doig NM, Kessar N, Duguid IC, Bogacz R, Butt SJB, Magill PJ (2015) Distinct developmental origins manifest in the specialized encoding of movement by adult neurons of the external globus pallidus. *Neuron* 86:501-513.
- Engel AK, Fries P (2010) Beta-band oscillations — signalling the status quo? *Curr Opin Neurobiol* 20:156-165.
- Escande MV, Taravini IR, Zold CL, Belforte JE, Murer MG (2016) Loss of Homeostasis in the Direct Pathway in a Mouse Model of Asymptomatic Parkinson's Disease. *J Neurosci* 36:5686-5698.
- Eusebio A, Cagnan H, Brown P (2012) Does suppression of oscillatory synchronisation mediate some of the therapeutic effects of DBS in patients with Parkinson's disease? *Front Integr Neurosci* 6:47.
- Faivre F, Joshi A, Bezard E, Barrot M (2019) The hidden side of Parkinson's disease: Studying pain, anxiety and depression in animal models. *Neurosci Biobehav Rev* 96:335-352.
- Fan KY, Baufreton J, Surmeier DJ, Chan CS, Bevan MD (2012) Proliferation of external globus pallidus-subthalamic nucleus synapses following degeneration of midbrain dopamine neurons. *J Neurosci* 32:13718-13728.
- Frank MJ, Samanta J, Moustafa AA, Sherman SJ (2007) Hold your horses: impulsivity, deep brain stimulation, and medication in parkinsonism. *Science* 318:1309-1312.
- Freeze BS, Kravitz AV, Hammack N, Berke JD, Kreitzer AC (2013) Control of basal ganglia output by direct and indirect pathway projection neurons. *J Neurosci* 33:18531-18539.

- Fu L, Shi Z, Luo G, Tu W, Wang X, Fang Z, Li X (2014) Multiple microRNAs regulate human FOXP2 gene expression by targeting sequences in its 3' untranslated region. *Mol Brain* 7:71.
- Galvan A, Smith Y (2011) The primate thalamostriatal systems: Anatomical organization, functional roles and possible involvement in Parkinson's disease. *Basal Ganglia* 1:179-189.
- Gerfen CR, Surmeier DJ (2011) Modulation of striatal projection systems by dopamine. *Annu Rev Neurosci* 34:441-466.
- Gerfen CR, Bolam JP (2016) The neuroanatomical organization of the basal ganglia. In: *Handbook of basal ganglia structure and function, 2nd Edition* (Seiner H, Tesng KY, eds), pp 2-32. Amsterdam: Elsevier/Academic Press.
- Gerfen CR, Engber TM, Mahan LC, Susel Z, Chase TN, Monsma FJ, Jr., Sibley DR (1990) D1 and D2 dopamine receptor-regulated gene expression of striatonigral and striatopallidal neurons. *Science* 250:1429-1432.
- Goldberg JH, Farries MA, Fee MS (2013) Basal ganglia output to the thalamus: still a paradox. *Trends Neurosci* 36:695-705.
- Gradinaru V, Mogri M, Thompson KR, Henderson JM, Deisseroth K (2009) Optical deconstruction of parkinsonian neural circuitry. *Science* 324:354-359.
- Grillner S, Robertson B (2015) The basal ganglia downstream control of brainstem motor centres--an evolutionarily conserved strategy. *Curr Opin Neurobiol* 33:47-52.
- Groves PM (1983) A theory of the functional organization of the neostriatum and the neostriatal control of voluntary movement. *Brain Res* 286:109-132.

- Guridi J, Alegre M (2017) Oscillatory activity in the basal ganglia and deep brain stimulation. *Mov Disord* 32:64-69.
- Haber SN, Fudge JL, McFarland NR (2000) Striatonigrostriatal pathways in primates form an ascending spiral from the shell to the dorsolateral striatum. *J Neurosci* 20:2369-2382.
- Hallworth NE, Bevan MD (2005) Globus pallidus neurons dynamically regulate the activity pattern of subthalamic nucleus neurons through the frequency-dependent activation of postsynaptic GABAA and GABAB receptors. *J Neurosci* 25:6304-6315.
- Hammond C, Bergman H, Brown P (2007) Pathological synchronization in Parkinson's disease: networks, models and treatments. *Trends Neurosci* 30:357-364.
- Hazrati LN, Parent A (1992) The striatopallidal projection displays a high degree of anatomical specificity in the primate. *Brain Res* 592:213-227.
- Hedreen JC, DeLong MR (1991) Organization of striatopallidal, striatonigral, and nigrostriatal projections in the macaque. *J Comp Neurol* 304:569-595.
- Heimer G, Bar-Gad I, Goldberg JA, Bergman H (2002) Dopamine replacement therapy reverses abnormal synchronization of pallidal neurons in the 1-methyl-4-phenyl-1,2,3,6-tetrahydropyridine primate model of parkinsonism. *J Neurosci* 22:7850-7855.
- Hermann A, Liewald JF, Gottschalk A (2015) A photosensitive degron enables acute light-induced protein degradation in the nervous system. *Curr Biol* 25:R749-750.
- Hernandez VM, Hegeman DJ, Cui Q, Kolver DA, Fiske MP, Glajch KE, Pitt JE, Huang TY, Justice NJ, Chan CS (2015) Parvalbumin⁺ neurons and Npas1⁺ neurons are distinct neuron classes in the mouse external globus pallidus. *J Neurosci* 35:11830-11847.
- Higley MJ, Sabatini BL (2010) Competitive regulation of synaptic Ca²⁺ influx by D2 dopamine and A2A adenosine receptors. *Nat Neurosci* 13:958-966.

- Hirtz D, Thurman DJ, Gwinn-Hardy K, Mohamed M, Chaudhuri AR, Zalutsky R (2007) How common are the "common" neurologic disorders? *Neurology* 68:326-337.
- Holgado AJ, Terry JR, Bogacz R (2010) Conditions for the generation of beta oscillations in the subthalamic nucleus-globus pallidus network. *J Neurosci* 30:12340-12352.
- Holm S (1997) A Simple Sequentially Rejective Multiple Test Procedure. *Scandinavian Journal of Statistics* 6:65-70.
- Inase M, Buford JA, Anderson ME (1996) Changes in the control of arm position, movement, and thalamic discharge during local inactivation in the globus pallidus of the monkey. *J Neurophysiol* 75:1087-1104.
- Isoda M, Hikosaka O (2008) Role for subthalamic nucleus neurons in switching from automatic to controlled eye movement. *J Neurosci* 28:7209-7218.
- Jahanshahi M, Obeso I, Rothwell JC, Obeso JA (2015) A fronto-striato-subthalamic-pallidal network for goal-directed and habitual inhibition. *Nat Rev Neurosci* 16:719-732.
- Jouve L, Salin P, Melon C, Kerkerian-Le Goff L (2010) Deep brain stimulation of the center median-parafascicular complex of the thalamus has efficient anti-parkinsonian action associated with widespread cellular responses in the basal ganglia network in a rat model of Parkinson's disease. *J Neurosci* 30:9919-9928.
- Kalia LV, Lang AE (2015) Parkinson's disease. *Lancet* 386:896-912.
- Keeler JF, Pretsell DO, Robbins TW (2014) Functional implications of dopamine D1 vs. D2 receptors: A 'prepare and select' model of the striatal direct vs. indirect pathways. *Neuroscience* 282:156-175.

- Ketzef M, Spigolon G, Johansson Y, Bonito-Oliva A, Fisone G, Silberberg G (2017) Dopamine depletion impairs bilateral sensory processing in the striatum in a pathway-dependent manner. *Neuron* 94:855-865.
- Kita H, Kita T (2011a) Role of Striatum in the Pause and Burst Generation in the Globus Pallidus of 6-OHDA-Treated Rats. *Front Syst Neurosci* 5:42.
- Kita H, Kita T (2011b) Cortical stimulation evokes abnormal responses in the dopamine-depleted rat basal ganglia. *J Neurosci* 31:10311-10322.
- Klaus A, Alves da Silva J, Costa RM (2019) What, If, and When to Move: Basal Ganglia Circuits and Self-Paced Action Initiation. *Annu Rev Neurosci* 42:459-483.
- Kordower JH, Olanow CW, Dodiya HB, Chu Y, Beach TG, Adler CH, Halliday GM, Bartus RT (2013) Disease duration and the integrity of the nigrostriatal system in Parkinson's disease. *Brain* 136:2419-2431.
- Koshimizu Y, Fujiyama F, Nakamura KC, Furuta T, Kaneko T (2013) Quantitative analysis of axon bouton distribution of subthalamic nucleus neurons in the rat by single neuron visualization with a viral vector. *J Comp Neurol* 521:2125-2146.
- Kotzadimitriou D, Nissen W, Paizs M, Newton K, Harrison PJ, Paulsen O, Lamsa K (2018) Neuregulin 1 Type I Overexpression Is Associated with Reduced NMDA Receptor-Mediated Synaptic Signaling in Hippocampal Interneurons Expressing PV or CCK. *eNeuro* 5:ENEURO.0418-0417.2018.
- Kovaleski RF, Callahan JW, Chazalon M, Wokosin DL, Baufreton J, Bevan MD (2020) Dysregulation of external globus pallidus-subthalamic nucleus network dynamics in parkinsonian mice during cortical slow-wave activity and activation. *The Journal of Physiology*.

- Kravitz AV, Freeze BS, Parker PR, Kay K, Thwin MT, Deisseroth K, Kreitzer AC (2010) Regulation of parkinsonian motor behaviours by optogenetic control of basal ganglia circuitry. *Nature* 466:622-626.
- Kuhn AA, Tsui A, Aziz T, Ray N, Brucke C, Kupsch A, Schneider GH, Brown P (2009) Pathological synchronisation in the subthalamic nucleus of patients with Parkinson's disease relates to both bradykinesia and rigidity. *Exp Neurol* 215:380-387.
- Le Van Quyen M, Foucher J, Lachaux J, Rodriguez E, Lutz A, Martinerie J, Varela FJ (2001) Comparison of Hilbert transform and wavelet methods for the analysis of neuronal synchrony. *J Neurosci Methods* 111:83-98.
- Leblois A, Boraud T, Meissner W, Bergman H, Hansel D (2006) Competition between feedback loops underlies normal and pathological dynamics in the basal ganglia. *J Neurosci* 26:3567-3583.
- Leblois A, Meissner W, Bioulac B, Gross CE, Hansel D, Boraud T (2007) Late emergence of synchronized oscillatory activity in the pallidum during progressive Parkinsonism. *Eur J Neurosci* 26:1701-1713.
- Lemos JC, Friend DM, Kaplan AR, Shin JH, Rubinstein M, Kravitz AV, Alvarez VA (2016) Enhanced GABA transmission drives bradykinesia following loss of dopamine D2 receptor signaling. *Neuron* 90:824-838.
- Lerner TN, Shilyansky C, Davidson TJ, Evans KE, Beier KT, Zalocusky KA, Crow AK, Malenka RC, Luo L, Tomer R, Deisseroth K (2015) Intact-Brain Analyses Reveal Distinct Information Carried by SNc Dopamine Subcircuits. *Cell* 162:635-647.

- Li Q, Ke Y, Chan DCW, Qian ZM, Yung KKL, Ko H, Arbuthnott GW, Yung WH (2012) Therapeutic Deep Brain Stimulation in Parkinsonian Rats Directly Influences Motor Cortex. *Neuron* 76:1030-1041.
- Lin JY, Sann SB, Zhou K, Nabavi S, Proulx CD, Malinow R, Jin Y, Tsien RY (2013) Optogenetic inhibition of synaptic release with chromophore-assisted light inactivation (CALI). *Neuron* 79:241-253.
- Lobb CJ, Jaeger D (2015) Bursting activity of substantia nigra pars reticulata neurons in mouse parkinsonism in awake and anesthetized states. *Neurobiol Dis* 75:177-185.
- Lu Y, Zhong C, Wang L, Wei P, He W, Huang K, Zhang Y, Zhan Y, Feng G, Wang L (2016) Optogenetic dissection of ictal propagation in the hippocampal-entorhinal cortex structures. *Nat Commun* 7:10962.
- Maccione A, Gandolfo M, Massobrio P, Novellino A, Martinoia S, Chiappalone M (2009) A novel algorithm for precise identification of spikes in extracellularly recorded neuronal signals. *J Neurosci Methods* 177:241-249.
- Magill PJ, Bolam JP, Bevan MD (2001) Dopamine regulates the impact of the cerebral cortex on the subthalamic nucleus-globus pallidus network. *Neuroscience* 106:313-330.
- Mahn M, Gibor L, Patil P, Cohen-Kashi Malina K, Oring S, Printz Y, Levy R, Lampl I, Yizhar O (2018) High-efficiency optogenetic silencing with soma-targeted anion-conducting channelrhodopsins. *Nat Commun* 9:4125.
- Mailly P, Aliane V, Groenewegen HJ, Haber SN, Deniau JM (2013) The rat prefrontostriatal system analyzed in 3D: evidence for multiple interacting functional units. *J Neurosci* 33:5718-5727.

- Mallet N, Ballion B, Le Moine C, Gonon F (2006) Cortical inputs and GABA interneurons imbalance projection neurons in the striatum of parkinsonian rats. *J Neurosci* 26:3875-3884.
- Mallet N, Delgado L, Chazalon M, Miguelez C, Baufreton J (2019) Cellular and Synaptic Dysfunctions in Parkinson's Disease: Stepping out of the Striatum. *Cells* 8.
- Mallet N, Pogosyan A, Marton LF, Bolam JP, Brown P, Magill PJ (2008a) Parkinsonian beta oscillations in the external globus pallidus and their relationship with subthalamic nucleus activity. *J Neurosci* 28:14245-14258.
- Mallet N, Pogosyan A, Sharott A, Csicsvari J, Bolam JP, Brown P, Magill PJ (2008b) Disrupted dopamine transmission and the emergence of exaggerated beta oscillations in subthalamic nucleus and cerebral cortex. *J Neurosci* 28:4795-4806.
- Mallet N, Schmidt R, Leventhal D, Chen F, Amer N, Boraud T, Berke JD (2016) Arky pallidal Cells Send a Stop Signal to Striatum. *Neuron* 89:308-316.
- Mallet N, Micklem BR, Henny P, Brown MT, Williams C, Bolam JP, Nakamura KC, Magill PJ (2012) Dichotomous organization of the external globus pallidus. *Neuron* 74:1075-1086.
- Maltese M, March JR, Bashaw AG, Tritsch NX (2019) Dopamine modulates the size of striatal projection neuron ensembles. *bioRxiv*.
- Markowitz JE, Gillis WF, Beron CC, Neufeld SQ, Robertson K, Bhagat ND, Peterson RE, Peterson E, Hyun M, Linderman SW, Sabatini BL, Datta SR (2018) The striatum organizes 3D behavior via moment-to-moment action selection. *Cell* 174:44-58.
- Mastro KJ, Bouchard RS, Holt HAK, Gittis AH (2014) Transgenic mouse lines subdivide external segment of the globus pallidus (GPe) neurons and reveal distinct GPe output pathways. *J Neurosci* 34:2087-2099.

- Mastro KJ, Zitelli KT, Willard AM, Leblanc KH, Kravitz AV, Gittis AH (2017) Cell-specific pallidal intervention induces long-lasting motor recovery in dopamine-depleted mice. *Nat Neurosci* 20:815-823.
- Mathai A, Ma Y, Pare JF, Villalba RM, Wichmann T, Smith Y (2015) Reduced cortical innervation of the subthalamic nucleus in MPTP-treated parkinsonian monkeys. *Brain* 138:946-962.
- McConnell GC, So RQ, Hilliard JD, Lopomo P, Grill WM (2012) Effective deep brain stimulation suppresses low-frequency network oscillations in the basal ganglia by regularizing neural firing patterns. *J Neurosci* 32:15657-15668.
- McGregor MM, Nelson AB (2019) Circuit Mechanisms of Parkinson's Disease. *Neuron* 101:1042-1056.
- McIver EL, Atherton JF, Chu HY, Cosgrove KE, Kondapalli J, Wokosin D, Surmeier DJ, Bevan MD (2019) Maladaptive downregulation of autonomous subthalamic nucleus activity following the loss of midbrain dopamine neurons. *Cell Reports* 28:992-1002.
- Mena-Segovia J (2016) Structural and functional considerations of the cholinergic brainstem. *J Neural Transm (Vienna)* 123:731-736.
- Mena-Segovia J, Bolam JP, Magill PJ (2004) Pedunculopontine nucleus and basal ganglia: distant relatives or part of the same family? *Trends Neurosci* 27:585-588.
- Miguelé C, Morin S, Martinez A, Goillandeau M, Bezard E, Bioulac B, Baufreton J (2012) Altered pallido-pallidal synaptic transmission leads to aberrant firing of globus pallidus neurons in a rat model of Parkinson's disease. *J Physiol* 590:5861-5875.
- Mink JW, Thach WT (1993) Basal ganglia intrinsic circuits and their role in behavior. *Curr Opin Neurobiol* 3:950-957.

- Moran RJ, Mallet N, Litvak V, Dolan RJ, Magill PJ, Friston KJ, Brown P (2011) Alterations in brain connectivity underlying beta oscillations in parkinsonism. *PLoS Comp Biol* 7.
- Muralidharan A, Jensen AL, Connolly A, Hendrix CM, Johnson MD, Baker KB, Vitek JL (2016) Physiological changes in the pallidum in a progressive model of Parkinson's disease: Are oscillations enough? *Exp Neurol* 279:187-196.
- Nambu A (2011) Somatotopic organization of the primate basal ganglia. *Front Neuroanat* 5:26.
- Nambu A, Tokuno H, Takada M (2002) Functional significance of the cortico-subthalamo-pallidal 'hyperdirect' pathway. *Neurosci Res* 43:111-117.
- Ni ZG, Bouali-Benazzouz R, Gao DM, Benabid AL, Benazzouz A (2001) Time-course of changes in firing rates and firing patterns of subthalamic nucleus neuronal activity after 6-OHDA-induced dopamine depletion in rats. *Brain Res* 899:142-147.
- Noether GE (1987) Sample size determination for some common nonparametric tests. *J Am Stat Assoc* 82:645-647.
- Nogueira LT, Costa DV, Gomes AS, Martins CS, Silva AM, Coelho-Aguiar JM, Castelucci P, Lima-Junior RC, Leitao RF, Moura-Neto V, Brito GA (2017) The involvement of mast cells in the irinotecan-induced enteric neurons loss and reactive gliosis. *J Neuroinflammation* 14:79.
- Oldenburg IA, Sabatini BL (2015) Antagonistic but Not Symmetric Regulation of Primary Motor Cortex by Basal Ganglia Direct and Indirect Pathways. *Neuron* 86:1174-1181.
- Pan MK, Kuo SH, Tai CH, Liou JY, Pei JC, Chang CY, Wang YM, Liu WC, Wang TR, Lai WS, Kuo CC (2016) Neuronal firing patterns outweigh circuitry oscillations in parkinsonian motor control. *J Clin Invest* 126:4516-4526.

- Parent M, Parent A (2004) The pallidofugal motor fiber system in primates. *Parkinsonism Relat Disord* 10:203-211.
- Parent M, Wallman MJ, Gagnon D, Parent A (2011) Serotonin innervation of basal ganglia in monkeys and humans. *J Chem Neuroanat* 41:256-265.
- Parker JG, Marshall JD, Ahanonu B, Wu YW, Kim TH, Grewe BF, Zhang Y, Li JZ, Ding JB, Ehlers MD, Schnitzer MJ (2018) Diametric neural ensemble dynamics in parkinsonian and dyskinetic states. *Nature* 557:177-182.
- Parker PR, Lalive AL, Kreitzer AC (2016) Pathway-Specific Remodeling of Thalamostriatal Synapses in Parkinsonian Mice. *Neuron* 89:734-740.
- Pavlidis A, Hogan SJ, Bogacz R (2015) Computational Models Describing Possible Mechanisms for Generation of Excessive Beta Oscillations in Parkinson's Disease. *PLoS Comput Biol* 11:e1004609.
- Paxinos G, Franklin KBJ (2001) *The Mouse Brain in Stereotaxic Coordinates* (2nd Edition). London: Academic Press.
- Peng X, Tehranian R, Dietrich P, Stefanis L, Perez RG (2005) Alpha-synuclein activation of protein phosphatase 2A reduces tyrosine hydroxylase phosphorylation in dopaminergic cells. *J Cell Sci* 118:3523-3530.
- Pessiglione M, Guehl D, Rolland AS, Francois C, Hirsch EC, Feger J, Tremblay L (2005) Thalamic neuronal activity in dopamine-depleted primates: evidence for a loss of functional segregation within basal ganglia circuits. *J Neurosci* 25:1523-1531.
- Pfeiffer RF (2016) Non-motor symptoms in Parkinson's disease. *Parkinsonism Relat Disord* 22 Suppl 1:S119-122.

- Planert H, Berger TK, Silberberg G (2013) Membrane properties of striatal direct and indirect pathway neurons in mouse and rat slices and their modulation by dopamine. *PLoS One* 8:e57054.
- Planert H, Szydlowski SN, Hjorth JJ, Grillner S, Silberberg G (2010) Dynamics of synaptic transmission between fast-spiking interneurons and striatal projection neurons of the direct and indirect pathways. *J Neurosci* 30:3499-3507.
- Plenz D, Kital ST (1999) A basal ganglia pacemaker formed by the subthalamic nucleus and external globus pallidus. *Nature* 400:677-682.
- Postuma RB, Aarsland D, Barone P, Burn DJ, Hawkes CH, Oertel W, Ziemssen T (2012) Identifying prodromal Parkinson's disease: pre-motor disorders in Parkinson's disease. *Mov Disord* 27:617-626.
- Postuma RB, Berg D, Stern M, Poewe W, Olanow CW, Oertel W, Obeso J, Marek K, Litvan I, Lang AE, Halliday G, Goetz CG, Gasser T, Dubois B, Chan P, Bloem BR, Adler CH, Deuschl G (2015) MDS clinical diagnostic criteria for Parkinson's disease. *Mov Disord* 30:1591-1601.
- Quiroga-Varela A, Walters JR, Brazhnik E, Marin C, Obeso JA (2013) What basal ganglia changes underlie the parkinsonian state? The significance of neuronal oscillatory activity. *Neurobiol Dis* 58:242-248.
- Redgrave P, Rodriguez M, Smith Y, Rodriguez-Oroz MC, Lehericy S, Bergman H, Agid Y, DeLong MR, Obeso JA (2010) Goal-directed and habitual control in the basal ganglia: implications for Parkinson's disease. *Nat Rev Neurosci* 11:760-772.
- Rommelfanger KS, Wichmann T (2010) Extrastriatal dopaminergic circuits of the Basal Ganglia. *Front Neuroanat* 4:139.

- Rosa M, Giannicola G, Servello D, Marceglia S, Pacchetti C, Porta M, Sassi M, Scelzo E, Barbieri S, Priori A (2011) Subthalamic local field beta oscillations during ongoing deep brain stimulation in Parkinson's disease in hyperacute and chronic phases. *Neurosignals* 19:151-162.
- Ryan MB, Bair-Marshall C, Nelson AB (2018) Aberrant Striatal Activity in Parkinsonism and Levodopa-Induced Dyskinesia. *Cell Rep* 23:3438-3446 e3435.
- Ryu SB, Bae EK, Hwang YS, Lee HJ, Im CK, Chang JW, Shin HC, Kim KH (2011) A quantitative comparison of basal ganglia neuronal activities of normal and Parkinson's disease model rats. *Neurosci Lett* 505:113-118.
- Sanders TH, Jaeger D (2016) Optogenetic stimulation of cortico-subthalamic projections is sufficient to ameliorate bradykinesia in 6-ohda lesioned mice. *Neurobiol Dis* 95:225-237.
- Sanders TH, Clements MA, Wichmann T (2013) Parkinsonism-related features of neuronal discharge in primates. *J Neurophysiol* 110:720-731.
- Saunders A, Oldenburg IA, Berezovskii VK, Johnson CA, Kingery ND, Elliott HL, Xie T, Gerfen CR, Sabatini BL (2015) A direct GABAergic output from the basal ganglia to frontal cortex. *Nature* 521:85-89.
- Schmidt R, Leventhal DK, Mallet N, Chen F, Berke JD (2013) Canceling actions involves a race between basal ganglia pathways. *Nat Neurosci* 16:1118-1124.
- Schor JS, Nelson AB (2019) Multiple stimulation parameters influence efficacy of deep brain stimulation in parkinsonian mice. *J Clin Invest* 130.
- Sharott A, Vinciati F, Nakamura KC, Magill PJ (2017) A population of indirect pathway striatal projection neurons is selectively entrained to parkinsonian beta oscillations. *J Neurosci* 37:9977-9998.

- Sharott A, Magill PJ, Harnack D, Kupsch A, Meissner W, Brown P (2005) Dopamine depletion increases the power and coherence of beta-oscillations in the cerebral cortex and subthalamic nucleus of the awake rat. *Eur J Neurosci* 21:1413-1422.
- Sharott A, Gulberti A, Zittel S, Tudor Jones AA, Fickel U, Munchau A, Koppen JA, Gerloff C, Westphal M, Buhmann C, Hamel W, Engel AK, Moll CK (2014) Activity parameters of subthalamic nucleus neurons selectively predict motor symptom severity in Parkinson's disease. *J Neurosci* 34:6273-6285.
- Shink E, Bevan MD, Bolam JP, Smith Y (1996) The subthalamic nucleus and the external pallidum: Two tightly interconnected structures that control the output of the basal ganglia in the monkey. *Neuroscience* 73:335-357.
- Shouno O, Tachibana Y, Nambu A, Doya K (2017) Computational Model of Recurrent Subthalamo-Pallidal Circuit for Generation of Parkinsonian Oscillations. *Front Neuroanat* 11:21.
- Shu X, Lev-Ram V, Deerinck TJ, Qi Y, Ramko EB, Davidson MW, Jin Y, Ellisman MH, Tsien RY (2011) A genetically encoded tag for correlated light and electron microscopy of intact cells, tissues, and organisms. *PLoS Biol* 9:e1001041.
- Siapas AG, Lubenov EV, Wilson MA (2005) Prefrontal phase locking to hippocampal theta oscillations. *Neuron* 46:141-151.
- Smith Y, Bevan MD, Shink E, Bolam JP (1998) Microcircuitry of the direct and indirect pathways of the basal ganglia. *Neuroscience* 86:353-387.
- Soares J, Kliem MA, Betarbet R, Greenamyre JT, Yamamoto B, Wichmann T (2004) Role of external pallidal segment in primate parkinsonism: comparison of the effects of 1-methyl-

- 4-phenyl-1,2,3,6-tetrahydropyridine-induced parkinsonism and lesions of the external pallidal segment. *J Neurosci* 24:6417-6426.
- St Louis EK, Boeve AR, Boeve BF (2017) REM Sleep Behavior Disorder in Parkinson's Disease and Other Synucleinopathies. *Mov Disord* 32:645-658.
- Steriade M (2000) Corticothalamic resonance, states of vigilance and mentation. *Neuroscience* 101:243-276.
- Tachibana Y, Kita H, Chiken S, Takada M, Nambu A (2008) Motor cortical control of internal pallidal activity through glutamatergic and GABAergic inputs in awake monkeys. *Eur J Neurosci* 27:238-253.
- Tachibana Y, Iwamuro H, Kita H, Takada M, Nambu A (2011) Subthalamo-pallidal interactions underlying parkinsonian neuronal oscillations in the primate basal ganglia. *Eur J Neurosci* 34:1470-1484.
- Tanimura A, Du Y, Kondapalli J, Wokosin DL, Surmeier DJ (2019) Cholinergic Interneurons Amplify Thalamostriatal Excitation of Striatal Indirect Pathway Neurons in Parkinson's Disease Models. *Neuron* 101:444-458 e446.
- Taverna S, Ilijic E, Surmeier DJ (2008) Recurrent collateral connections of striatal medium spiny neurons are disrupted in models of Parkinson's disease. *J Neurosci* 28:5504-5512.
- Tecuapetla F, Jin X, Lima SQ, Costa RM (2016) Complementary Contributions of Striatal Projection Pathways to Action Initiation and Execution. *Cell* 166:703-715.
- Tepper JM, Koos T, Ibanez-Sandoval O, Tecuapetla F, Faust TW, Assous M (2018) Heterogeneity and Diversity of Striatal GABAergic Interneurons: Update 2018. *Front Neuroanat* 12:91.

- Villalba RM, Smith Y (2018) Loss and remodeling of striatal dendritic spines in Parkinson's disease: from homeostasis to maladaptive plasticity? *J Neural Transm (Vienna)* 125:431-447.
- Walters JR, Hu D, Itoga CA, Parr-Brownlie LC, Bergstrom DA (2007) Phase relationships support a role for coordinated activity in the indirect pathway in organizing slow oscillations in basal ganglia output after loss of dopamine. *Neuroscience* 144:762-776.
- Wang YY, Wang Y, Jiang HF, Liu JH, Jia J, Wang K, Zhao F, Luo MH, Luo MM, Wang XM (2018) Impaired glutamatergic projection from the motor cortex to the subthalamic nucleus in 6-hydroxydopamine-lesioned hemi-parkinsonian rats. *Exp Neurol* 300:135-148.
- West MJ, Slomianka L, Gundersen HJ (1991) Unbiased stereological estimation of the total number of neurons in the subdivisions of the rat hippocampus using the optical fractionator. *Anat Rec* 231:482-497.
- West MO (1998) Anesthetics eliminate somatosensory-evoked discharges of neurons in the somatotopically organized sensorimotor striatum of the rat. *J Neurosci* 18:9055-9068.
- Whitmer D, de Solages C, Hill B, Yu H, Henderson JM, Bronte-Stewart H (2012) High frequency deep brain stimulation attenuates subthalamic and cortical rhythms in Parkinson's disease. *Frontiers in Human Neuroscience* 6:155.
- Wichmann T, DeLong MR (1996) Functional and pathophysiological models of the basal ganglia. *Curr Opin Neurobiol* 6:751-758.
- Willard AM, Isett BR, Whalen TC, Mastro KJ, Ki CS, Mao X, Gittis AH (2019) State transitions in the substantia nigra reticulata predict the onset of motor deficits in models of progressive dopamine depletion in mice. *Elife* 8:e42746.

- Wilson CJ, Phelan KD (1982) Dual topographic representation of neostriatum in the globus pallidus of rats. *Brain Res* 243:354-359.
- Wilson CL, Cash D, Galley K, Chapman H, Lacey MG, Stanford IM (2006) Subthalamic nucleus neurones in slices from 1-methyl-4-phenyl-1,2,3,6-tetrahydropyridine-lesioned mice show irregular, dopamine-reversible firing pattern changes, but without synchronous activity. *Neuroscience* 143:565-572.
- Wu Y, Richard S, Parent A (2000) The organization of the striatal output system: a single-cell juxtacellular labeling study in the rat. *Neurosci Res* 38:49-62.
- Xu B, Lian S, Li SZ, Guo JR, Wang JF, Wang D, Zhang LP, Yang HM (2018) GABAB receptor mediate hippocampal neuroinflammation in adolescent male and female mice after cold expose. *Brain Res Bull* 142:163-175.
- Yin HH, Knowlton BJ (2006) The role of the basal ganglia in habit formation. *Nat Rev Neurosci* 7:464-476.
- Zavala B, Zaghoul K, Brown P (2015) The subthalamic nucleus, oscillations, and conflict. *Mov Disord* 30:328-338.
- Zhu Z, Bartol M, Shen K, Johnson SW (2002) Excitatory effects of dopamine on subthalamic nucleus neurons: in vitro study of rats pretreated with 6-hydroxydopamine and levodopa. *Brain Res* 945:31-40.
- Zold CL, Escande MV, Pomata PE, Riquelme LA, Murer MG (2012) Striatal NMDA receptors gate cortico-pallidal synchronization in a rat model of Parkinson's disease. *Neurobiol Dis* 47:38-48.